Design, Characterization and Analysis of Polydimethylsiloxane (PDMS) Based Flexible Antenna

THESIS

Submitted in the partial fulfillment
of the requirement for the degree of

DOCTOR OF PHILOSOPHY

by

Praveen Kumar Sharma
ID No. 2016PHXF0502P

Under the supervision of

Prof. Navneet Gupta

BITS Pilani
Pilani | Dubai | Goa | Hyderabad

BIRLA INSTITUTE OF TECHNOLOGY & SCIENCE,

PILANI-333031 (RAJASTHAN), INDIA

JULY 2022

BIRLA INSTITUTE OF TECHNOLOGY & SCIENCE
PILANI-333031 (RAJASTHAN) INDIA

CERTIFICATE

This is to certify that the thesis titled **"Design, Characterization and Analysis of Polydimethylsiloxane (PDMS) Based Flexible Antenna"**, submitted by **Praveen Kumar Sharma**, ID.No. **2016PHXF0502P** for the award of Ph.D. of the Institute embodies original work done by him under my supervision.

Date:-_____

Signature of the Supervisor

Prof. Navneet Gupta,
Professor
Department of Electrical & Electronics Engineering
BITS-Pilani, Pilani Campus

Dedicated to my little princess Kaavya Praveen Sharma.....

Acknowledgements

"Perseverance, inspiration and motivation have always played a key role in success of any venture". This thesis, as I see it, is not the end but just the beginning of my research journey. However before continuing the journey further, I would like to thank those who made possible all my ventures.

At the outset, I would like to thank the Almighty for everything that I am/have today.

At this level of understanding it is often difficult to understand the wide spectrum of knowledge without proper guidance and advice. Hence, I extend my sincere gratitude to my mentor Prof. Navneet Gupta, Professor, Department of Electrical and Electronics Engineering, BITS Pilani, for his support and guidance throughout my thesis. He gave me the freedom to choose my research topics and he created the environment where I could concentrate on my research without being disturbed by various financial and administrative issues. Despite his at times busy schedule, he was always available when I was in need of his scientific intuition and insights. He gave me a once-in-a-lifetime opportunity by sending me to Sofia, Bulgaria, to work as a Co-PI on a joint DST research project between BITS-Pilani, India, and Sofia University, Bulgaria, which provided me with a worldwide research platform. I am most grateful to him for giving me the opportunity to work under his supervision and for offering me the moral and scientific support to achieve my academic goals.

I am thankful to my Doctoral Advisory Committee (DAC) members Prof. Rahul Singhal and Prof. Praveen Kumar A.V, Associate Professor(s), Department of Electrical and Electronics Engineering, BITS Pilani who spared their valuable time to review my proposal and draft thesis. I am also grateful to Prof. H.D Mathur, Head of the Department and members of Departmental Research Committee (DRC) for their valuable guidance and motivation throughout this research.

Let me thank to the Vice-Chancellor, Directors and Deans of Birla Institute of Technology & Science (BITS), Pilani for providing me the opportunity to pursue my doctoral studies by providing necessary facilities and financial support.

Enormous help and kindness shown to others is never forgotten. My sincere gratitude towards Late Prof. Plamen I. Dankov, Associate Professor, Faculty of Physics and Ms. Valda Levcheva, Engineer, Sofia University "St. Kliment Ohridski", Sofia University Sofia, Bulgaria, with whom I got a chance to work as Co-PI in the joint research project between BITS Pilani and Sofia University, Bulgaria.

I would like to thank all my friends and fellow research scholars of BITS Pilani, in particular, Mr Suraj Baloda for his timely support to my research work.

Mr. Ravinder Kumar, Mr. Ashok Saini, Mr. Manoj Kumar, Mr. Amitabh Jangir, Mr. Sanjay Bhargava and all the staff of the EEE Department are also to be thanked for their assistance in the laboratory and with other official duties. Mr. Mahesh Chandra deserves special recognition for his technical assistance and support.

I am also grateful to my nephew, Deepak Jangid for his help to solve my all technical problems related to thesis writing.

I am most grateful to my parents, Mrs. Manju and Mr. J. P. Sharma, my In-laws, Mrs. Vimla and Mr. P.C. Jangid, brothers, Rahul and Jayant, sisters, Reya and Rajni & her family for their love and support.

And of course, my wife, Dr. Rashmi, and daughter, Kaavya Praveen Sharma, for always be ready to help me and stand with me in every situation, without them none of this would have been possible.

Praveen Kumar Sharma ...

Abstract

The field of flexible and wearable electronics has seen considerable expansion in recent years. Flexible electronics' remarkable mechanical qualities, such as bending, stretching, and twisting, make them promising for modern electronic devices to operate in real-world conformal and varied environmental operating circumstances. With the emergence of flexible electronics, flexible antennas have piqued the interest of academicians and industry personnel worldwide. They have a lot of appealing features, such as delivering adequate performance under a variety of operating conditions, which makes them a good contender for next-generation wireless communication systems.

There are a lot of choices of flexible substrates for the development of flexible and wearable antennas available in the literature which includes, fabric, polymer and paper-based substrates. Due to their multiple advantages over rigid and fabric substrates, polymers have been increasingly popular as a substrate for the design of flexible/wearable antennas in the previous few years. Flexible antennas require bending, stretching, and twisting, whereas rigid substrates do not perform well under these conditions. Fabric substrates, though can be employed for flexible antenna designs, but they are more susceptible to environmental influences like moisture absorption, temperature changes, and so on, which have negative impact on the antenna's radiating characteristics. Therefore, researchers are continuously exploring new conducting and substrate materials for the design of flexible antennas. In this research, the silicone-based polymer Polydimethylsiloxane (PDMS), which belongs to the category of polymeric organo-silicon compounds (silicones) $(C_2H_6OSi)_n$, is chosen as the polymer substrate. In addition to flexible antennas, it can also be employed as a flexible substrate in microchips, thin membranes, sensors, hydrophobic antenna coating, and other applications. PDMS possesses favorable attributes for its employment as a flexible antenna substrate like it is chemically inert, thermally stable, permeable to gases, easy to handle, and with reasonably isotropic and homogeneous qualities in addition to flexibility, transparency, and water resistance properties.

However, it has been observed that varied values of its dielectric parameters are employed by the researchers for the frequency range 0.1-40 GHz. These parameters include dielectric constant (ϵ_r) values ranging from 2.32 to 3.2 and loss tangent ($\tan\delta_{\epsilon_r}$) values ranging from 0.01 to 0.08. The values in the range of ∼2.7-2.8 represent parallel dielectric constant values, whereas values in the range of ∼2.65 or below represent perpendicular dielectric constant values. This variance in PDMS dielectric parameter values is undesirable since it degrades design accuracy. This gives the motivation for the development of novel PDMS characterization methods for calculating the precise value of its dielectric parameters.

Two experimental methods for PDMS characterization are proposed in this research. The first method is based on resonance measurements using PDMS samples in the shape of discs to excite two types of TE- and TM-mode cylinder resonators. This method ensures that the dielectric constant and dielectric loss tangent values in parallel and perpendicular directions are accurately determined. The second method is based on the close coverage of planar microstrip ring resonators with non-metalized PDMS samples, and it provides accurate equivalent dielectric parameters. The obtained results reveal that PDMS substrate posses modest but measurable uniaxial anisotropy, as well as well-expressed frequency dependence of the derived dielectric parameters in the 1-40 GHz range, notably ϵ_{par} ∼2.7-2.82; ϵ_{perp} ∼ 2.52-2.73 and ϵ_{eq} ∼2.64- 2.75, $\tan\delta_{\epsilon_{eq}}$ ∼ 0.017-0.048. Several other complementary methods confirm the results obtained.

After successfully evaluating important electromagnetic properties of PDMS, the first antenna prototype for various wireless applications is designed. The key objective of this prototype is to show that, PDMS can be used as a flexible antenna substrate that offers various advantages over fabric-based substrates. To present the comparative analysis, the fabric-based substrate Jean is chosen. Various researchers have employed Metamaterial for the enhancement of the radiation properties of rigid substrate-based antennas. A very limited literature is available on the use of metamaterial in the flexible antennas, particularly those employing polymer-based substrates like PDMS. So, this prompted us to incorporate it in the second antenna prototype as metamaterial inspired flexible antenna. A single split ring resonator (SRR) is employed in this proposed design on the same side

of the patch in addition to the rectangular slot on the ground. This offers the requisite frequency notched characteristics for the intended frequency bands, and the provided antenna resonates at 5 GHz, 5.8 GHz, and 6.6 GHz for WLAN and WBAN applications, as per the IEEE 802.11ac, 802.16d, and 802.11ax requirements. The SRR structure and slots with the applied coplanar waveguide (CPW) feed also helped in achieving compactness, minimize losses, and backward radiation, when the proposed antenna is used in close proximity to the human body. Both the presented flexible antennas have been tested in a variety of operating situations including bending, and wet environments, and they consistently provide good performance characteristics. The specific absorption rate (SAR) analysis is also performed in this research using three layered simulation model to analyze the effect of antenna on human body. The presented flexible antennas are fabricated and characterized using the KEYSIGHT N9928A vector network analyzer (VNA) to validate the simulation results.

Keywords: Anisotropy, Dielectric materials, Dielectric constant, Flexible antenna, Material characterization, Metamaterial, PDMS, Polymers, Resonators, SRR, SAR.

Contents

List of Figures

List of Tables

List of Abbreviations

COP	**C**yclo **O**lefin **P**olymer
CST	**C**omputer **S**imulation **T**echnology
CTE	**C**oefficient of **T**hermal **E**xpansion
CNT	**C**arbon **N**anotubes
DOD	**D**rop **o**n **D**emand
E- field	**E**lectric **F**ield
ENG	**E**psilon **N**egative
FSS	**F**requency **S**elective **S**urface
GSM	**G**lobal **S**ystem for **M**obile Communication
HMSIW	**H**alf-**M**ode **S**ubstrate **I**ntegrated **W**aveguide
HFSS	**H**igh **F**requency **S**tructure **S**imulator
ISM	**I**ndustrial **S**cientific and **M**edical
IEEE	**I**nstitute of **E**lectrical and **E**lectronics **E**ngineers
LCP	**L**iquid **C**rystal **P**olymer
LR	**L**inear **R**esonator
MSL	**M**icrostrip **L**ine
MTM	**M**etamaterial
NRM	**N**egative **R**efractive **I**ndex **M**aterials
NWCF	**N**onwoven **C**onductive **F**abrics
NP	**N**anoparticle
PCB	**P**rinted **C**ircuit **B**oard
PET	**P**olyethylene **T**erephthalate
PEN	**P**olyethylene **N**aphthalate
PC	**P**olycarbonate
PES	**P**olyethersulfone
PI	**P**olyamide
PSS	**P**olyethylenedioxythiophene **P**olystyrene **S**ulfonate

PANI	**P**olyaniline
PPV	**P**olyphenylene **V**inylene
PEC	**P**erfect **E**lectric **C**onductor
PDMS	**P**olydimethylsiloxane
PTFE	**P**olytetrafluoroethylene
Q	**Q**uality Factor
RR	**R**ing **R**esonator
RFID	**R**adio **F**requency **I**dentification
RP	**R**esonant **P**article
SAR	**S**pecific **A**bsorption **R**ate
SMA	**S**ub **M**iniature version **A**
SEM	**S**canning **E**lectron **M**icroscope
SIW	**S**ubstrate **I**ntegrated **W**aveguide
SRR	**S**plit **R**ing **R**esonator
TE	**T**ransverse **E**lectric
TM	**T**ransverse **M**agnetic
TEM	**T**ransverse **E**lectric and **M**agnetic
UWB	**U**ltra **W**ideband
VSWR	**V**oltage **S**tanding **W**ave **R**atio
VNA	**V**ector **N**etwork **A**nalyzer
WBAN	**W**ireless **B**ody **A**rea **N**etworks
WLAN	**W**ireless **L**ocal **A**rea **N**etworks
Wi-Fi	**Wi**reless **Fi**delity
WiMAX	**W**orldwide **I**nteroperability for **M**icrowave **A**ccess

Chapter 1

Introduction

1.1 Background

The 'Fourth Industrial Revolution' piqued researcher's interest in flexible electronics, which is one of the most recent innovations in the electronics sector. The 5G network's technological breakthroughs, such as higher data speeds, range, and capacity with reduced latency, have sparked this revolution. As a result, researchers are constantly looking for novel materials that can meet all of these requirements while also providing flexible characteristics to address the drawbacks of rigid materials.The flexible devices are light, compact, easy to integrate, inexpensive, and, most significantly, environmentally beneficial, especially in light of today's high pollution levels. By 2023, the flexible electronics sector market is expected to be worth more than 40 billion dollars [1]. The demand for wireless, implantable and flexible devices for the number of applications like health monitoring systems and other day-to-day devices such as mobiles, computers, laptops, etc., has increased tremendously in recent years. Therefore, the demand and requirement for flexible antennas, the crucial component of flexible wireless communication systems, has increased proportionally. So, to design a flexible antenna that is compact, flexible, and low profile, satisfying all the system requirements in terms of small size, number of frequency bands supported, gain and bandwidth, etc., is still a challenging task [2].

Traditional stiff substrates and conducting materials are not suited for designing flexible antennas because they cannot withstand the requirements mentioned above

of flexibility and conformal circumstances. Therefore, the researchers are constantly looking for new materials with the necessary properties for specific applications. Various materials for flexible antennas have been suggested in the literature. As illustrated in Fig 1.1, in order to design a flexible antenna, materials for conductive sections such as patch, ground and feed, as well as substrate material should be carefully chosen, that mainly depends on the target applications in consideration. The conductive materials like silver and cooper are most commonly used in the form of nanoparticle (NP) inks. Nowadays, conductive textile fabrics known as electro-textiles such as taffeta and conductive polymers such as polyaniline, polypyrrole etc. are also becoming increasingly popular because of their high conductivity and better performance under conformal conditions.

The three main types of flexible substates that can be employed for flexible antenna design are fabric, polymers, and paper-based substrates. Fabric substrates are more prone to environmental factors such as moisture absorption and temperature variations. Under flexible, stretchable, and conformal circumstances, they deliver a limited performance. Paper-based substrates have comparable constraints, therefore polymer-based substrates are preferred in this research.

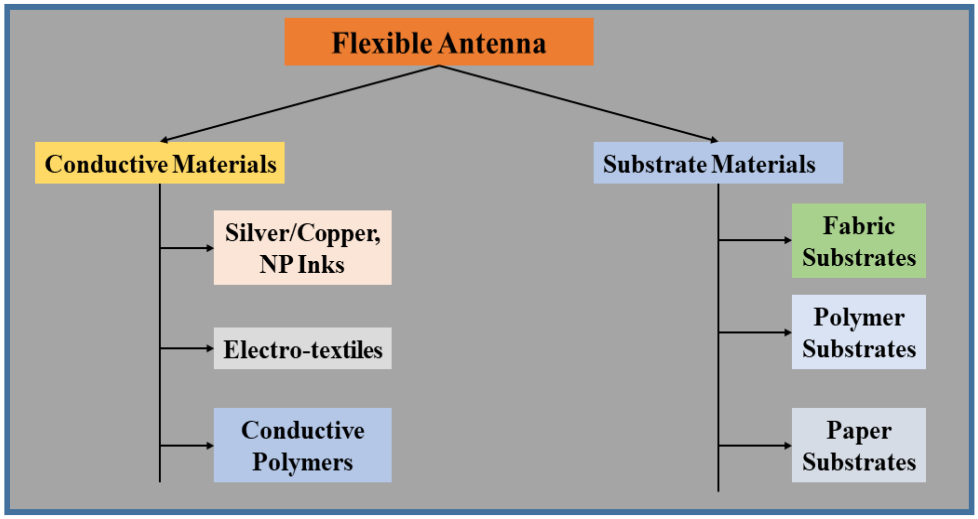

FIGURE 1.1: Different materials for flexible antenna design

With the advancements in printing technology, a variety of new techniques for fabricating flexible antenna have emerged in recent years. Conventional fabrication procedures such as chemical itching and embroidery have certain drawbacks.

These include being slow, inaccurate and using chemicals that are not very environmentally friendly. The latest manufacturing techniques, like inkjet printing, screen printing, and substrate intigrated waveguide (SIW), are faster and antenna design is directly transferred on the substrates utilising conducting NP inks and modern printers. These manufacturing procedures create relatively little waste and are also non-hazardous to the environment. A comprehensive review of various types materials and fabrication methods employed by different researchers to develop flexible antennas for multiple applications is presented in chapter 2.

In order to design the flexible antennas, the conventional procedure to be followed is illustrated in Fig.1.2. The initial and most crucial step in the design process is the material selection and characterization of the dielectric properties of these materials mainly dielectric constant ϵ_r, dielectric loss tangent $\tan\delta_{\epsilon_r}$ and conductivity σ_r. Then depending upon the applications, suitable geometry of the antenna structure is selected, which includes the radiating patch, ground and feed lines. After that, the antenna is simulated and optimized using the appropriate 3D electromagnetic solvers like Ansys HFSS or CST, etc. In this research, all simulations are performed using the Ansys HFSS. At last, the simulation results are validated by developing the appropriate prototype, measurements and performance evaluation of the designed antenna are then performed using the suitable vector network analyzer (VNA) based setup.

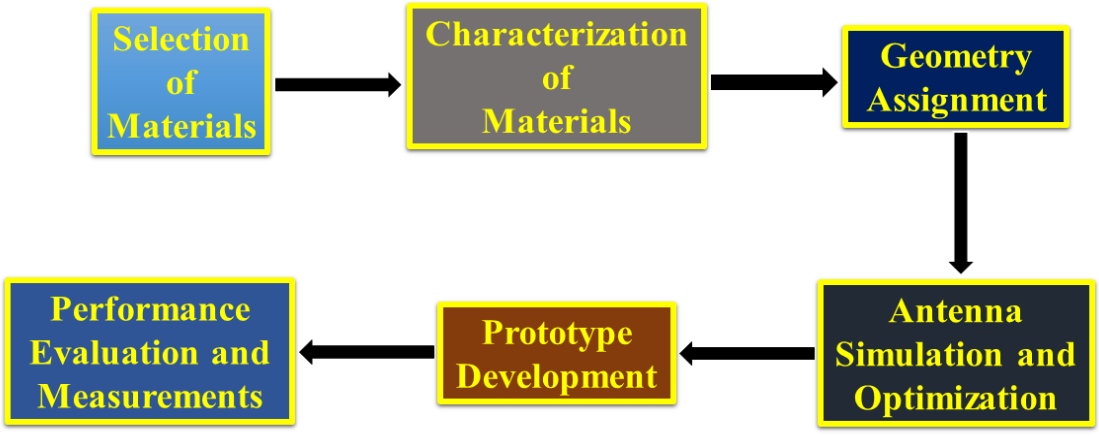

FIGURE 1.2: Design steps of Flexible Antennas

This chapter is divided into four sections. The first section 1.1 provides a quick background of flexible antennas. The challenges of the flexible antenna designs

are highlighted in section 1.2, followed by section 1.3, which explains the research motivation and objectives. The thesis's organization is then presented in section 1.4.

1.2 Challenges of Flexible Antenna Design

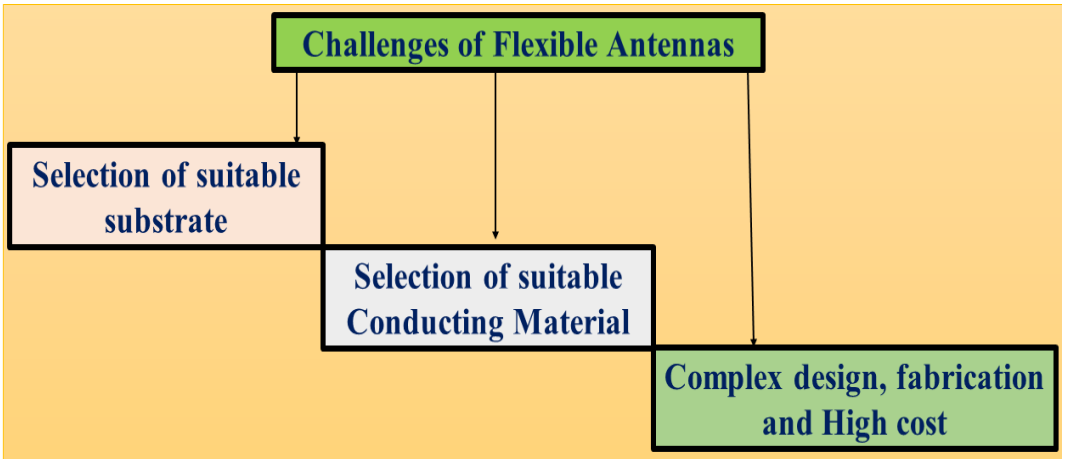

FIGURE 1.3: Challenges for Flexible antenna design

The different issues and challenges of flexible antennas as shown in Fig (1.3), in terms of design, fabrication, and implementation are as follows:

A. Selection of suitable substrate: The substrate plays a vital role in flexible antenna design, which should be flexible and operate well under different conformal conditions. So, the first task is to replace the conventional rigid substrate with a flexible substrate depending upon the requirement and target applications. There are various choices of flexible substrates available these days. The typical flexible substrates have a low value of dielectric parameters as compared to standard rigid substrates like FR4 or Rogers, which have a dielectric constant of 3–10 and a loss tangent of 0.001–0.02. Despite having a low value of dielectric parameters that allows to achieve a high bandwidth and gain, downsizing of the flexible antenna is still a challenging task. The uneven surface thickness of flexible substrates like polymers is another problem. We also faced this problem while developing Polydimethylsiloxane (PDMS) in our lab but performing different iterations gave us satisfactory results. The fabric-based and paper substrates are more prone to environmental variations like absorption of moisture, inability to withstand high

temperatures, which may lead to the degradation of the antenna's performance. That's why polymer-based substrates like PDMS are preferred here in this research. Excessive bending or twisting of the polymer-based antenna might result in micro-cracks in the substrate, which can be a concern. This will reduce the antenna's electrical conductivity and increase the chance of failure. This constraint can be solved by inserting ultra-thin metallic nanowires on the surface of PDMS to make them highly conductive and flexible.

B. Selection of suitable conducting material: Another issue in developing flexible antennas is finding acceptable conducting materials that can withstand a variety of bending and twisting situations while maintaining a tolerable resistance value that does not degrade the antenna's performance. Different conducting material choices for flexible antennas are available in the literature. Also, there are many ways to develop conductive substrates, such as chemically altering fabric surfaces or physically combining numerous conductive materials.

C. Complex design, fabrication, and high cost: The choice of different available fabrication methods and designs to develop flexible antenna mainly depends on the targeted applications and budget, so optimizing these two parameters is also a challenging task. In this research, in order to reduce the cost and design complexity, we have used the substrate PDMS developed and characterized in our lab, conducting parts of the flexible antenna are made from the adhesive copper tape. A single split-ring resonator structure (SRR) is also used to enhance the performance of the proposed antenna.

1.3 Motivation and Objective of the Thesis

The following are the three primary components that drive this research's motivation:

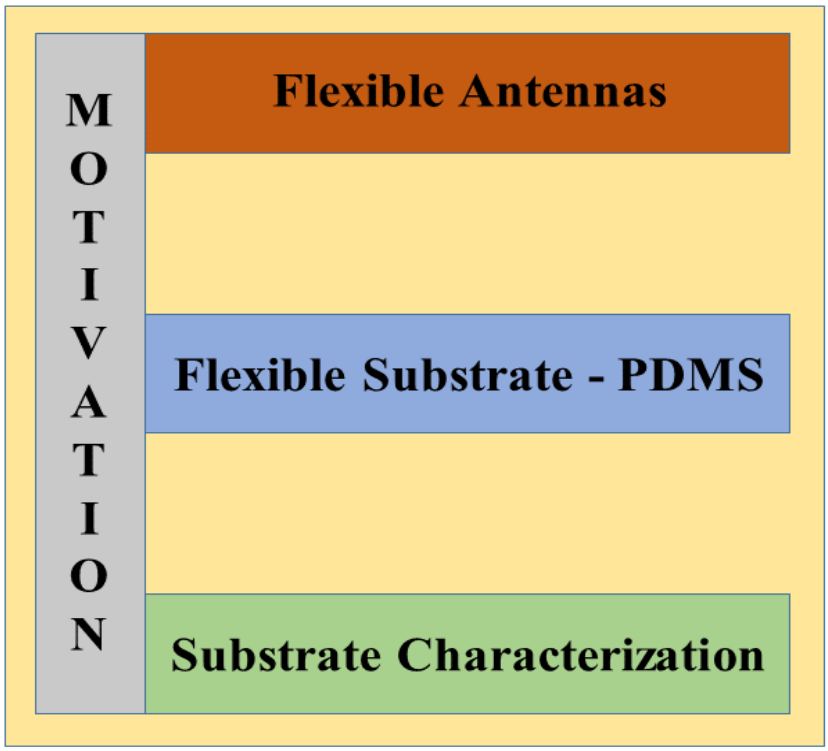

FIGURE 1.4: Thesis Motivation

A. Flexible Antennas: With the rapid rise of flexible electronics, flexible antennas have piqued the interest of researchers, academia, and business in recent years. They are preferred over rigid antennas for a variety of reasons, including their broad range of WBAN and WLAN applications, their non-traditional operating environment-bending, stretching, and so on, and the fact that they can be used in close proximity to the human body. However, previous research has shown that developing a flexible antenna with decent performance under a variety of operating situations remains a challenge. As a result, in this research, a flexible antenna for WBAN and WLAN applications is fabricated and tested for various operating scenarios with satisfactory results.

B. Flexible Substrate- PDMS: Various types of substrates have been documented in the literature to design flexible and wearable antennas; a complete overview is addressed in chapter 2. Because of its numerous advantages, such as being highly flexible, transparent, chemically inert, adhesive, performing well under conformal conditions, withstanding high temperatures, and suitable for a variety of applications, Polydimethylsiloxane (PDMS) is preferred over the fabric and other

types of substrate options in this research (comparative analysis of PDMS with denim substrate is also performed in the chapter- 5).

C. Substrate Characterization: As inferred from the previous works, different researchers have used a diverse variety of dielectric constant and loss tangent values of PDMS, affecting the antenna's performance directly or indirectly. Therefore, different experimental methods for the exact characterization of the dielectric properties of PDMS and similar substrates have been proposed in chapter 3 of this thesis. Parallel and perpendicular dielectric parameters of PDMS and comparable substrates can be obtained simulteneously using the proposed methods, and their frequency and temperature dependence have also been investigated.

The development and characterization of Polydimethylsiloxane (PDMS) as a flexible antenna substrate, as well as the design and analysis of the flexible antenna using PDMS substrate for WLAN and WBAN applications, are the key themes of this thesis. The following are the thesis objectives:

1. Development and dielectric characterization of the flexible antenna substrate.
2. Investigation of the dielectric anisotropy and bending effect of the flexible substrates.
3. Design, simulation and analysis of the antenna on the developed flexible substrate.
4. Fabrication and testing of the developed flexible antenna under various operating conditions.

1.4 Organization of the Thesis

The thesis is organized into seven chapters, of which **Chapter 1** introduces the background of flexible antennas, with design challenges, motivation and objectives of the research. The following six chapters of this thesis are outlined below:
Chapter 2 provides an overview of flexible antennas, including different conducting and substrate material options and various fabrication procedures for flexible antenna design. In the later sections of this chapter, the benefits of using Metamaterial to improve the performance of flexible antennas are discussed.

Chapter 3 deals with the development and characterization of the Polydimethylsiloxane (PDMS) as a substrate for flexible antennas. The fabrication procedure used at the BITS-Pilani lab to develop PDMS is illustrated in this chapter. To characterize the dielectric properties of PDMS, two experimental methods are applied. The first method is based on resonance measurements by the two-resonator method. This method allows the determination of the dielectric constant ϵ_r and dielectric loss tangent $\tan\delta_{\epsilon_r}$ of non-metalized samples in parallel and perpendicular directions. The second method is based on the application of different planar structures (resonators and transmission lines) by integrating the PDMS samples without metallization. The results obtained by analyzing PDMS samples are compared with results for isotropic Polytetrafluoroethylene (PTFE) and Cyclo Olefin Polymer (COP) samples. The analysis performed experimentally proves that PDMS is a good choice as a flexible and wearable antenna substrate.

Chapter 4 highlights the bending effect of the substrates for the flexible antennas. The simultaneous effect of the substrate anisotropy and bending are numerically and experimentally investigated in this chapter for planar resonators on flexible textile and polymer substrates. With the help of properly selected flexible isotropic substrates, the pure bending effect has been investigated. The effect of anisotropy is quantitatively split from the effect of bending, and it has been demonstrated for the first time that both phenomena have nearly similar but opposite effects on the resonance characteristics of planar resonators. The opposite influence of both effects, anisotropy and bending, has been experimentally demonstrated for rectangular resonators after selecting different anisotropic textile fabrics, polymers, and flexible reinforced substrates with measured anisotropy.

Chapter 5 presents a comparitive analysis of polymer and fabric substrate based flexible antenna. The denim (Jean) is selected as a fabric substrate and PDMS is used as a polymer substrate. The flexible antenna with PDMS substrate shows a better results in terms of its performance parameters like S-parameters and VSWR as compared to the jean substrate based antenna. The discripancy between the simulated and measured results of the presented antenna using PDMS substrate is likewise less then the jean substrate based antenna. Also, the PDMS substrate based antenna shows a stable performance under varying operating conditions like

bending and wet conditions.

Chapter 6 describe the performance and geometric analysis, fabrication, and measurements of a flexible antenna for WLAN and WBAN applications. In this design a single split ring resonator (SRR) structure is also used at the same side of the patch to further improve the antenna's performance. This proposed antenna have also been tested in various operating conditions, including bending and wet conditions. The specific absorption rate (SAR) analysis is performed using a three layer simulation model in order to analyse the effect of the antenna when it is used in the close proximity to the human body.

Chapter 7 presents the conclusions drawn from the work, thesis highlights, and provides directions for possible future works.

Chapter 2

Flexible Antenna: An Overview

2.1 Introduction

Electronic devices using flexible substrate materials provide numerous advantages over traditional electronic devices using rigid substrates. These flexible devices can withstand unusual operating situations such as bending, stretching, and twisting. Due to the increased demand for novel wireless communication systems in recent years, antenna designers have had to overcome a number of technological challenges as a result of additional unusual performance requirements. It is better to have a flexible, small, lightweight, easily integrable, and low-cost antenna for such purposes. These characteristics are likewise desirable for wearable antennas for body-worn applications, without causing potential harm to the user's health. As a result, flexible antennas that are developed using flexible substrates are preferred to meet such requirements over conventional antennas using rigid substrates. Different types of flexible antennas for various applications using a variety of substrates have been reported in the literature in recent years. In 2001, the authors [3] used fabric substrates to design a flexible antenna to conform to wear. Then, in 2002 a flexible antenna was designed for WLAN (2.04 GHz) and UMTS (2.1 GHz) applications using the fabric-based substrates [4] again. The flexible antennas for wearable applications used in the military and safety were developed from 2003 to 2007 [5,6]. A wearable antenna operating under variable humid conditions was reported in [7]. Implementing flexible antennas for biomedical applications has gained popularity in recent years [8, 9]. Flexible antennas, in particular, are the vital component

in the implementation of vital sign monitoring systems, organ function regulation systems, brain interfaces, intracranial sensors, drug administration systems, and a variety of other activities related to health monitoring systems [10, 11].

The flexible antenna sensors are also becoming popular in modern electronics due to their number of advantages like easy to integrate, reducing the overall cost of the systems, perform well under bent or stretched conditions, or non-flat conditions. They have simple configurations, and most importantly, they can handle both sensing and communication, allowing the system's size to be lowered significantly. The first antenna sensor [12], based on the Bottcher model, was implemented in 1995 to monitor moisture content using a circular patch antenna. Since then, a number of flexible antenna sensors have been reported in various studies for measuring the dielectric characteristics of snow, soil, gas [13, 14], pH level [15], glucose level, humidity, and moisture etc. [16–20] content. These flexible antenna sensors fall under the category of dielectric antenna sensors. The dielectric properties of the materials used in the flexible antennas define the relation of the experimental measurements and the radiation characteristics of the antennas. There are no exact analytical models present in the literature to evaluate the actual dielectric parameters of the flexible materials (substrates), which is one of the significant barriers in the creation of the flexible dielectric antennas. This research also presents different experimental methods for measuring the dielectric properties of flexible antenna substrates like Polydimethylsiloxane (PDMS) in Chapter 3.

This chapter provides a brief overview of flexible antennas. The various materials used as substrates and conducting parts are discussed in section 2.2. In Section 2.3, the different fabrication procedures for the construction of flexible antennas are presented. Section 2.4 explains how metamaterial can be used in flexible antennas to improve their performance for a variety of applications. Finally, the complete study is summarized in section 2.5 as the conclusion.

2.2 Materials for Flexible Antennas

Different choices of materials for the substrates and conductive parts are available to develop flexible antennas. The selection of these materials is based on the type of

the target applications, required radiation characteristics of the flexible antennas, dielectric properties, tolerance limits according to the working environment like mechanical deformations- bending, twisting, and stretching conditions, and required compactness. Materials are chosen such that they retain their usefulness even when exposed to the worst working circumstances, such as rough and uneven surfaces. All such requirements have triggered the researchers to continuously search and develop new materials with the latest fabrication methods that are more precise in terms of dielectric characteristics, flexibility, reliability, weight, and efficiency.

The dielectric characteristics of the selected substrates directly affect the radiation behavior of the flexible antennas. The dielectric constant, loss tangent and height of the substrates must be adequately evaluated with sufficient accuracy so that the required expectation of the antenna's behavior for a selected application must be reached. For example different characterization methods for polymer substrate are available in the literature like waveguide method, two-resonator method, coplanar method, ring-resonator method, planar methods, etc. [21–23].

Different materials for the development of flexible antennas are presented in this section. The conductive materials used to form the conducting layers, such as patch, ground, and feed, are first explained. Following that, three main types of substrate materials are discussed: fabric, polymers, and paper-based substrates.

2.2.1 Conducting Materials

The choice of conductive material for the patch, ground, feed, and other parts should have a high electrical conductivity, which is essential for attaining acceptable performance of flexible antenna. Another desirable attribute for the conductive material is to resist performance degradation due to the flexible antenna's different conformal geometries. Because of their excellent electrical conductivity, materials such as silver and copper, in the form of nanoparticle (NP) inks, are frequently used to fabricate conductive parts of flexible antennas. These materials have their own advantages, like silver has less oxidation rate than copper, which is more cost-effective than silver [24]. Electro-textile materials such as Flectron, copper-coated nylon fabric, Ni/Ag-plated threads, and nonwoven conductive fabrics (NWCFs) are

commonly utilized in flexible textile-based antennas in addition to copper and silver. In [25], the authors have reviewed different conductive materials used for flexible antennas. The self-adhesive tapes of copper [26], [27] are also employed to create flexible antennas. Conducting polymers are also becoming increasingly popular for developing the conducting sections of flexible antennas. Different polymers, such as Polyethylenedioxythiophene polystyrene sulfonate (PSS) [28], Polyaniline [29], and Polypyrrole [30], are examples of popular conducting polymer materials that could be used in flexible antennas.

By adding elements like graphene [31], carbon nanoparticles [32], and nanotubes [33], the conductivity of these polymer composites can be improved even more. Due to their high electrical conductivity and higher performance in conformal environments, graphene-based flexible antennas are getting a lot of attraction. Different stretchable conductive materials use doping to increase their conductivity to accommodate mechanical strain and deformation without compromising the antenna's effectiveness. Silver nanowire silicone [34], fluorine rubber loaded silver, conductive polymers based on carbon nanotubes (CNT) [35], [36], and metals in liquid state in flexible substrates are just a few examples. Table 2.1 shows the conductivity values of the various conductive materials utilized to produce a flexible antenna.

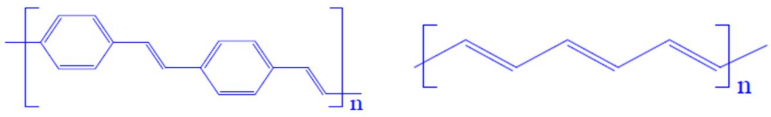

(a) Polyaniline (PANI) (b) Polyacetylene $(CH)_x$

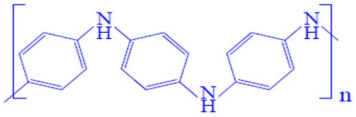

(c) Polyphenylene vinylene (PPV)

FIGURE 2.1: Typical examples of conducting polymers used in the flexible antennas

TABLE 2.1: Different conducting materials for flexible antennas

Conductive Material Category	**Examples**	**Conductivity value, σ (S/m)**	**Ref.**
Metal nanoparticles	Ag nanoparticle	2.173×10^7	[37]
	Cu nanoparticle	1×10^6	[38]
Conductive Polymers	PEDOT: PSS	100-1500	[39]
	Polyaniline (Pani)	5	
	Polypyrrole (PPy)	40-200	
	Polyleurethene nanoparticle composite sheet	1.1×10^6	[40]
Conductive Polymers with additives	C nanotube	4000-7000	[41]
	PANI/CCo Composite	7.3×10^3	[42]
	AgNW/PDMS	8130	[26]
	Ag flakes + Fluorine Rubber	8.5×10^4	[27]
	Zoflex FL45 + Cu	1.93×10^5	[43]
Graphene Based materials	Nanoflakes	6×10^5	[44]
	Paper	4.2×10^5	[45]
Liquid Metal	Eutectic GaIn	3.4×10^6	[46]
	EgaIn liquid fillet	2.5×10^5	[47]
Conductive Fabrics	Copper coated taffetta	3.4×10^6	[48]
	Meshed Fabric	2×10^5	[49]

2.2.2 Substrate Materials

The three types of substrate materials that are widely employed in the design of flexible antennas are as follows:

A. Fabric (Textile) Substrates

The fabric substrates are a promising candidate for flexible antennas, particularly for different wearable applications like Body centric wireless communications. The IEEE 802.15.6 standards group was formed in November 2007 [50] to support the growing interest in antennas and propagation research for body communication systems. A flexible wearable antenna is a type of antenna in which textile materials are utilized to produce an antenna segment that may be conveniently employed in close proximity to the human body for communication purposes. They are easily interagable, lightweight with acceptable performance in different conformal conditions. These fabric-based antennas can be categorized as per the materials used in the antenna structure. In the first category, the antenna substrate is a non-conductive textile material. For other segments like patch, ground, and feed,

different conductive Nanoparticle inks like silver and copper as described above can be used. In the following category, both substrate and other conducting antenna segments are textile materials.

Electro-textile (e-fabrics) materials are utilized to produce the conductive segments of the antenna in the second category of flexible wearable antenna. These e-fabrics are typically metal-plated fabrics in which various types of metals are implanted in standard textile fabric materials by weaving various metal wires in different directions (the orthogonal arrangement generally is chosen). Knitting is another method in which woven mesh is used to embed metal conductors into ordinary fabric materials, as shown in Fig.2.2. In terms of conductivity, durability, and mechanical strength, the percentage of metal conductors added to the pure fabric materials defines the fiber's potential [51]. The typical examples of the frequently used e-fabric materials for the flexible wearable antennas are Flectron®, Nora®, and Zelt®. Different fabric substrates used to develop flexible antennas for multiple applications are listed in Table 2.2.

The fabric substrates can also be divided into natural or artificial (synthetic) textile materials. The artificial textile substrates derive their properties from their molecular structure, unlike the natural textile materials such as wool, silk and cotton, which are sourced from nature. The textile substrates are preferred for specific wearable applications as they generally have a low dielectric constant value, which reduces losses due to the surface waves and enhances the performance characteristics of the antenna like efficiency and bandwidth. But different conformal conditions of the flexible antennas might affect the overall radiation characteristics of the antenna. The effect of bending and variation of the substrate height on the resonant frequencies and other performance parameters is explained in detail in chapter 4 [52, 53].

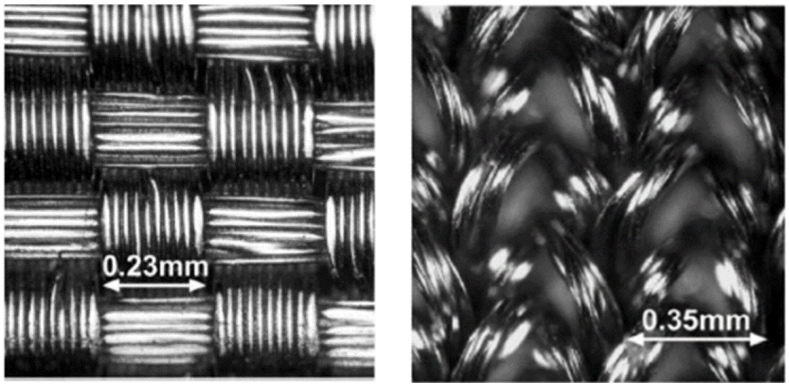

(a) (b)

FIGURE 2.2: Examples of Electro- textile materials (e-fabrics) (a) AgCuNi- Plated Fabric, and (b) Ag- Plated Fabric [51]

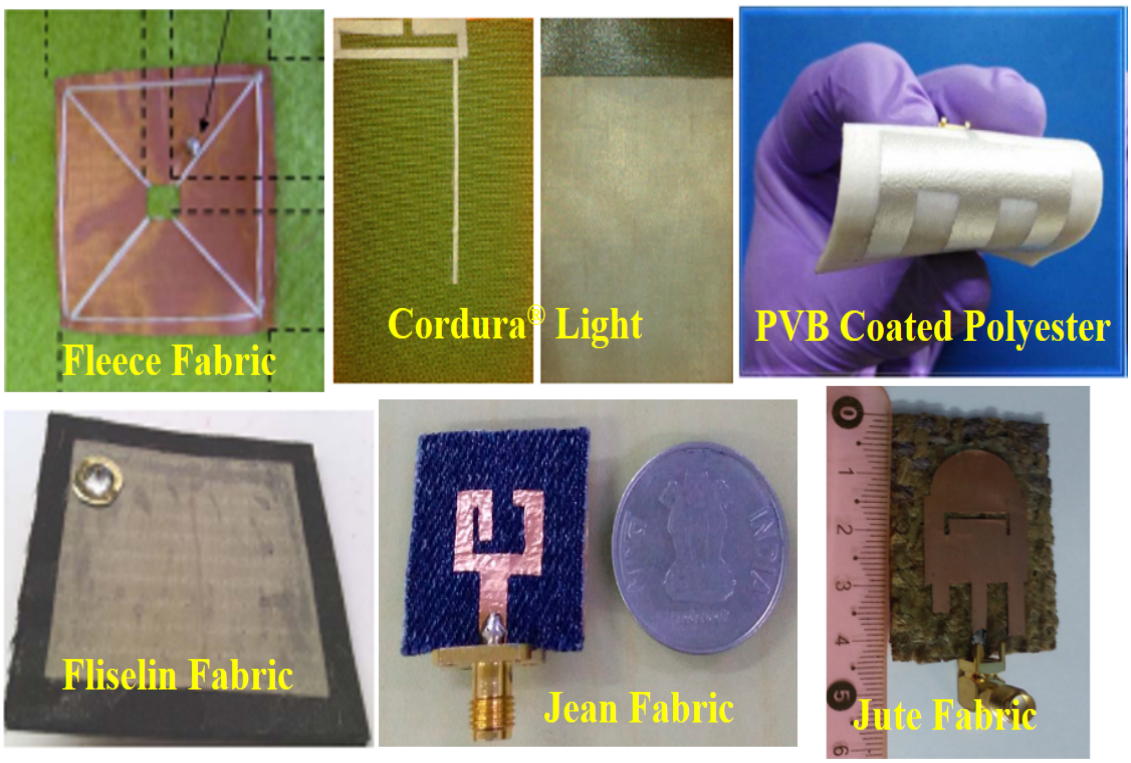

FIGURE 2.3: Examples of Fabric Substrate based Flexible Antennas [54–59]

TABLE 2.2: Different fabric substrates for flexible antennas

Antenna type/Structure used	**Substrate used**	**Advantages/ frequency band**	**Ref.**
Planar inverted F antenna (PIFA)	Not specified	First wearable antenna proposed for GSM (900 MHz) and Bluetooth (2.4 GHz)	[60]
Microstrip patch antenna	textile substrate	WLAN and GPS systems	[54], [61]
Rectangular ring-type antenna	Fleece fabric	Integrated well in garments and bending characteristics well tested for 2.4 GHz	[62]
Dual-band coplanar patch antenna	Zelt fabric	2.45 and 5.8 GHz	[63]
Dual polarized patch antenna, dual-band patch antenna	Fire-retardant foam, flexible felt substrate	Easily interagable into fire fighter suits, 2.45 and 5.8 GHz	[64], [65]
Yagi–Uda antenna with an end-fire radiation pattern	Commercial fabric	Reflection and radiation characteristics have been tested in free space and on a skin-equivalent phantom for on-body communications over the entire 57–64-GHz range	[66]
Dual-band antenna using the suspended plate concept	Conductive textiles	277 MHz (2.22–2.48 GHz) in the ISM and 850 MHz (4.95–5.80 GHz) in the Hiper LAN band	[67]
LV shaped logo antenna	Leather	ISM frequency band, 2.4 and 4.5 GHz	[68], [69]
T-shaped antenna	Cordura® Light, zelt	GSM900 and DCS1800 frequency bands based Smart coat	[55]
E-shaped microstrip patch antenna	Polyvinyl butyral (PVB) coated polyester fabric	WiMAX applications	[56]
Rectangular sleeve-badge antenna	Fliselin fabric and polyester fabric.	2.45 GHz frequency band	[57]
Square- slot antenna	Silver-plated cotton	UWB applications	[58]
Defected ground plane antenna	Jean	WLAN, C band and X/Ku frequency bands	[70]
Rectangular patch antenna	Jute fiber	3.23 GHz	[59]
Rectangular patch antenna	Polyester	26 GHz, 5G-IoT Millimeter-wave applications	[71]

B. Polymer Substrates

The electrical behavior of polymers was first reported in 1977. Since then, the applications of polymers in the electronics sector have gained much popularity by progressive refinement in their characteristics like flexibility, conductivity etc. [72].

Polymers have become increasingly popular as a substrate for the design of flexible/wearable antennas in recent years due to their numerous advantages over the fabric and rigid substrates like rigid substrates cannot be used for flexible antennas. They fail to operate correctly under bending, stretching, and twisting processes, which are the significant requirements of flexible antennas. However, fabric substrates can be used for flexible antenna designs. Still, these substrates also have some limitations, like such substrates are more prone to environmental effects like moisture absorption, temperature variations, etc., which affect the antenna's radiation characteristics. On the other hand, the polymer substrates provide flexibility, stretchability, and bending characteristics in addition to robustness, less dielectric loss, high thermal conductivity, and high transition temperature to the antenna designs.

A variety of polymer substrate materials for the design of flexible antennas have been documented in the literature, including liquid crystal polymer (LCP) [73], [74] , polypyrrole (PPY) [75], [76], thermoplastic semi-crystalline polymers like polyethylene terephthalate (PET) [10, 77, 78] and polyethylene naphthalate (PEN) [79–81] which provides very good conformal, mechanical, electrical and resistant to moisture absorption properties, thermoplastic non-crystalline polymers like polycarbonate (PC) [82] and polyethersulfone (PES) [83], high transition temperature, Tg polymers like polyimide (PI) [30, 84–86] which becomes very popular in recent years. When the flexible antenna is designed for wearable applications like in health monitoring systems etc. it should possess some essential characteristics such as stable and high performance under different conformnal and environmental conditions, robustness and high mechanical strength, transparent and last but not the least it should not affect the health of the users (low SAR). Wearable antennas built on fabric substrates may meet some of the requirements, but limiting their visibility and shielding against changing external conditions is practically difficult. That is why polymer-based antennas are becoming increasingly popular.

The polydimethylsiloxane (PDMS) used in this research (its development and characterization are detailed in Chapters 3) is an emerging silicone polymer substrate with all of the desirable properties such as transparency, flexibility (with

Young's modulus <3 MPa), water resistance, thermal stability, isotropy, and homogeneity that confirm its suitability as a potential substrate for flexible wearable antennas [87–89]. The substrate selection is one of the critical steps in antenna designing as antenna properties are directly affected by its substrate's dielectric characteristics. Therefore, the proper characterization of the dielectric properties of the substrate is required. It has been observed from the literature (Table 2.3) that the authors have applied quite different values of the dielectric parameters (dielectric constants ϵ_r and loss tangent $\tan\delta_{\epsilon_r}$) of polymer substrates like PDMS. Therefore, in Chapter 3, the various experimental characterization methods for the characterization of PDMS and comparable polymer substrates are proposed. The issues of polymers for their employment as a substrate in flexible antennas are also highlighted.

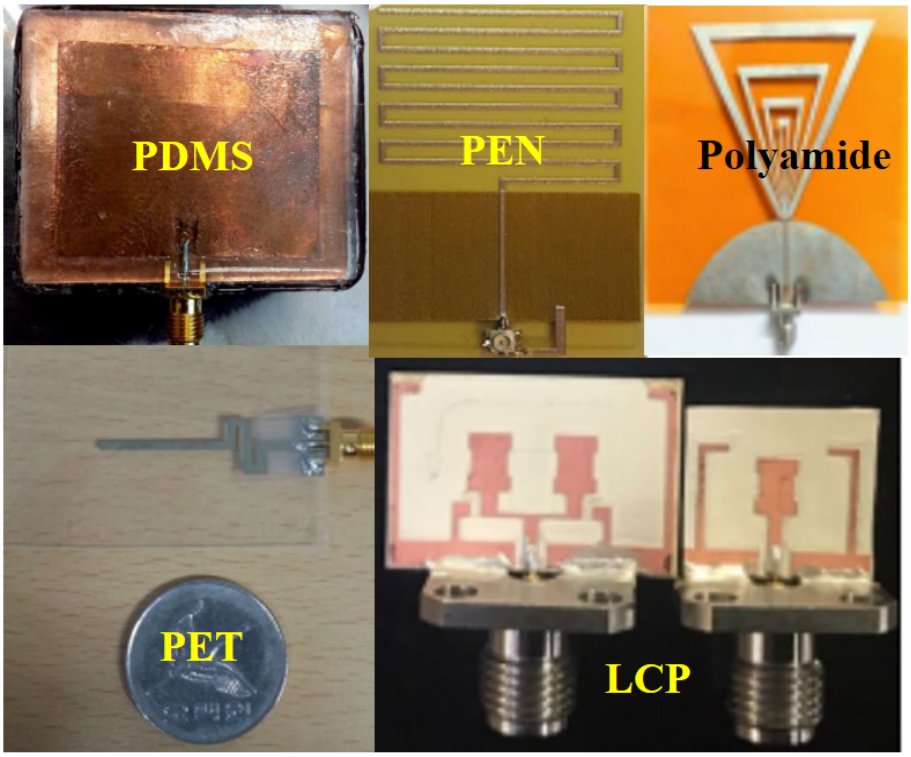

FIGURE 2.4: Examples of Polymer Substrate based Flexible Antennas [88], [90], [80], [91], [92]

TABLE 2.3: Different Polymer substrates for Flexible Antennas

Substrate	**Dielectric Properties** ($\epsilon_r / \tan\delta_{\epsilon_r}$)	**Antenna type**	**Frequency band/Applications**	**Ref.**
PDMS	2.8/0.002	Circular Patch Antenna	2.45/5.8 GHz, ISM band	[87]
	2.8/0.002	Circular Patch Antenna	2.45/5.8 GHz, ISM band	[88]
	3/0.001	Monopole Slotted Antenna	3.43-11.1 GHz	[89]
	2.67/0.001	Microstrip Patch Antenna	3-4 GHz, Conformal Applications	[93]
PET	3/0.008	Microstrip Patch Antenna	2.35 GHz, BAN and IoT Applications	[94]
	2.8/0.003	Monopole Antenna	1.8 GHz, Wearable Applications	[90]
	3.2/0.022	Bowtie shaped slot antenna	2.1-4.5 GHz, WLAN and WiMAX Applications	[95]
	3.2/0.022	Slotted Disc Monopole Antenna	2.45 GHz, ISM Band	[96]
PEN	2.9/0.005	Microstrip Patch Antenna	Sub-6GHz, 5G Applications	[97]
	2.9/0.005	Meander Antenna	800 MHz, UHF Applications	[80]
	2.9/0.005	PIFA Antenna	3.81/6.22 GHz, 5G Applications	[79]
Polyamide	2.8/0.002	PIFA Antenna	5.18–5.32 GHz, WLAN Applications	[98]
	3.5/0.0027	MIMO Antenna	2.39- 5.86 GHz, WLAN and applications	[99]
	3.5/0.002	Planar Monopole	1.2-3.4 GHz, Wearable Applications	[91]
	3.5/0.003	Monopole Antenna	2.5/5.2 GHz, WLAN applications	[100]
	4.3/0.004	Monopole Antenna	UWB and Body centric Wireless Communication	[101]
	4.3/0.004	Flower Shaped Antenna	3.5 GHz, WiMAX Applications	[102]
Crystal Polymer (LCP)	2.9/0.0025	Tapered Patch Antenna	Ka-band (26.5-40 GHz), 5G Applications	[92]
	2.9/0.0025	Circularly Polarized Antenna	3.5/5.8/5.9 GHz, WiMAX/WLAN/Vehicular Comm. Band Applications	[103]
	2.9/0.0025	Tuning Fork Shaped Patch Antenna	20.7-36 GHz, 5G Applications	[104]

C. Paper Substrates

In recent years, the utilization of paper as a substrate for the design of flexible antennas has increased tremendously with the advancements in print technology. The word 'Paper' is derived from the Latin word 'papyrus', which is a Cyeprus papyrus plant; it is an organic material that, because of its mass manufacture, is readily available at a low cost. Paper comes in various densities, coatings, thicknesses, and textures. Instead of standard metal etching procedures, paper can be used with quick printing processes. Because of the ongoing concern about environmental issues, using these paper-based antennas, which are environmentally benign, is a significant step toward the development of 'green' electronic products. Paper is a suitable candidate as substrates for different latest RF devices, such as microwave filters, RFID tags, and wearable/flexible antennas, due to their lightweight, low profile structures and minimal thickness.

The paper can be used for quick printing processes with the suitable coating like calcium carbonate or Kaolin, which can be applied either on one side or both sides to make the surface water resistant and increase its suitability for high-resolution halftone screens. Both uncoated and coated paper's surfaces can be polished by the calendaring process. The coated papers are available in various finishes, including matte, semi-matte and gloss. Glossy paper is often preferred for printing images as it produces the highest optical density.

Instead of using the classic metal etching procedures, direct-write methodologies can be applied on paper substrates. Electronics circuits can be printed on these paper substrates using different quick printing processes like inkjet printing using specific printers like material printer by Dimatic^{TM}, *n*Scrypt system by *n*Scrypt^{TM}, and the Maskless Mesoscale Material Deposition (M^{3}D) system by Optomec^{TM}. The Flexible antennas, RFIDs, and sensors can all be easily incorporated in or on paper as a result of this [105]. Like any other substrate, the dielectric characterization of paper before using it as a substrate for different RF applications is important. It can be characterized by the proposed methods in chapter-3 (future objectives), various other methods like parallel-plate resonators, cavity resonators have also been applied by other researchers for its dielectric characterization [106].

The flexible antennas designed using paper substrates exhibit good efficiency

(>80-85%) due to their low profile structure and thin width. The initial research using paper as a substrate for the design of flexible antennas was related to RFIDs like in [104] the authors have proposed a U-shaped dipole passive RFID antenna. The same design is extended to design a paper-based wireless module, then this U-shaped was converted to S-shaped in [107]. The first antenna using paper substrate radiating above 1 GHz was proposed in [108–110] for Wi-Fi applications having a PIFA (planar inverted F antenna) structure. The antenna was fabricated using M^3D technology for 2.4 GHz and it was observed that the antenna was more than 82% efficient with good SAR characteristics. In [111], a double-slotted Ultra-wideband antenna was proposed for Wi-Fi and WLAN applications at 5.2 and 5.7 GHz. This antenna was fabricated using nScrtpt^{TM} printing technology using Dupont^{TM} ink. Since then, continuous progress in the fabrication of paper substrate-based antennas is going on with the advancements in printing technology. Some of these antennas with different printing methods are summarized in Table 2.4.

TABLE 2.4: Different Paper substrate-based Flexible Antennas

Substrate	**Dielectric Properties** ($\epsilon_r/\tan\delta_{\epsilon_r}$)	**Antenna type**	**Frequency band/Applications**	**Fabrication Technology**	**Ref.**
Organic paper	3.4/0.065	Inverted F Antenna	2.45 GHz, WLAN applications	Direct write (M3D) technology	[108]
Organic Paper	3.28/0.061	RFID antenna	0.71, 1.44 GHz, UHF applications	Inkjet printing technology	[105]
Organic Paper	3.4/0.06	Planar antenna	4.5 GHz, Ammonia Gas Sensor	Inkjet printing technology	[112]
Glossy paper	4.01/0.07	Z-shaped monopole antenna	1.57 GHz, RFID Applications	Inkjet printing technology	[113]
Glossy paper	4.01/0.05	Folded Strip monopole antenna	2.48, 6.2 GHz, IoT Applications	Inkjet printing technology	[114]
Commercial paper	3.3/0.06	Vivaldi antenna	UWB applications	Inkjet printing technology	[115]
Organic paper	3.4/0.06	Meandered line dipole antenna	1 GHz, RFID applications	Screen printing using grapheme nanoflake ink	[116]

2.3 Fabrication Methods for Flexible Antennas

The fabrication method utilized to develop the flexible antennas also governs its performance, which varies depending on the substrate and antenna design. This section presents the commonly used fabrication techniques available for flexible antennas.

2.3.1 Chemical Etching

The method of corrosively etching away the undesirable area to obtain the desired metallic patterns is the chemical etching process, which is often accompanied by photolithography, as shown in Fig.2.5. This technology first arose in the 1960s with the rise of the Printed Circuit Board (PCB) sector. It has since grown in popularity because of its ability to make high-resolution patterns with fine details. The etching process is carried out by applying certain chemicals known as photoresists. Photoresists are the organic polymers that change their chemical properties when exposed to ultra-violet light.

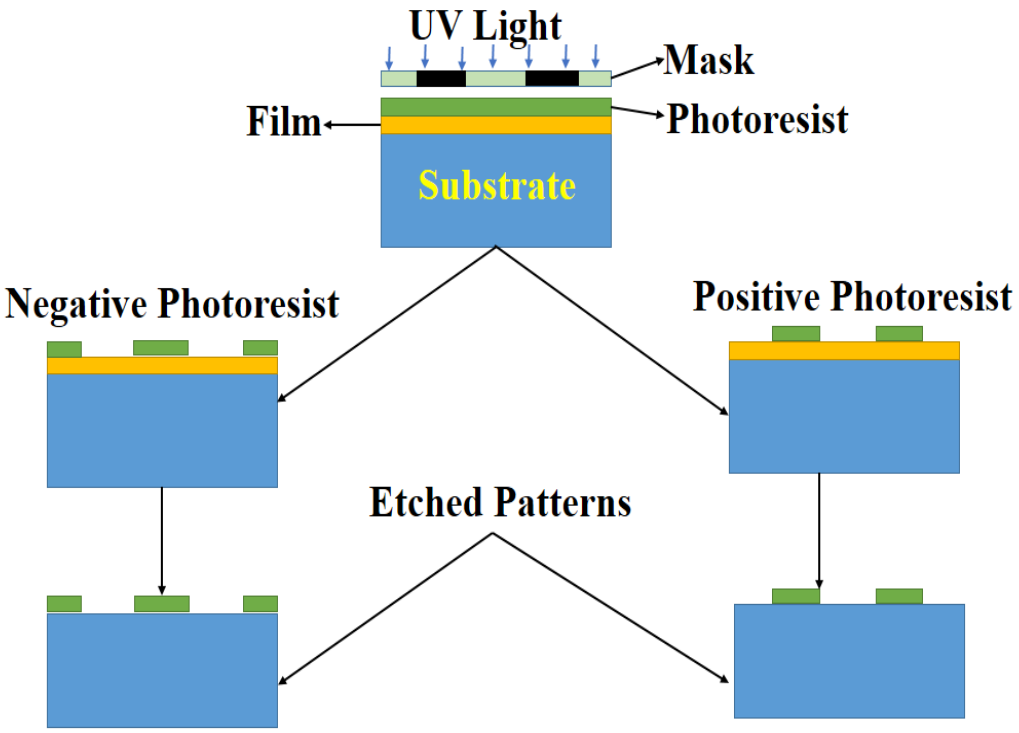

FIGURE 2.5: Chemical Etching Process

Positive photoresists are preferred in this procedure over negative photoresists due to the better resolution of the patterns. Although chemical etching is a standard process for producing flexible/wearable antennas, it has a limited throughput and requires hazardous chemicals, which have significant environmental consequences [117–119].

2.3.2 Inkjet Printing

Inkjet printing technology has emerged as an alternative to the conventional printing method to develop flexible antennas [120–123]. This is a direct write method in which the pattern is directly transferred on the substrate using conductive inks like silver nanoparticle ink, graphene nano flake inks, other organic metal inks, etc. The viscosity, surface tension, and particle size of the ink significantly impact printing quality. In contrast to the chemical etching approach described above, which involves removing the undesirable conductive component from the substrate surface, inkjet printing involves depositing a controlled quantity of ink droplets from the nozzle to a specific location. As a result, no waste is produced, and chemical compounds are removed, resulting in a cost-effective, quick, and environmentally friendly solution. The inkjet printing setup and method are shown in Fig.2.6.

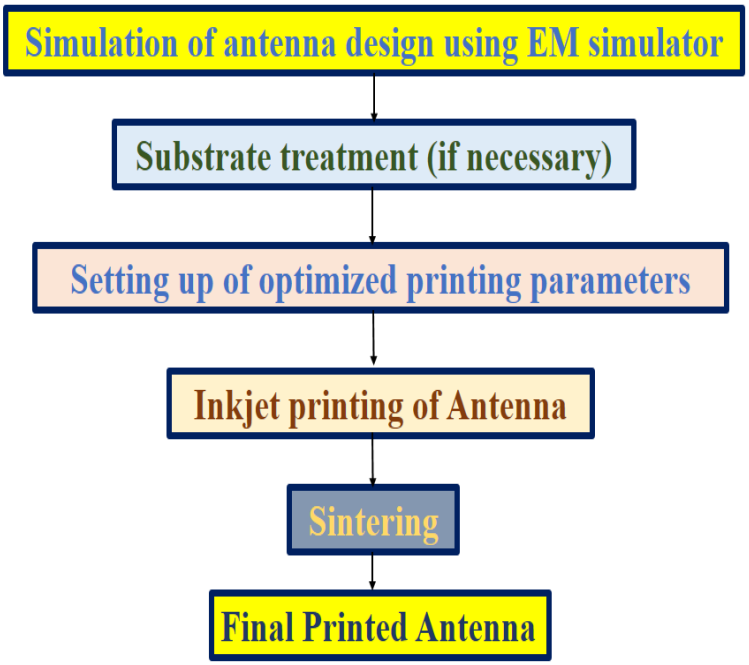

(a)

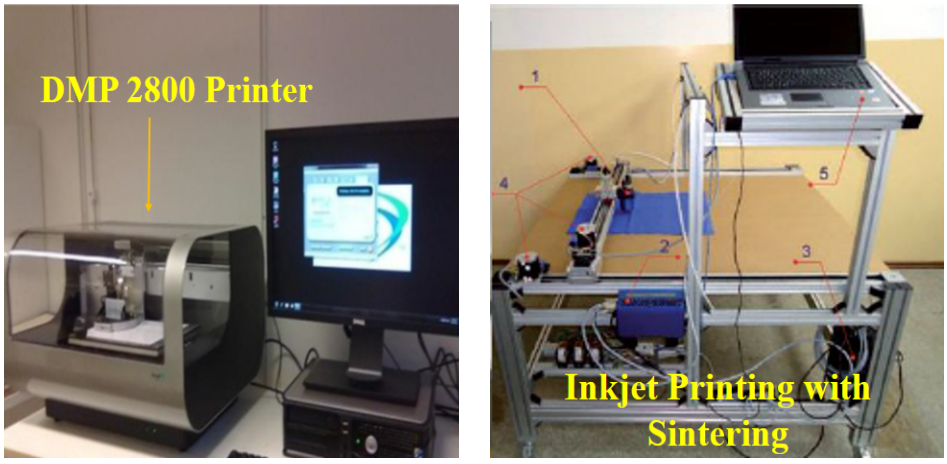

(b) (c)

FIGURE 2.6: Inkjet Printing process, (a) Printing steps, (b) Commercial DMP 2800 Dimatrix printer, and (c) Inkjet printing setup with sintering process [124].

The inkjet printing process is categorized as (i) Continuous printing and (ii) Drop on Demand (DoD) printing. In DoD, the print heads use a piezo or thermoelement to impart pressure pulses to ink, pushing a drop from a nozzle when needed. With Pico-litre volume cartridges, new generation printers provide precise printing. The jetting waveform, the nozzle's jetting voltage, the jetting frequency, the cartridge temperature, the platen temperature for the substrate, and the pattern resolution affect printing quality [125–127]. Sintering is required once the antenna design has been printed to remove the solvent and capping agent and achieve electrical conductivity.

2.3.3 Screen Printing

The screen printing process is another potential option for fabricating flexible antennas [56, 128–131]. This is a quick and straightforward process for manufacturing a low cost antenna. The screen used in this method is woven with a mesh of fabric threads having different thicknesses and densities. The non-printable regions of the screen are blocked using a stencil or emulsion, but the print areas are left open. A squeeze blade is driven down to create a printed pattern, forcing the screen to contact the substrate. Ink ejects through the exposed screen portions on the

substrate, forming the desired pattern. Like inkjet printing, this process of fabricating the flexible antennas is an additive process rather than a subtractive one like chemical etching, so it's less expensive and better for the environment. Despite its many advantages, it has significant drawbacks, such as resolution being dependent on substrate surface quality, limited layer control, and no thickness control for the conductive layer. Due to these considerations, the implementation of such a technique has been limited, as the printing technology for flexible antennas needs greater precision for better performance under different operating conditions.

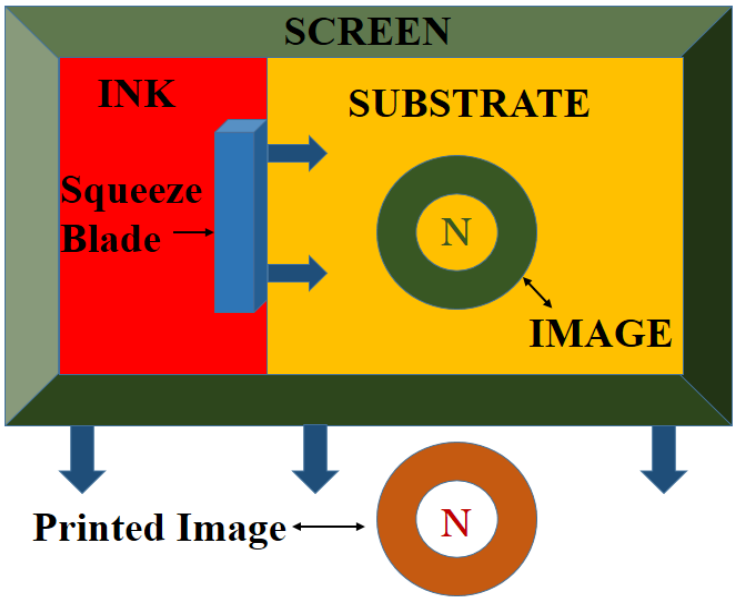

FIGURE 2.7: Screen Printing Process

2.3.4 Embroidery and Sewing

This is one of the conventional methods employed to fabricate flexible antennas. In this method, no adhesive material like copper tape or conductive ink is used on the substrate for making conductive parts. A conductive textile yarn is woven or stitched on the non-conductive textile substrate to make the flexible antenna's conducting sections [132], [133]. Additionally, using a computer-aided embroidery machine, these antennas can be directly embroidered onto the non-conductive textile fabric [134]. The flexibility and strength of the conductive threads, high accuracy of the embroidery machine, as well as the direction and density of stitching on

the fabric substrate are some of the critical factors to be considered while creating an efficient antenna design using this method [135–137].

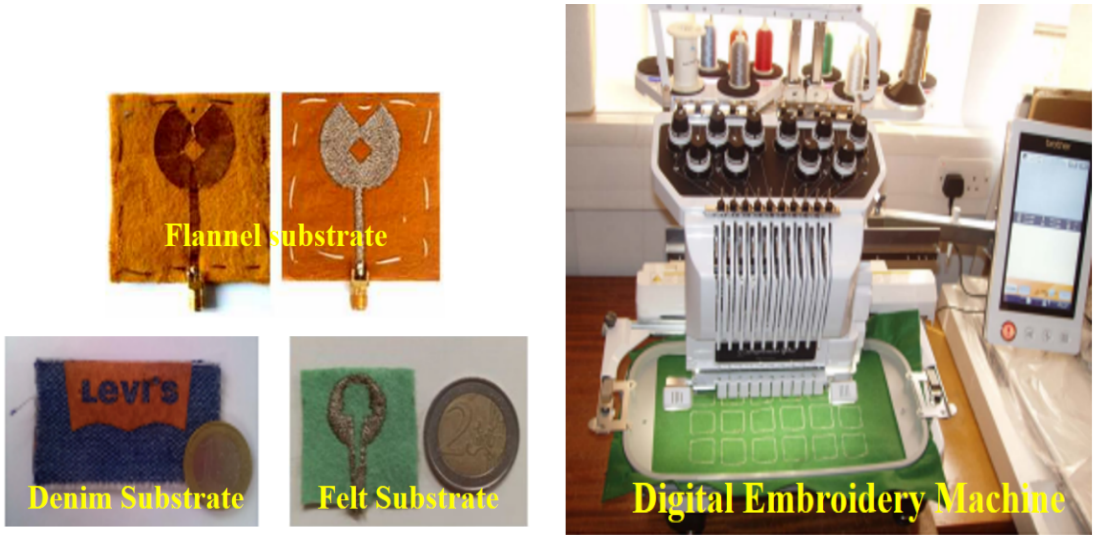

(a) (b)

FIGURE 2.8: (a) Embroidered Flexible Antennas [136], [138], [139], (b) Entrepreneur Pro PR1000e Digital Embroidery Machine [134]

2.3.5 Substrate Integrated Waveguide (SIW)

Substrate Integrated Waveguide (SIW) is recent technology for fabricating a wearable system on a single platform. This technology allows future 'System on Substrate (SoS)' systems to be realized, which are essential to building cost-effective and easy-to-fabricate high-performance mm-wave systems [140], [141]. These structures, by employing shorting vias on the cavity's sidewalls, backed by the entire ground plane, ensure the containment of electric fields inside the cavity. This improves the structure's quality factor while also boosting the isolation between the antenna and the human body for wearable applications [142–144].

The review of various fabrication methods for constructing flexible antennas is presented in Table 2.5.

TABLE 2.5: Review of different fabrication methods for flexible/wearable antennas

Methods	Antenna type	Substrate	Applications	Ref.
Chemical Etching	Tapered Antenna	Gold wire	Optical communication applications	[145]
	RFID antenna	FR4	UHF applications	[118]
	Half-wave dipole antenna	PDMS	1.53 GHz RF applications	[146]
	Circularly polarized antenna	LCP	WiMAX (3.5 GHz), WLAN (5.8 GHz), and vehicular communication band (5.9 GHz) applications	[103]
Inkjet Printing	Patch antenna	Polyester cotton	2.45 GHz ISM band applications	[120]
	Z-shaped antenna	PET	2.45 GHz ISM band applications	[121]
	Triangular antenna	Kapton Polyimide	1.2, 2.0, 2.6 and 3.4 GHz, wireless communication applications	[91]
	Microstrip antenna	Kapton Polyimide	UWB applications	[123]
	Patch antenna	Polyester cotton	2.4 GHz wearable applications	[120]
Screen Printing	E-shaped Microstrip antenna	Polyester cotton	3.3 GHz WiMAX applications	[56]
	Patch antenna	PDMS	2.45 GHz, ISM band applications	[128]
	Elliptical dipole antenna	Kapton Polyimide	2-5 GHz, wireless communication applications	[129]
	Microstrip antenna (with parasitic array)	flexible substrate from PremixGroup	77 GHz, MM-wave applications	[130]
	Microstrip antenna	Twill cotton	2.45 GHz, ISM band applications	[131]
Embroidery and Sewing	Fractal antenna	Nomex	868 MHz and 915 MHz ISM band applications	[133]
	Monopole antenna	Jean	3.03-3.76 GHz,5.48-6.24 GHz,7.10-7.40 GHz, and 7.93-8.22 GHz bands WBAN applications	[135]
	Patch antenna	Felt	UWB applications	[136]
	Patch antenna	Nylon	2.40 GHz, Wearable applications	[137]
Substrate integrated waveguide (SIW)	Leaky wave antenna with C-shaped slots	Carbon	IoT applications	[140]
	Self-triplexing antenna	Rogers 4003	3.5 GHz, 4.8 GHz, and 5.4 GHz, 5G, WiMAX, WLAN applications	[141]
	Leaky wave antenna with C-shaped slots	Rogers RT/Duroid 5870	16.7 GHz and 19.8 GHz applications	[142]
	Planar antenna	FR4	1.8 GHz, sub-6 GHz wireless	[144]

2.4 Metamaterial in Flexible Antennas

The word 'Meta' comes from Greek that means 'beyond'. Metamaterial have electromagnetic properties beyond the naturally occurring materials [147]. They are built up of periodically arranged components called unit cells of different shapes like squares or circles, holding a fixed side length [148,149]. These unit cells are set in a specific pattern, yielding resonant structures that govern their electromagnetic behaviour. The components can be arranged in a single, two, or three-dimensional configuration, and variations in metamaterial properties can be observed [150,151].

The researchers are always experimenting with new approaches and materials to improve the performance of flexible and wearable antennas. The use of metamaterial loading in flexible/wearable antennas is one of them. Different metamaterial structures, such as split-ring resonators (SRRs), can further improve the performance of flexible antennas, by miniaturizing the size, increasing bandwidth, efficiency, directivity, and improving radiation patterns [152–154]. Surface wave reduction, wave polarisation, and wave absorption are all aided by these structures. Resonant metamaterial structures, on the other hand, sometimes suffer from losses caused by conducting inclusions.

Metamaterial surfaces also become popular for reducing the specific absorption rate (SAR) of flexible/wearable antennas. These metamaterial structures may hinder the propagation of surface currents/waves within a given frequency range, so they are recommended as a ground plane to improve the antenna's performance [155–157]. Metamaterial are commonly used to shield the human body from harmful radiations by lowering the amount of energy received by the body [158]. There's no denying that they're useful in antenna design. However, there's still a lot more work to be done in this area for various reasons, including a limited selection of substrates for employing metamaterial structures in antennas. On the other hand, conducting inclusions can lead to losses in resonant metamaterial structures [159, 160].

Different flexible antennas using metamaterial loading have been reported in the literature for various applications, a short review of which is presented in Table 2.6.

TABLE 2.6: Review of metamaterial loaded flexible antennas

Antenna Type	**Substrate**	**Applications**	**Metamaterial Structure**	**Advantages of using Metamaterial**	**Ref.**
Elliptical patch antenna	Denim and Felt	UWB and WBAN- Breast Imaging applications	Elliptical and grain rice-shaped SRR	High BW, gain and directivity	[152]
Microstrip patch antenna	Cotton	2.45 GHz, wearable applications	Mushroom-type electromagnetic bandgap (EBG)	Low SAR and high efficiency	[153]
Planar monopole antenna	Viscose-wool felt	UWB applications	Rectangular- and nonagon-shaped	High BW 2.55 to 15 GHz	[154]
Patch antenna	Nickel oxide polymer-ized palm fiber	RF energy harvesting	Hilbert-shaped	High gain at 5.8 GHz- 4.56 dBi and 8 GHz- 7.38 dBi	[161]
Patch antenna	Denim	Sub-6 GHz IoT and wearable applications	Grain rice-shaped SRR	Broad BW (6.5-35 GHz), High Gain (8.85 dBi), Directivity (10 dB) and $>$ 80%efficiency	[156]
Microstrip antenna	Polymer	BAN and ISM band applications	Minkowski fractal geometry	Low SAR 0.25 W/kg and 0.33 W/kg at 403 MHz and 2.45 GHz	[157]
Patch antenna	Jean	IEEE 802.11 a and b/g/n WLAN, WiMAX 2.3 and 5.5 GHz and GSM 1800 MHz bands applications	Square SRR	High BW- 1.6 to 2.56 GHz (46%) and 4.24 to 7 GHz (49.11%)	[158]
Patch antenna	Polyamide	WBAN applications	Square SRR	High gain- 9.3 dBi and 5.37 dBi, and the radiation efficiency-48.4% and 35.7%, at 2.45 and 5.8 GHz, 70% reduction in SAR	[159]

Continued on next page

Table 2.6 – continued from previous page

Antenna Type	**Substrate**	**Applications**	**Metamaterial Structure**	**Advantages of using Metamaterial**	**Ref.**
Patch antenna	Liquid crystal polymer (LCP)	WiMAX (3.5 GHz), WLAN (5.8 GHz), Vehicular communication band (5.9 GHz) applications	Circular SRR	Compact size and circular polarization (axial ratio < 3 dB)	[103]
Patch antenna	Semi-flexible Rogers RT/duroid 5880	UWB applications	Ring shaped	High gain-8 dBi and radiation efficiency-85%	[160]

2.5 Conclusion

Flexible antenna research encompasses a wide range of engineering and scientific disciplines. Material science, mechanical engineering, electrical and electronics engineering are all involved in this intriguing and diverse field of research. Flexible antennas are one of the critical components of modern, flexible electronic devices. Flexible antennas are good contender for present and future wireless communication systems, sensing, biomedical, and other wearable applications due to their multiple advantages such as lightweight, reduced form factor, low-cost manufacture, and flexibility to suit non-planar surfaces. This chapter briefly introduces flexible antennas, covering design procedures, substrate and conducting material options, and manufacturing techniques with applications.

Chapter 3

Development and Dielectric Characterization of Polydimethylsiloxane (PDMS) Substrate

3.1 Introduction

Modern electronics, particularly microwave devices, antennas, and sensors, rely heavily on discovering and developing novel materials. Today, the outcomes of the combined efforts of research groups of physicists, chemists, technologists, mechanics and engineers are becoming more visible in their goals to create materials with new desirable properties, to mix two or more materials to get new characteristics, to provide dielectric matrices for the incorporation of diverse inclusions in order to develop engineered materials and metamaterial with naturally unexpected properties, or to develop unique materials which can replace others in specific applications.

Nowadays, many materials apart from their traditional applications can be used for different untraditional applications like; for example, textile materials can be used as flexible substrates for antennas, sensors and wearable devices [162], [163]. The use of polymer-based substrates is the most recent trend in the field. These polymers with different conductive coatings [164], [165] can also be utilized as a flexible substrate in antenna designing [166]. In this context, the present RF and antenna design approach necessitate adequate characterization of such materials in the microwave region [167], [168], which remains challenging. The proposed

research in this chapter focuses on an in-depth analysis of the dielectric characterization of Polydimethylsiloxane (PDMS) [169], a widely used silicon-based elastomer that has been used as a flexible substrate for a variety of flexible and wearable antenna applications [48, 87–89, 170]; as thin membranes [171] for mm-wave applications, as sensors [172] and microchips [173], as a hydrophobic antenna coating [174], as a dielectric matrix for the incorporation of a variety of inclusions for control of the dielectric constant or as metamaterial [175], [176], with suitable metallization [177], in microfluidic systems [178], etc. PDMS is a silicon-based organic polymer that belongs to the category of polymeric organo-silicon compounds (silicones) $(C_2H_6OSi)_n$ [179, 180].

The properties of PDMS like perfect flexibility, water resistivity, transparency, chemically inert, thermally stable, permeable to gases, easy to handle, with relatively isotropic and homogenous nature make it a very suitable candidate as a substrate for the design of flexible antennas [169]. However, it has been observed from the literature that researchers have used quite different values of the dielectric loss tangent (from 0.01 up to 0.08; 8 times) and of the dielectric constant without inclusions (from 2.32 up to 3.2; or $\sim 33\%$ scatter) of this material. Some sources claim that the dielectric characteristics of pure PDMS samples have an explicit frequency dependence [181], which is a typical property for this type of polymer. However, the results obtained may be influenced by the characterization approach used.

The dielectric constant ϵ_r values given by different researchers can be divided into three groups. For the frequency range 0.1-40 GHz [88], [170], most of the authors have applied the values of ϵ_r in the interval ∼2.7-2.8 (typically 2.71). These ϵ_r values are generally employed for the frequencies below 6 GHz [87], [48] and [176]. A prevalent case here is that the coaxial resonators [182] or open coaxial dielectric probes [48] are used to measure the dielectric constant, which is parallel to the sample surface. The authors who propose the application of PDMS in the mm-wavelength range typically apply the ϵ_r values $\sim 2.64 - 2.69$ for example, 60 GHz, 77 GHz and beyond [171]; nevertheless, ϵ_r values ~ 2.65 have also been used by authors at lower frequencies [170], [172], and planar measurement (for example, microstrip T-resonator) methods are used to obtain these values.

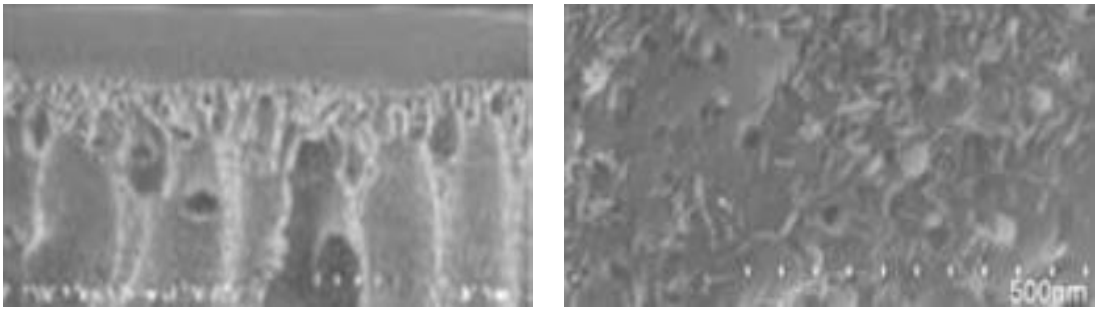

(a) (b)

FIGURE 3.1: SEM images of pure PDMS membranes: (a) cross-section view, (b) surface view.

Quite a few researchers have utilized extremely low values of $\epsilon_r \sim 2.3 - 2.4$ [175], these are obtained by Impedance (capacitance) measurement methods at frequencies below 1 MHz and represent the perpendicular dielectric constant of PDMS samples. Flexible substrates like PDMS and related polymers cannot be characterized by the reference planar IPC TM-650 2.5.5.5 test procedures [183], which are used for commercial microwave substrates due to the applied controlled pressure during the testing.

The wide applicability of this organic material as a substrate, however, does not correlate to the observed scattering of the utilized dielectric parameters by RF engineers; this fact is undesirable and may reduce the design accuracy of wearable/flexible antennas on this material to some extent. This reasoned that the PDMS might have small but measurable uniaxial anisotropy, which is different dielectric characteristics in perpendicular and parallel directions to the sample surface and weak frequency dependence, some clues of this behavior are also present in the literature. SEM images of pure PDMS samples taken with scanning electron microscopes reveal an expressed micro-porous structure [179], [180] (Fig. 3.1), which could be a source of the putative anisotropy. Similar weak uniaxial anisotropy has been seen in woven and knitted textile fabrics used for wearable antennas [184], and its genesis is linked to the oriented mixing of threads and air filling.

The proposed chapter mainly focuses on the individual investigation of the perpendicular and parallel dielectric parameters of the developed PDMS samples as described in section 3.2 by the different proposed methods within the frequency

interval of 40 GHz and verifying their frequency dependencies and possible uniaxial anisotropy. In section 3.3, two proposed experimental methods used to characterize PDMS samples are described in detail. In section 3.4, all the obtained results by proposed methods are discussed, and frequency dependencies of the dielectric parameters and anisotropy are also investigated. The temperature dependences of dielectric anisotropy and equivalent dielectric parameters of PDMS samples are measured and described for the first time in the same section, in the temperature range of –40°C to +70°C. Finally, the acquired results are summarized in the conclusion section, and their usefulness in the wearable/flexible antennas using PDMS substrates has been assessed.

3.2 Preparation of PDMS Samples for Characterization

As shown in Fig. 3.2, the following are the steps involved in the PDMS fabrication process: initially, the silicone elastomer base and silicone elastomer curing agent are mixed thoroughly in a 10:1 ratio. The PDMS solution is then stored in desiccators to eliminate air bubbles which forms during the mixing of the solution. After that, the solution is placed onto a silicon wafer and allowed to settle for 15 minutes before being cured at 70°C for around an hour. Finally, the transparent PDMS layer on the silicon wafer is peeled away. The obtained PDMS sample is now ready for characterization testing.

Different PDMS samples in the shape of disks having diameter ∼47 mm with thickness ∼0.65-0.80 mm are fabricated using the above procedure in order to perform the characterization of dielectric properties. Using specific cutters, smaller discs of diameters 30, 18.1, 15, 10 and 8 mm with more consistent thicknesses are

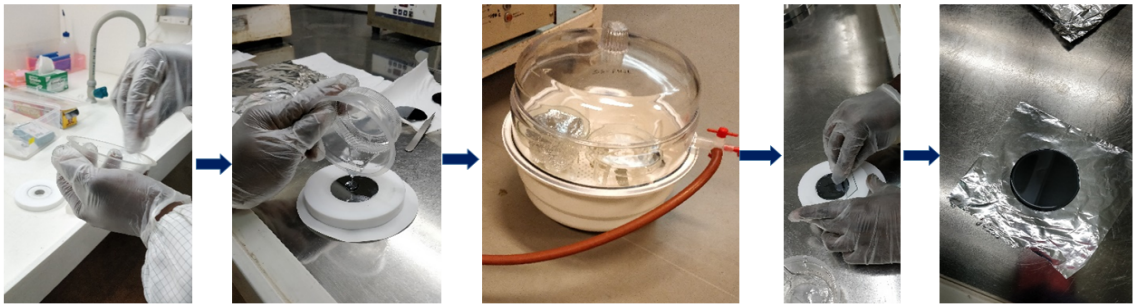

FIGURE 3.2: Fabrication of PDMS (at BITS-Pilani, EEE Laboratory).

prepared from big PDMS samples, as shown in Fig. 3.3(a). These samples are utilized in tests spanning the frequency range of 0.01 to 40 GHz. Samples from the other organic materials with isotropic and near-to-isotropic properties like Silicone elastomers, Polytetrafluoroethylene (PTFE), Cyclo Olefin Polymer (COP) (Fig. 3.3 (b), (c), (d)) and Polycarbonate (PC) are also measured in order to perform a comparison and verifying the measurement procedures.

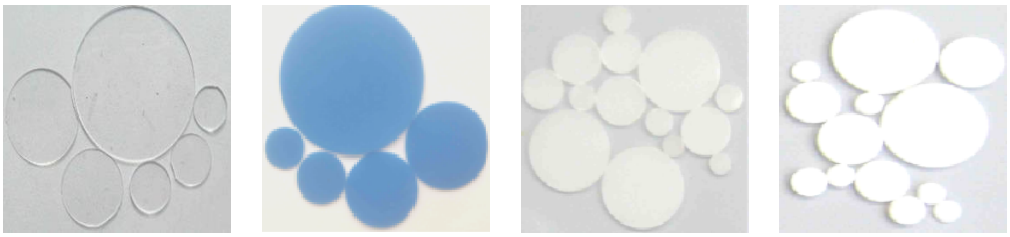

(a) (b) (c) (d)

FIGURE 3.3: PDMS and other polymer samples: (a) PDMS disks of diameters 30, 18.1, 15, 10 and 8 mm; (b) disks from commercial Silicone elastomer; (c) disks from COP (Cyclo Olefin Polymer) delivered as a trademark ZEONEX® RS420; (d) PTFE (Polytetrafluoroethylene) disks

3.3 Characterization Methods

There is no universal method present in the literature for the accurate and reliable evaluation of the dielectric properties of the polymers and reinforced substrates in various directions to their surface [185]. In order to extract the dielectric parameters parallel to the surface of the substrate, a set of classical methods like Courtney's method, Kent's evanescent-mode tester, free-space method, split-post dielectric resonator, NIST's mode-filtered resonator, coaxial- probe method can be employed [186–191]. On the other hand, different methods like the reference IPC TM-650 2.5.5.5 test methods [183], re-entrant cavities, TM-mode resonance cavities, balanced TM-mode resonators, substrate-integrated waveguides (SIW), etc. can be used to measure the dielectric parameters in perpendicular direction [182, 192–194]. When these methods are applied to the anisotropic substrates, they will give different results; moreover, not all of them are suitable for polymer substrates.

When anisotropic substrates are substituted with isotropic substrates, the third set of methods based on planar transmission lines or resonators delivers the equivalent parameters of the anisotropic substrates [195]. Only few approaches allow for direct measurements of substrate uniaxial or biaxial anisotropy. To do this, resonance or propagation modes with mutually perpendicular electric field directions must be used to extract dielectric characteristics in different directions from a single sample. Triple-mode waveguide perturbation method, suitable for characterization of liquid-crystal substrates [196], determination of low-loss crystal anisotropy by whispering-gallery resonators [197], anisotropy characterization of all-dielectric metamaterials [198], coupled microstrip resonator method for characterization of the uniaxial anisotropy of reinforced substrates [199], etc. are some of the selected examples present in the literature.

In this chapter, two experimental methods are proposed to characterize the selected polymer-based substrate PDMS. The first method involves the resonance measurements by the two-resonator method, which utilizes two types of TE and TM mode cylindrical resonators to measure the dielectric parameters of non-metalized PDMS samples in both perpendicular (ϵ_{perp} and $\tan\delta_{\epsilon_{perp}}$) and parallel ($\epsilon_{par}$ and $\tan\delta_{\epsilon_{par}}$) directions to the surface using the single sample. This method can be successfully applied for the uniaxial anisotropy characterization of a variety of artificial materials: reinforced and textile substrates, antenna radomes, nano- and gradient absorbers, thin films, 3-D printed samples, plant tissues, all-dielectric metamaterials, etc. [200].

The origin of the anisotropy of these materials could be different; however, the determination of this property in each case gives valued information for the structure, content and applicability of the considered materials. The second method is based on implementing the different planar structures like resonators and transmission lines where the PDMS sample under test (SUT) has been integrated. This method cannot separate the parallel and perpendicular dielectric parameters, but it allows determination of the sample's equivalent dielectric parameters (ϵ_{eq} and $\tan\delta_{\epsilon_{eq}}$), considered an isotropic material.

3.3.1 Resonance Measurements: Two Resonator Method

The notion of the presented method is illustrated in Fig. 3.4(a), where the PDMS sample is sequentially placed in two resonators R1 and R2, for characterization. Due to the exciting TE_{0mn} modes in resonators of type R1 and TM_{0mn} modes in resonators of type R2, the pure parallel and perpendicular dielectric constant can be measured. The perpendicular and parallel values could coincide to some degree for this present case of pure isotropic or near-to-isotropic material. In the resonators of type R1 and R2, the azimuthally symmetrical modes TE_{011} and TM_{010} are used, respectively. Additionally, selected higher-order azimuthally symmetrical modes have been used for the measurements (e.g., mode TE_{021} in resonators R11 and R12, and mode TM_{020} in resonators R21 and R22), ensuring acceptable accuracy.

The resonance curves of certain high-order TE modes can sometimes coincide with the resonance curves of other high-order TM modes and vice versa. Some resonances become wide two-peak curves due to this effect, making determining the dielectric loss tangent extremely difficult and erroneous (and even impossible). Hence, only the resonance curves that can be measured are chosen. To ensure the finest possible conditions for the excited TE or TM modes and maximum separation between these modes, the sample is placed in the middle in resonator R1 and at the bottom in R2 (for example, the height of the resonator R1 must be equal to its diameter ($H_1 \sim D_1$), and the height of the resonator R2 must be less than its diameter ($H_2 < D_2$)) with the orientation of the coupling probes so that only TE modes in R1 and TM modes in R2 are excited.

Fig. 3.5 shows a family of eight silver-plated resonators (4 each resonator of type R1 and R2); these resonators ensure the reliable and accurate measurements of PDMS anisotropy within the frequency range of 6-38 GHz by a vector network analyzer of 0.01-40 GHz. The resonance measurement setup for evaluating the dielectric characteristics of PDMS substrate samples is illustrated in Fig. 3.6.

The steps involved in the experiment are as follows: To obtain the equivalent resonator parameters: equivalent diameter D_{eq} (mm) and equivalent wall conductivity σ_{eq}(S/m), the empty resonators are measured initially (resonance frequency and unloaded quality (Q) factors of the selected modes).

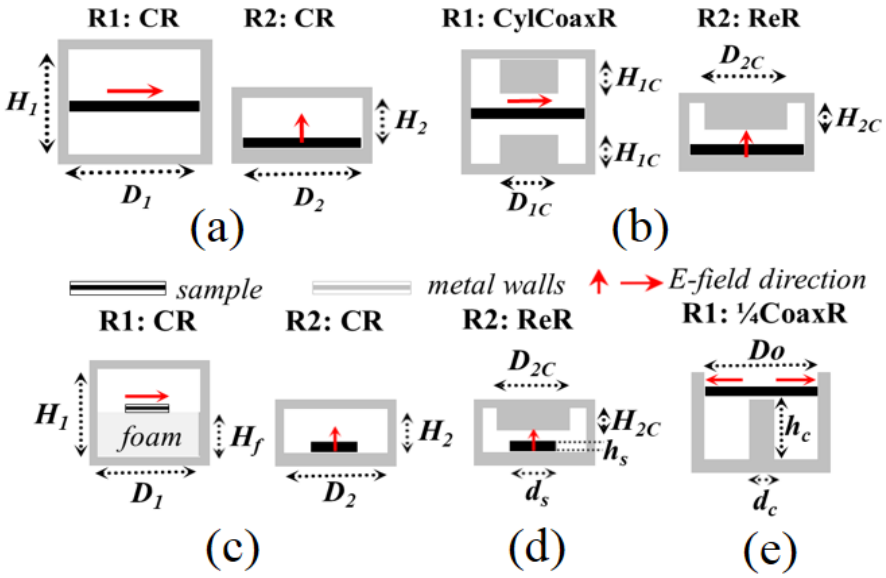

FIGURE 3.4: Resonators for measurement of parallel (R1) and perpendicular (R2) dielectric parameters of disk samples: (a) cylindrical TE- (R1) and TM- mode (R2) resonators; (b) cylindrical resonators with coaxial rods: R1 (CylCoax; TE-mode resonator with pair of tunable coaxial cylindrical flanges) and R2 (ReR; TM-mode tunable re-entrant resonator); (c) cylindrical TE- and TM-mode resonators with samples of smaller diameters ($d_S < D_{1,2}$); (d) re- entrant resonator with smaller samples ($d_S < D_2$); (e) quarter wave-length resonator. Legend: $D_{1,2}, H_{1,2}$ – resonators diameters and heights; $D_{1,2C}, H_{1,2C}$ – coaxial rod (piston) diameters and heights; d_C, h_C – coaxial core diameter and length; d_S, h_S – disk sample diameter and height (thickness); D_0 – coaxial outer diameter.

The resonators with samples are then measured again and the corresponding new resonance frequencies and unloaded Q factors for the same modes (well-identified) are calculated. The appropriate extraction procedure is applied to evaluate parallel values, ϵ_{par} and $\tan\delta_{\epsilon_{par}}$ in resonators R1 and perpendicular values,ϵ_{per} and $\tan\delta_{\epsilon_{perp}}$ in R2.

The sample diameter d_S can be chosen in two ways: to match the resonator diameters $D_{1,2}$ (Fig. 3.4(a)) or to be smaller ($d_S < D_{1,2}$; Fig. 3.4(c)). Low-permittivity foam support must be employed in the second scenario, whose dielectric parameters must be measured and taken into account. If $d_S \sim D_{1,2}$, the analytical model proposed in [201,202] can accurately extract the dielectric parameters. Finally, the acquired data enable numerical determination of the dielectric constant and loss tangent in parallel (ϵ_{par} and $\tan\delta_{\epsilon_{par}}$) and perpendicular ($\epsilon_{perp}$

and $\tan\delta_{\epsilon_{perp}}$) directions in resonators R1 and R2, respectively. In the Ku band, the evaluated measurement uncertainty is relatively small: 3-5 % for ϵ_{perp}, 1-1.5% for ϵ_{par}, 5-7 % for $\tan\delta_{\epsilon_{par}}$ and 10-15% for $\tan\delta_{\epsilon_{perp}}$ in the case of 0.5-1.5 mm thick substrates with dielectric constants $\sim$ 2-5.

The uncertainty in determining the sample thickness and the method chosen contribute to measurement inaccuracy; in the wide range of substrate anisotropy and thickness, the measuring resonators determine the corresponding "pure" parameters (perpendicular ones in R2 and parallel ones in R1) with selective uncertainty less than ±3-0.4% for the dielectric constant and less than ±5-1.0% for the dielectric loss tangent due to the E-fields orientation [202]. This analytical method cannot be applied if the sample diameter is smaller than the resonator diameter. Instead, appropriate 3-D simulations can be applied (as illustrated in Figs. 3.7-3.9; for this present case, ANSYS® HFSS simulations are used), and the dielectric parameters of the samples can be fine-tuned throughout the simulations until the simulated resonance frequency and unloaded Q factor match the measured values [203] (usually 1-2 % coincidence is enough).

FIGURE 3.5: Family of optimized silver-plated measuring resonators: (a) TE-mode resonators R1 (D_1 = 30, 18.1, 15, 10 mm) and (b) TM-mode resonators R2 (D_2 = 30, 18.1,10, 8 mm) which cover the frequency range of 6- 38 GHz (see Table 3.1).

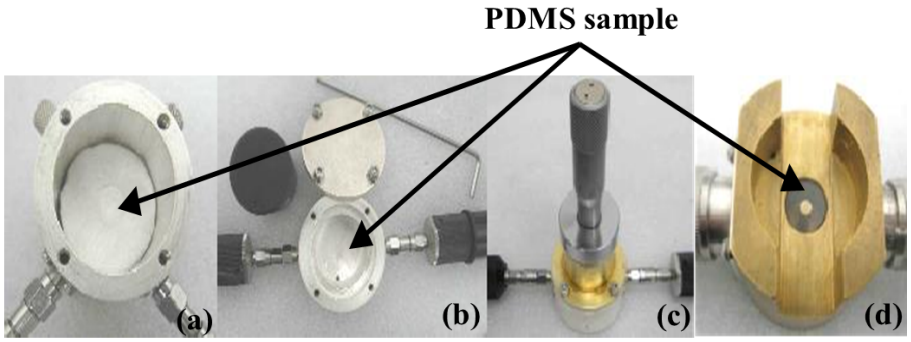

FIGURE 3.6: PDMS samples in measuring resonators: (a) sample with $d_S < D_1$ in resonator R11 (Fig. 3.4(c)); (b) sample with $d_S \sim D_2$ in resonator R22 (Fig. 3.4(a)); (c) ReR on the base of resonators R21 (Fig. 3.4(d)); (d) quarter-wavelength coaxial resonator with PDMS sample d_S=10 mm (1/4CoaxR in Fig 3.4(e)).

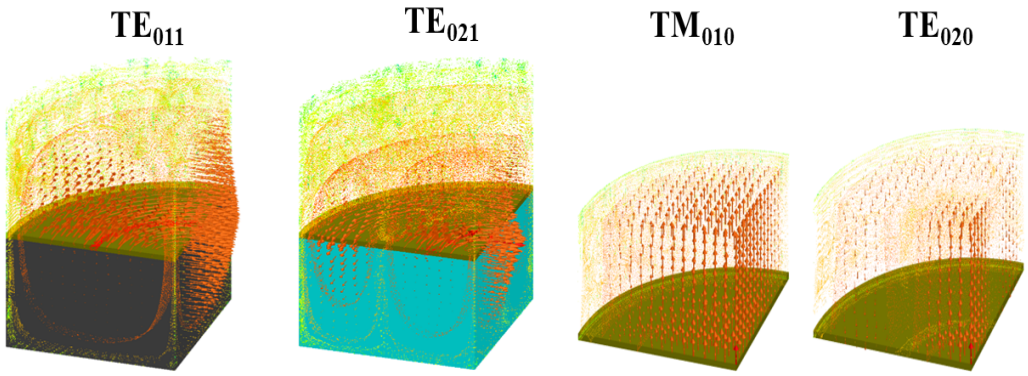

FIGURE 3.7: E-field distributions in resonator R11 (modes TE_{011} and TE_{021}) and resonator R21 (modes TM_{010} and TM_{020}), in which the sample diameter coincides with the resonator diameter (30 mm).

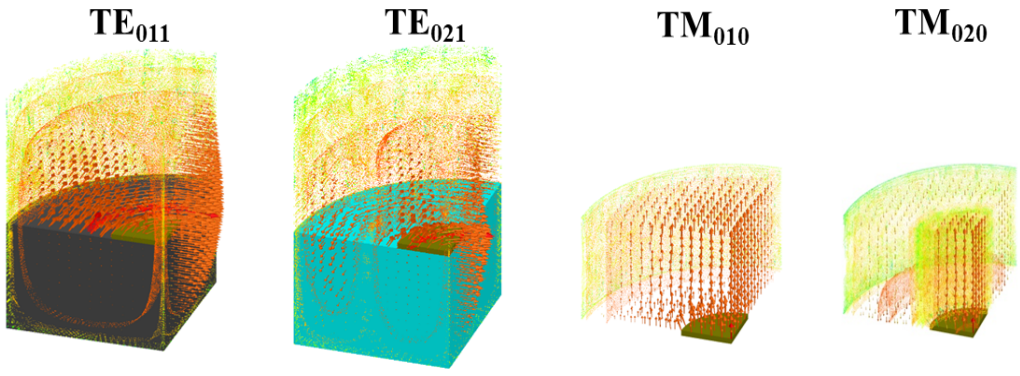

FIGURE 3.8: E-field distributions in resonator R11 (modes TE_{011} and TE_{021}) and resonator R21 (modes TM_{010} and TM_{020}), in which the sample diameter is smaller than the resonator diameter (30 mm).

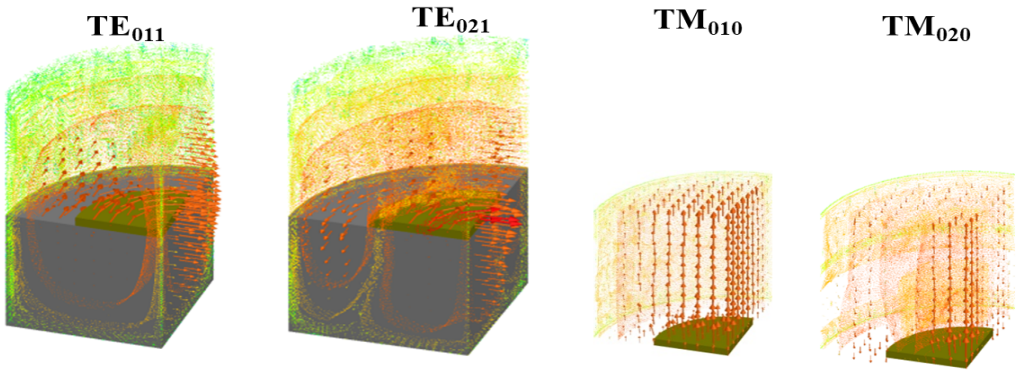

FIGURE 3.9: E-field distributions in resonator R12 (modes TE_{011} and TE_{021}) and resonator R22 (modes TM_{010} and TM_{020}), in which sample diameter is smaller than the resonator diameter (18.1 mm).

3.3.2 Planar Structure Measurements: Linear and Ring Microstrip Resonator Method

Planar resonance methods are very popular for the characterization of the dielectric properties of commercial reinforced substrates because they provide appropriate metallization that enables the use of various planar resonance structures, such as the linear resonator (LR) or the ring resonator (RR). They make it possible to extract the equivalent dielectric parameters of anisotropic materials in microstrip-line configurations (MSL) [195], often known as "design values," which are typically provided by substrate manufacturers. The inescapable influence of the metallization – its thickness and roughness – is an issue with these methods.

In order to characterize PDMS samples (or other similar substrates) without metallization, these planar methods cannot be applied directly with reliable accuracy. Therefore, two different strategies are followed in this chapter to use the considered planar methods. Firstly, different hand-made LR and RR resonators are made on the raw PDMS sample with a diameter of 46 mm, as shown in Fig. 3.10. Coaxial probes with magnetic loops are used to elicit the resonances. To avoid parasitic resonances, the probes have been tuned for coupling below -40 dB, and the resonator has been side-stepped with absorbers. Only 3-4 quasi-TEM resonances in the frequency range 2-10 GHz have been measured, and the values of effective dielectric constant ϵ_{eff} and equivalent dielectric constant ϵ_{eq} are calculated using standard transmission line (TRL) calculator [185]. The other strategy for planar

measurements is to cover raw PDMS samples of ring resonators photolithographically printed as a layout on commercial reinforced substrates having good resonance performances over a wide frequency range. The E-field distribution in the sample above the RR structure follows the E-field distribution into the substrate, following the method for characterization of reinforced substrates as described in [204]. As a result, this method enables the accurate estimation of the equivalent parameters of the covering substrate. However, as there are no credible analytical models for extracting the covering sample parameters, appropriate 3D simulations using ANSYS® HFSS in both "driven solution" and "eigenmode solution" options are applied.

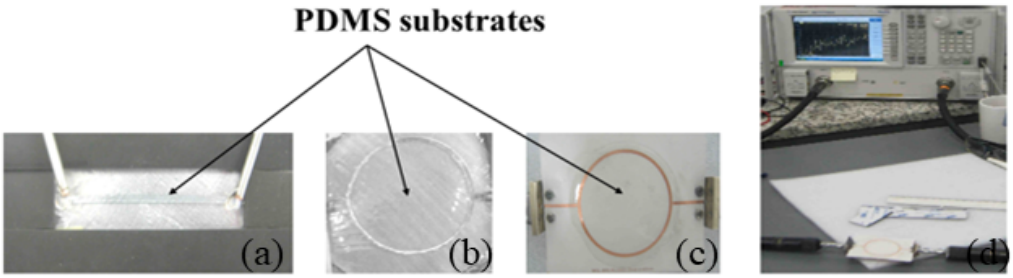

FIGURE 3.10: Planar microstrip resonators: hand-made linear (LR) (a) and ring (RR) (b) resonators on PDMS substrate; the metal layout is made by a high-quality self-adhesive aluminium foil; (c) PDMS sample covers a ring resonator on commercial Ro3003 substrate; (d) measurement scheme by VNA in the frequency range 0.01-40 GHz.

3.4 Results and Discussion

3.4.1 Resonance Measurements by TE and TM mode cylindrical resonators

In this method, the resonance characteristics of empty resonators are measured, and the crucial equivalent parameters: equivalent resonator diameter $D_{eq1,2}$ (in mm), and equivalent wall conductivity $\sigma_{eq1,2}$ (in S/m), are investigated. Then these parameters are utilized for the extraction of the dielectric parameters of the samples. Table 3.1 illustrates the typical parameters of the used measuring resonators– dimensions, measured resonance parameters, and determined equivalent diameters and wall conductivity. The last two parameters have daily variations

due to the actual room temperature, tuning screws' position, technological holes, surface roughness, eccentricity and excited mode. The resonators of type R1 ensure total frequency interval 11-39 GHz and unloaded Q factors 4700-17000 by the exited dominant symmetrical TE_{011} modes, while the R2 resonators – frequency interval 6-29 GHz and unloaded Q factors 4700-6500 by the exited dominant symmetrical TM_{010} modes. Because of these high Q factors, the dielectric loss tangent of such low-loss materials like PTFE and similar dielectrics can be determined with acceptable accuracy. Even the higher-order modes (TE_{021} and TE_{031} in R1 resonators and TM_{020} and TM_{030} in R2 resonators) could also be applied if they are well identified and relatively far from other parasitic modes in the range. TE modes with last index $n = 3, 5, \ldots$, which are also exited in the specified range and allow extraction of the parallel parameters, are not considered in the measurements because of the increased influence of the sample positioning, which degrades the acceptable accuracy. The foam support with height $H_f \sim (H_1\text{-}h_S)/2$ used in the R1 type resonators is also measured; the dielectric parameters are measured as 1.0218/0.00004 in the Ku band.

A full set of measurement results of PDMS samples with thickness 0.66-0.77 mm for the dielectric constant and dielectric loss tangent in the parallel (in R1 resonators) and perpendicular (in R2 resonators) directions are presented in Table 3.2. For the case when $d_S = D_{1,2}$, each reported value of these parameters is derived by averaging results from 5 samples (including sample thickness); the presented measurement uncertainty is linked to the standard deviation from this averaging. The R11 and R21 resonators are only used for the measurements of samples with $d_S < D_{1,2}$; in this case, the averaging of the dielectric parameters is performed for five consecutive positioning of every single sample near to the resonator centre. The dielectric constant is determined with adequate precision when the samples are measured with $d_S < D_{1,2}$; however, the precision of the loss tangent determination is reduced. It is essential during the measurements in the resonator R2 that the samples should lie tightly on the resonator bottom (particularly when $d_S = D_2$). It is noticed that the measured dielectric constant values in TE and TM mode resonators are different, with mean values of $\epsilon_{par} \sim 2.71$ (in R1 resonators) and $\epsilon_{perp} \sim 2.558$ (in R2 resonators) (the similar difference is also observed for the

dielectric loss tangent, $\tan\delta_{\epsilon_{par}} \sim 0.027$ and $\tan\delta_{\epsilon_{perp}} \sim .0197$; as shown in Table 3.3). In order to calculate these mean values, samples with a thickness larger than 0.6 mm are only selected. These differences are more substantial than measurement errors; for example, the relative errors for a single measurement are estimated as $\pm.5\%$ for ϵ_{par}; $\pm5\%$ for ϵ_{perp}; $\pm5-7\%$ for $\tan\delta_{\epsilon_{par}}$ and $\pm25\%$ for $\tan\delta_{\epsilon_{perp}}$ [203].

Probably, the modest discrepancies between the ϵ_{par} and ϵ_{perp} values for the PDMS are most likely due to the porous structure of this polymer. However, over the frequency range of 2-40 GHz it is reasonable to consider the PDMS samples as isotropic with approximate isotropic parameters $\epsilon_r = \epsilon_{isotropic} = 1/2(\epsilon_{r_{par}}+\epsilon_{r_{perp}}) \sim 2.64\pm0.02$ and $\tan\delta_{\epsilon_r} = \tan\delta_{\epsilon_{risotropic}} \sim 0.023\pm0.0045$ as shown in Fig. 3.11, which shows the dependencies for $\epsilon_{par}, \epsilon_{perp}$ (by two-resonators method) and ϵ_{eq} (by the planar methods; next section).

The analysis of the presented results definitely shows that the PDMS substrate really has a measurable anisotropy. All data obtained by R1 and R2 resonators differ; even expressed frequency dependences can be observed. Nevertheless, the averaged values for the parallel and perpendicular parameters are presented in Table 3.3 for the PDMS samples and several other organic materials, obtained by the set of measuring resonators from Fig. 3.5 in one measurement campaign. As measures of the uni-axial anisotropy the following parameters are used:

$$\Delta A_\epsilon = \frac{2(\epsilon_{par} - \epsilon_{perp})}{(\epsilon_{par} + \epsilon_{perp})} \tag{3.1}$$

for the dielectric constant and

$$\Delta A_{\tan\delta_\epsilon} = \frac{2(\tan\delta_{\epsilon_{perp}} - \tan\delta_{\epsilon_{perp}})}{(\tan\delta_{\epsilon_{perp}} + \tan\delta_{\epsilon_{perp}})} \tag{3.2}$$

for the dielectric loss tangent, introduced in [198]. The obtained anisotropy of the investigated PDMS samples is ΔA_ϵ ~6.3 % and $\Delta A_{\tan\delta_\epsilon}$ ~5 %. Regarding parameter ΔA_ϵ, the PDMS samples are pretty similar to the textile fabrics, whose anisotropy is typically ΔA_ϵ ~3-6 % [184] due to the mixture between the textile fibers and air. For comparison, the applied method accurately predicts the

practical isotropy of materials like Polycarbonate (PC) (0.33 %) and Polytetrafluoroethylene (PTFE) (0.68 %), and same silicone-based materials (the last two rows in Table 3.3), and the weak anisotropy of Cyclo Olefin Polymer (COP) (1.6 %) (the parameter $\Delta A_{\tan\delta_\epsilon}$ less informative for low-loss materials in the considered comparison).

The other observable fact is that the measured dielectric parameters in each measurement resonator have very substantial scattering (as per the results in Table 3.2). The values for ϵ_{par} from $\sim$ 2.54 up to 2.83 and for ϵ_{perp} from $\sim$ 2.32 to 2.69 are measured. These differences are far too significant to be regarded as typical measurement errors for this method. Furthermore, it can be observed that the smaller dielectric constant values have been measured only for thinner samples, e.g., $\epsilon_{par} \sim$ 2.54-2.65 for samples with a thickness of $\sim$0.45-0.51 mm, while $\epsilon_{par} \sim$ 2.65-2.8 for samples with a thickness of $\sim$ 0.63-0.71 mm for measuring resonators R1. Other measuring resonators R2 show a similar effect: $\epsilon_{perp} \sim$ 2.34-2.45 for samples with thickness $\sim$ 0.45-0.51 mm, while ϵ_{perp} $\sim$2.53-2.68 for samples with thickness $\sim 0.63 - 0.71$ mm. These findings show that the dielectric constant of PDMS samples is affected by material thickness.

TABLE 3.1: Typical parameters of eight silver-plated measuring resonators

No	**D,**mm	**H,**mm	f_0, **GHz; mode**	Q_0	D_{eq}, **mm**	σ_{eq}, **S/m**
R11	30.0	30.0	13.1531; TE_{011}	16800	30.0522	2.41×10^7
			21.8338; TE_{021}	5610	30.0477	1.55×10^6
			32.6824; TE_{031}	4980	30.0581	8.53×10^5
R12	18.10	18.0	21.7983; TE_{011}	11445	18.1509	1.85×10^7
			37.8507; TE_{021}	2200	18.1315	3.95×105
R13	15.00	14.08	26.5477; TE_{011}	11170	15.0351	2.15×10^7
R14	10.00	10.0	39.3166; TE_{011}	4720	10.0599	5.69×10^6
R21	30.00	12.13	7.6460; TM_{010}	6280	30.0136	2.90×10^7
			17.5401; TM_{020}	8470	30.0320	2.30×10^7
			27.4956; TM_{030}	7820	30.0338	1.25×10^7
R22	18.10	12.12	12.6480; TM_{010}	6544	18.1440	3.19×10^7
			29.0036; TM_{020}	7250	18.1620	1.71×10^7
R23	10.00	10.12	22.8782; TM_{010}	6150	10.0307	3.72×10^7
R24	8.00	8.08	28.5299; TM_{010}	4750	8.0436	2.78×10^7

TABLE 3.2: Dielectric parameters of PDMS samples, obtained by measurements with a set of resonators R1 and R2 and different excited modes

R1	d_S, **mm**	h_S, **mm**	ϵ_{par}	$\tan\delta_{\epsilon_{par}}$	f_ϵ, GHz/Q_ϵ, (mode)
R11	30	0.68 ± 0.08	2.718 ± 0.005	0.022 ± 0.0010	12.61/260 TE_{011}
			2.712 ± 0.008	0.030 ± 0.0015	21.67/175 TE_{021}
			2.700 ± 0.010	-	30.49/- TE_{031}
	18.1	0.74 ± 0.02	2.723 ± 0.005	0.021 ± 0.0012	12.72/500 TE_{011}
			2.720 ± 0.007	0.023 ± 0.0015	22.10/390 TE_{021}
	15	0.74 ± 0.02	2.719 ± 0.005	0.024 ± 0.0010	12.86/620 TE_{011}
			2.722 ± 0.007	0.026 ± 0.0015	22.11/430 TE_{021}
	10	0.75 ± 0.02	2.717 ± 0.005	0.023 ± 0.0010	13.02/2180 TE_{011}
			2.719 ± 0.008	0.025 ± 0.0015	22.33/500 TE_{021}
	8		2.733 ± 0.005	0.031 ± 0.0015	13.06/3700 TE_{011}
			2.702 ± 0.008	0.028 ± 0.0030	22.84/730 TE_{021}
R12	18.1	0.74 ± 0.04	2.711 ± 0.004	0.031 ± 0.0015	20.17/120 TE_{011}
			2.702 ± 0.008		34.11/- TE_{021}
R13	15	0.75 ± 0.02	2.718 ± 0.004	0.035 ± 0.0022	24.01/105 TE_{011}
R14	10	0.73 ± 0.01	2.705 ± 0.004	0.045 ± 0.0030	34.24/67 TE_{011}
R2	d_S, **mm**	h_S, **mm**	ϵ_{perp}	$\tan\delta_{\epsilon_{perp}}$	f_ϵ, GHz/Q_ϵ, (mode)
R21	30	0.68 ± 0.08	2.584 ± 0.005	0.017 ± 0.0005	7.508/1540TM_{010}
			2.540 ± 0.013	0.023 ± 0.0012	17.16/890 TM_{020}
			2.520 ± 0.015	0.035 ± 0.0020	26.64/385 TM_{030}
	18.1	0.74 ± 0.08	2.603 ± 0.005	0.020 ± 0.0005	7.52/1560 TM_{010}
			2.580 ± 0.010	0.026 ± 0.0009	17.32/1450 TM_{020}
	15	0.74 ± 0.08	2.595 ± 0.006	0.021 ± 0.0005	7.54/1740 TM_{010}
			2.575 ± 0.011	0.025 ± 0.0009	17.38/1900 TM_{020}
	10	0.75 ± 0.08	2.590 ± 0.006	0.019 ± 0.0004	7.58/2650 TM_{010}
			2.570 ± 0.012	0.026 ± 0.0009	17.33/2000 TM_{020}
	8	0.70±0.08	2.597±0.007	0.022±0.0010	7.61/2800 TM_{010}
			2.575±0.013	0.025±0.0012	17.43/2290 TM_{020}
R22	18.1	0.74 ± 0.07	2.548 ± 0.008	0.021 ± 0.0008	12.35/1190 TM_{010}
			2.540 ± 0.013	0.027 ± 0.0012	27.84/330 TM_{020}
R23	10	0.73 ± 0.03	2.546 ± 0.009	0.026 ± 0.0011	22.15/480 TM_{010}
R24	8	0.66 ± 0.01	2.505 ± 0.008	$0.032 \pm .0013$	27.45/340 TM_{010}

TABLE 3.3: Summarized results for the dielectric parameters of several organic materials obtained by the Two-Resonator Method

Material	$\epsilon_{par}; \tan\delta_{\epsilon_{par}}$ **(12-35 GHz)**	$\epsilon_{perp}; \tan\delta_{\epsilon_{perp}}$ **(7-28 GHz)**	$\Delta A_\epsilon; \Delta A \tan\delta_\epsilon, \%$
PDMS	2.716 ± 0.009 0.031 ± 0.008	2.55 ± 0.028 0.024 ± 0.007	6.3 25.5
PTFE	2.054 ± 0.005 0.00029 ± 0.00001	2.04 ± 0.020 0.00026 ± 0.00003	0.68 -
COP	2.327 ± 0.006 0.00051 ± 0.00006	2.29 ± 0.028 0.00029 ± 0.00003	1.60 -
PC	2.767 ± 0.003 0.0056 ± 0.0001	2.758 ± 0.009 0.0055 ± 0.0002	0.33 1.8
Silicone elastomer	2.21 ± 0.04 0.0010 ± 0.0001	2.19 ± 0.08 0.0008 ± 0.0003	0.91 1.8
Commercial silicone glue	2.34 ± 0.02 0.0096 ± 0.001	2.33 ± 0.05 0.0077 ± 0.0008	0.43 22.0

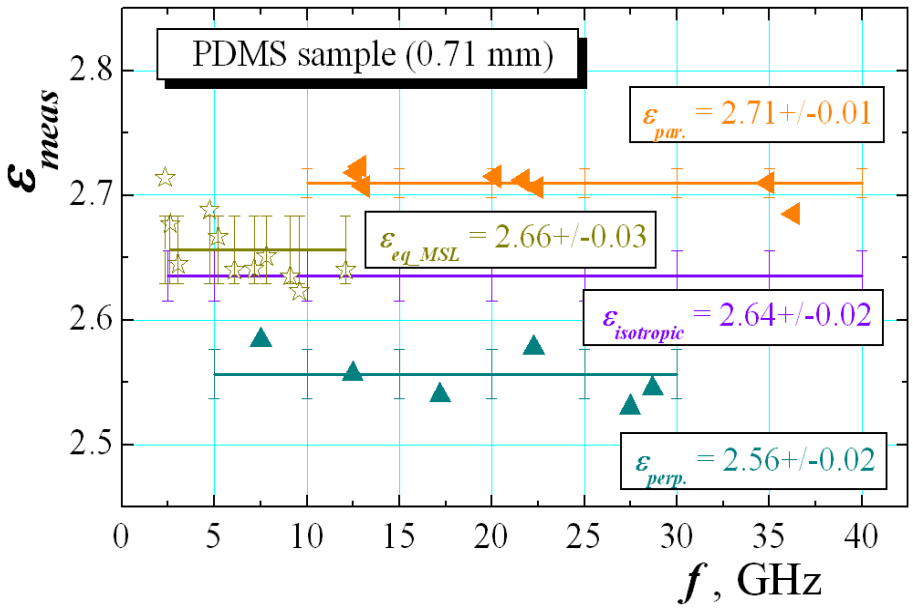

FIGURE 3.11: Measured parallel and perpendicular dielectric constants of PDMS substrate with thickness 0.71 mm by the two-resonator method compared with the equivalent dielectric constant from the planar measurements.

3.4.2 Frequency Dependence of PDMS Anisotropy

The fact that the PDMS anisotropy is frequency-dependent is also interesting. Additional auxiliary methods are applied to expand the dependencies for ϵ_{par} and ϵ_{perp} to prove this fact (the loss tangents are not measured by some of these methods

due to the lower accuracy). The so-called re-entrant resonator ReR (as shown in Fig. 3.4 (b), Fig. 3.6 (c)) [193] based methods are one of the most accurate methods for determining ϵ_{perp} at lower frequencies. A tunable version is applied on the base of resonator R21; the parameters are extracted using 3D simulations in the frequency range from 1.65 to 7.6 GHz. The obtained results reveal that ϵ_{perp} increase from 2.59 to 2.69 (and a decreasing of $\tan\delta_{\epsilon_{perp}}$ from 0.017 to 0.012) – see the corresponding data in Fig. 3.12 for ϵ_{perp}. The parallel parameter ϵ_{par} has been determined by a cylinder-coaxial resonator (Fig. 3.4(b)), based on the resonator R11 with coaxial pistons on the flanges [201]. The measured values $\epsilon_{par} \sim 2.73$ and $\tan\delta_{\epsilon_{par}} \sim 0.021$ at a single frequency 6.53 GHz have also been confirmed by a quarter wavelength coaxial resonator (Fig. 3.4 (e) and Fig. 3.6 (d)): $\epsilon_{par} \sim 2.75$ and $\tan\delta_{\epsilon_{par}} \sim 0.017$ at 5.78 GHz (Fig. 3.12).

The classical waveguide method, which measures the phase delay in flat thin PDMS samples placed between pairs of waveguide flanges as shown in Fig. 3.13 (a), can provide valuable auxiliary information for ϵ_{par} in wide frequency range but with less accuracy. Simple numerical simulations can be easily used to determine the parallel dielectric constant if the sample completely covers the waveguide aperture with $\sim$ 10-15% margin. From S to Ka-band, seven pairs of waveguides are applied to measure the additional phase delay in the middle of each waveguide operating range (see the examples for the frequency range 3.5-14 GHz in Fig. 3.14 (a)). Despite the lower accuracy, the extracted values of $\epsilon_{par} \sim 2.78$ at 3.5 GHz to 2.68 at 34 GHz confirm the frequency behavior of the parallel dielectric constant (Fig. 3.12). Simple perturbation resonance measurements with excited first three dominant TM modes in the X band using a waveguide (WR90) resonator with small PDMS prism (as shown in Fig. 3.13 (b)) also yield comparable results – $\epsilon_{par} \sim 2.76$ at 6.95 GHz, 2.75 at 9.53 GHz, and 2.73 at 13.3 GHz.

The last step is to extend the frequency dependence for ϵ_{perp} beyond 29 GHz. There are a limited number of options. The corresponding dependencies in the K and Ka bands are shown in Fig. 3.14 (b) obtained by applying the method of comparison between the measured and simulated phase delays in waveguides with a small PDMS prism placed in the middle of the waveguide in a horizontal position for an approximate determination of ϵ_{perp} (the prism in a vertical position

has also been measured for determination of ϵ_{par}). Both dependencies, ϵ_{perp} and ϵ_{par}, indicate a weak saturation over 30 GHz, according to the measurements.

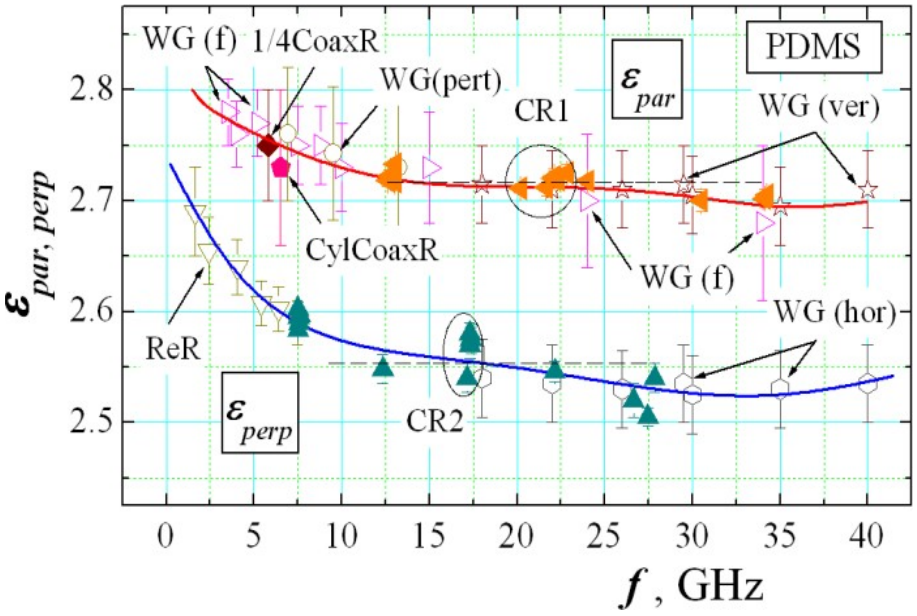

FIGURE 3.12: Summarized dependencies of the parallel and perpendicular dielectric constants of PDMS samples by the two-resonator method. Results from other methods have been also added. Legend: CR1,2 – data obtained by all cylinder resonators R1 and R2, taken from Table 3.2; ReR – data from a re-entrant resonator on the base of R21 with $d_S = D_2$; $D_{2C} = 18.0$; $H_{2C} = 0 - 11.4$ (Fig. 3.4(b) and Fig. 3.6 (c)); CylCoaxR and 1/4CoaxR – data from a cylinder- coaxial resonator (Fig. 3.4 (b); on the base of R11; $D_{1C} = 18.0$; $H_{1C} = 8.6 - 11.0$) and quarter wave- length resonator (Fig. 3.4 (e) and Fig. 3.6 (d); $d_C = 3.1$, $h_C = 10.43$, $D_0 = 10.43$); WG(f)–PDMS samples between flanges (Fig. 3.13 (a)) of waveguides WR229; WR137; WR112, WR90, WR75, WR42, WR28; WG(ver/hor) – PDMS prism 0.78 x 3.0 x 6.0 in vertical or horizontal positions (Fig. 3.13 (c)) in waveguides WR42 and WR28; WG(pert) – small PDMS prism 0.78 × 0.8 × 10.16 in WR90 resonator of length $L_R = 64.85$ (Fig. 3.13 (b)) with exited $TM_{101,103,105}$ modes. Solid curves are polynomial fits of all presented data; dashed lines – averaged values from the two-resonator method only in the corresponding frequency ranges.

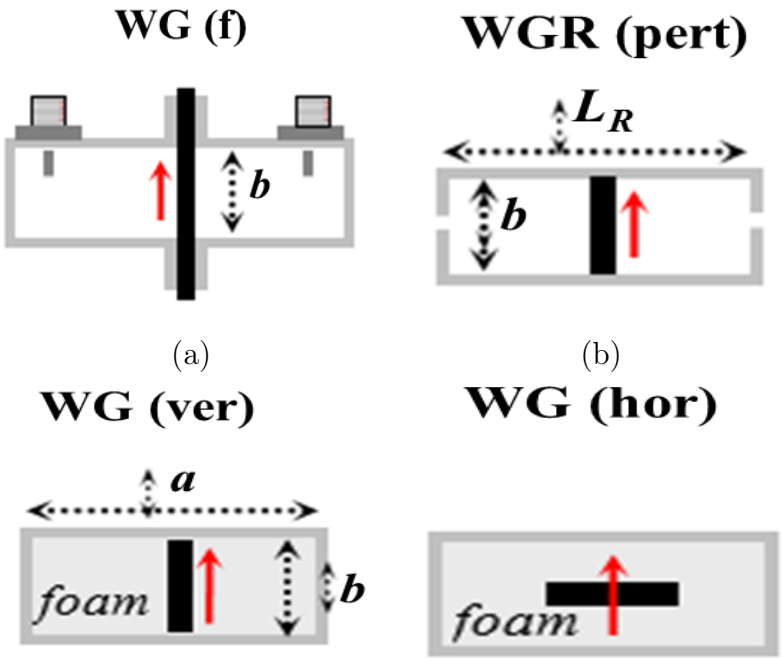

FIGURE 3.13: Illustration of auxiliary waveguide methods for determination of substrate anisotropy: (a) substrate between waveguide flanges; (b) Perturbation method – waveguide resonators with a small prism; (c) sample prism in a vertical, and (d) horizontal position if waveguide with foam support. Legend: a, b – waveguide width and height; L_R – waveguide resonator length.

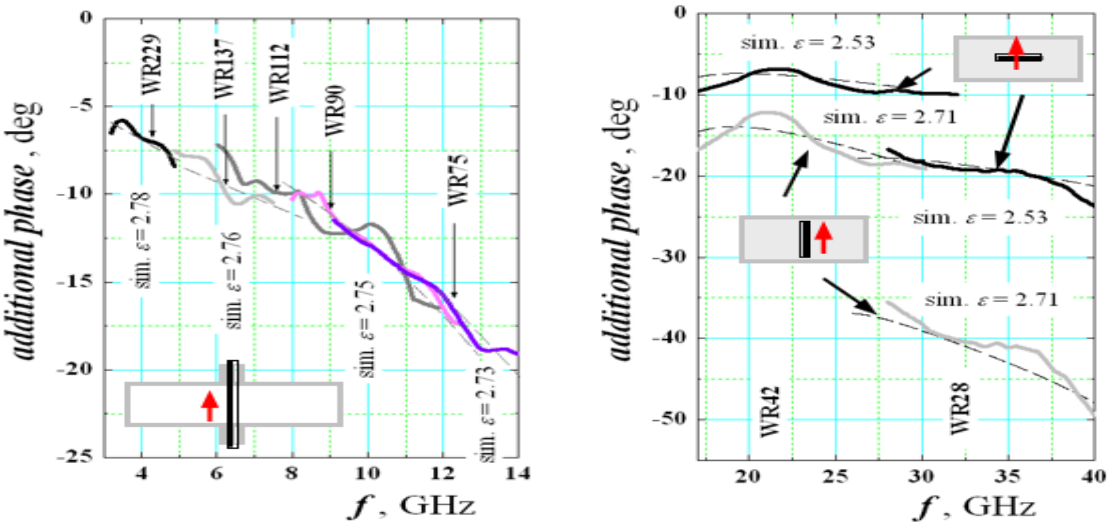

FIGURE 3.14: Measured and simulated phase delays from PDMS samples in rectangular waveguides: (a) flat sample between pairs of waveguide flanges; (b) Prism samples in vertical and horizontal positions in waveguides.

3.4.3 Planar Structure Measurements

A. Linear (LR) and Ring Microstrip resonator (RR) method

Initially, the investigations of the frequency behavior of classical linear and ring resonators on non-metalized PDMS substrates are carried out. Self-adhesive metal (aluminum or copper) foil (50 μm thick) can be used to create the metal layout carefully, as shown in Fig. 3.10 (a), (b). Several attempts have been made, utilizing special coaxial punchers, for LR on PDMS substrate with lengths L_{LR} ranging from 25 up to 44 mm and width w_{LR} from 1 to 4 mm and for RR with diameters D_{RR} ranging from 18.1 to 33 mm. Despite the ensured accuracy, measurable 3-4 quasi-TEM resonances without parasitic peaks are only detected in the frequency range 2-10 GHz; three cases are shown in Fig. 3.15 for references. Table 3.4 shows the values of the estimated effective dielectric constant ϵ_{eff} and the recalculated equivalent dielectric constant ϵ_{eq} (using conventional TRL calculators).

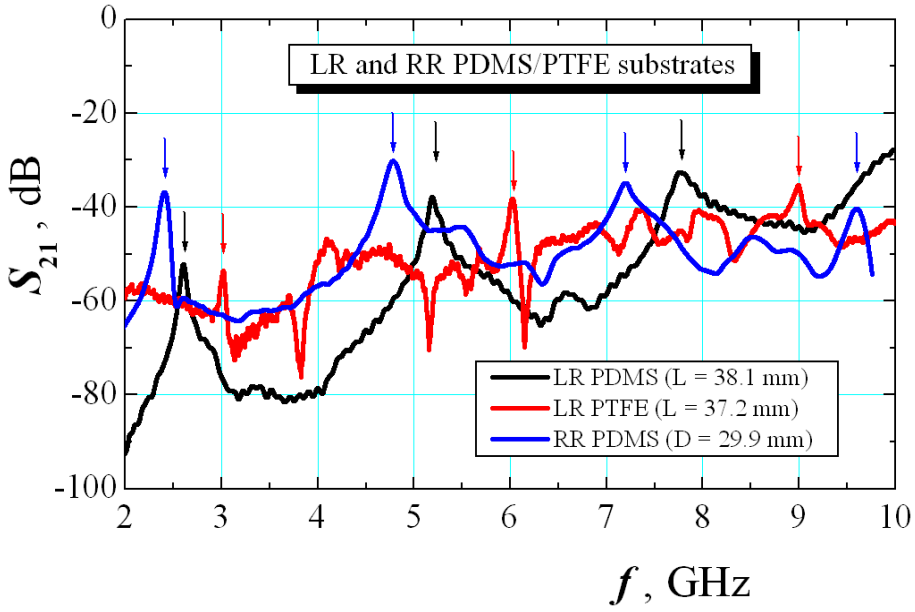

FIGURE 3.15: Measured resonance curves (2-10 GHz) of the first 3-4 q-TEM modes in linear (LR) and ring (RR) microstrip resonators on PDMS (0.75 mm thick) and PTFE (0.48 mm thick) substrates.

The calculated results for the mean equivalent value of the dielectric constant of the PDMS sample ($\epsilon_{eq} \sim 2.664 \pm 0.020$) is extremely close to the predicted isotropic value as presented in Table 3.3 (similar results are achieved for PTFE samples: $\epsilon_{eq} \sim 2.059 \pm 0.007$)). However, as the sizes of the manufactured resonators aren't

known with certainty so to rely on these results only is not acceptable. Furthermore, with similar measurements, sufficient accuracy for the dielectric loss tangent cannot be reached.

TABLE 3.4: Measured effective and equivalent dielectric constant of PDMS and PTFE substrate by LR/RR method

Substrates	**Resonance frequencies, GHz**	**Averaged ϵ_{eff}**	**Extracted ϵ_{eq}**
PDMS (0.71 mm) LR(L_{LR}= 38.1mm)	2.60	2.156 ± 0.013	2.677 ± 0.014
	5.21		2.667 ± 0.014
	7.82		2.651 ± 0.014
			Averaged: 2.66 ± 0.014
PTFE (0.48 mm) LR(L_{LR} = 37.2mm)	3.017	1.792 ± 0.007	2.677 ± 0.014
	6.029		2.060 ± 0.008
	9.016		2.052 ± 0.008
			Averaged: 2.059 ± 0.008
PDMS(0.71 mm) RR (D_{RR}=29.9 mm)	2.34	2.071 ± 0.046	2.714 ± 0.020
	4.73		2.688 ± 0.020
	7.14		2.641 ± 0.020
	9.59		2.623 ± 0.020
			Averaged: 2.67 ± 0.020

B. By Covered Ring Resonator (CovRR) Method:

For microstrip ring resonators (MSL-RR) of diameter D_{RR} = 4cm covered by PDMS disk sample, the resonance parameters (resonance frequencies and unloaded Q factors) are determined as shown in Fig. 3.10 (c), (d). The RR conductor layout is now accurately manufactured by photo-lithography on commercial substrates (in this case, near-to-isotropic materials like 20-mils thick Isola Astra MT and Ro3003 with dielectric constant close to 3 and with relatively small losses are used). The resonance curves of a microstrip ring resonator on substrate ISOLA Astra MT 3.0 without and with a covering PDMS sample are shown in Fig. 3.16. Fig. 3.17 (a) illustrates the corresponding resonance frequencies of the TEM modes shifts owing to the PDMS sample influence, whereas Fig. 3.17 (b) shows the corresponding unloaded Q factors. The dielectric parameters of the PDMS sample are extracted using this data. The sample should completely cover the RR substrate's surface with no air gaps, which is not an issue for such a flexible and self-adhesive sample and is easy to control.

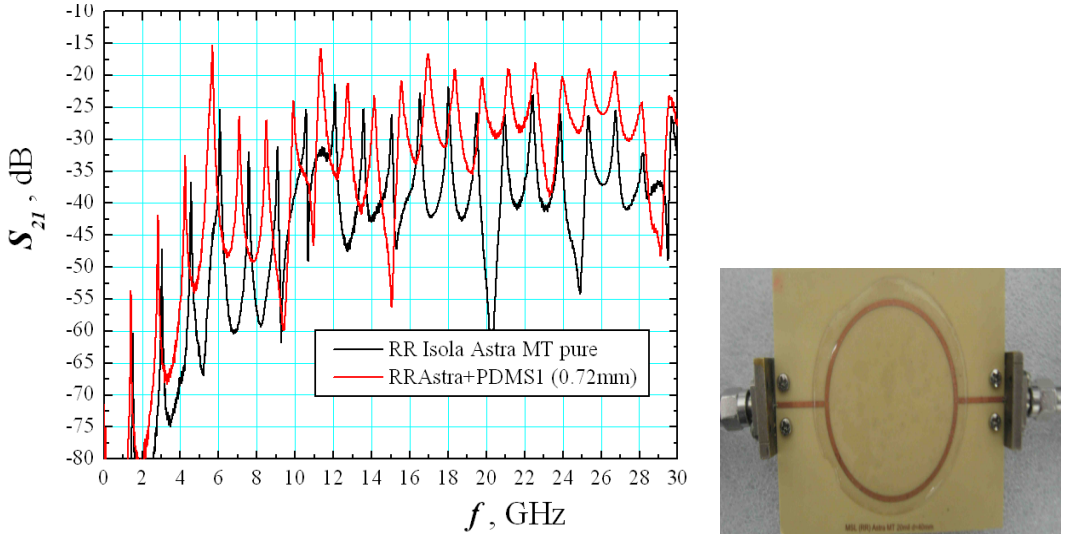

(a) (b)

FIGURE 3.16: Resonance curves of microstrip RR of averaged diameter 40 mm on substrate ISOLA Astra MT 3.0 without and with covering PDMS sample and (b) image of the covered RR by PDMS sample of diameter 46 mm.

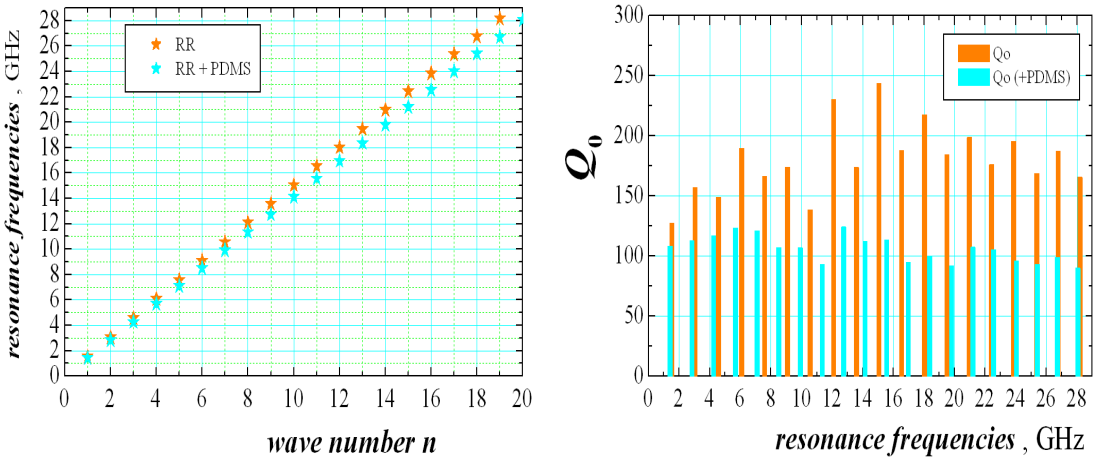

(a) (b)

FIGURE 3.17: (a) Resonance curves of microstrip ring resonator on substrate ISOLA Astra MT 3.0 without and with covering PDMS sample according to the wavenumber and (b) corresponding unloaded Q factors.

The dependencies of the calculated effective dielectric constant ϵ_{eff} and attenuation α of a microstrip line (MSL) on the used substrate with and without PDMS

sample is calculated by the simple expression,

$$\epsilon_{eff} = \left(\frac{30p}{2\pi\, D_{RR}\, f_p} \right)^2, \tag{3.3}$$

where the resonance frequencies f_p ($p = 1, 2, 3\ldots$) are in GHz and D_{RR} is in cm;

$$\alpha\,(\mathrm{dB/cm}) = \frac{27.3(\epsilon_{\mathrm{eff}})^{0.5}}{\mathrm{Q_p}.\lambda_0}, \tag{3.4}$$

where λ_0 is the free-space wavelength in cm, Q_p is the unloaded factor [205]. The dependencies are presented in Fig. 3.18. Actually, three RRs with different PDMS samples are measured; these RRs of diameter $D_{RR} = 40$ mm are printed on different commercial substrates with ϵ_r close to 3.0 (Ro3003, CLTE, Isola Astra MT). The final results presented below (e.g., in Fig. 3.19) are averaged from these several measurements. Thus, two pairs of dependencies are obtained for each RR without and with covering sample, namely: $\epsilon_{eff_{MSL}}$, $\alpha_{eq_{MSL}}$, and $\epsilon_{eff_{covMSL}}$, $\alpha_{eq_{covMSL}}$. The question now is how to extract the equivalent parameters ϵ_{eq_S}, $\tan\delta_{\epsilon_{eq_s}}$ of the covering (PDMS) samples from these dependencies. There are two approaches: to use an appropriate analytical model (e.g., presented in [206]) or to perform relevant 3D simulations (as in [21]).

If the RR substrate has a dielectric constant $\epsilon_m > \epsilon_{eq_s}$ and thickness d_m; if the width of the RR conductors is w_m ($w_m > 2d_m$) (see the inset in Fig. 3.19 (b)), the following pairs of expressions can be used for the calculation of the effective dielectric constant $\epsilon_{eff_{covMSL}}$ of the MSL structure with covering sample (superstrate) of thickness d_s [206]:

$$\epsilon_{eff_{covMSL}} = 0.5(\epsilon_m + \epsilon_{cov}) + 0.52(\epsilon_m - \epsilon_{cov})\left(1 + \frac{12d_m}{w_m}\right)^{-0.5} \tag{3.5}$$

where

$$\epsilon_{cov} = 1 + \left(\frac{2}{\pi}\right)(\epsilon_{eq_s} - 1)\arctan\left[1.877\left(\frac{d_s}{d_m}\right)^{0.904}\left(\frac{w_m}{d_m}\right)^{0.367}\right] \tag{3.6}$$

is an effective dielectric constant of the layers above the MSL, including the covering sample and the air above. Thus, the equivalent superstrate dielectric

constant $\epsilon_{calc} = \epsilon_{eq_s}$ can be successfully extracted from Eq.(3.6) when the calculated $\epsilon_{eff_{covMSL}}$ value by Eq.(3.5) coincides with the measured one from Fig. 3.18 (a). The ϵ_{calc} dependence is presented on the same figure for RR on Isola Astra substrate (with mean equivalent dielectric parameters 3.098/0.0029); it simply follows the slope of $\epsilon_{eff_{covMSL}}$ curve and does not represent the actual frequency behavior. The approach based on applying 3D simulation models explained below of MSL structures to assist the RR measurements is more effective and accurate.

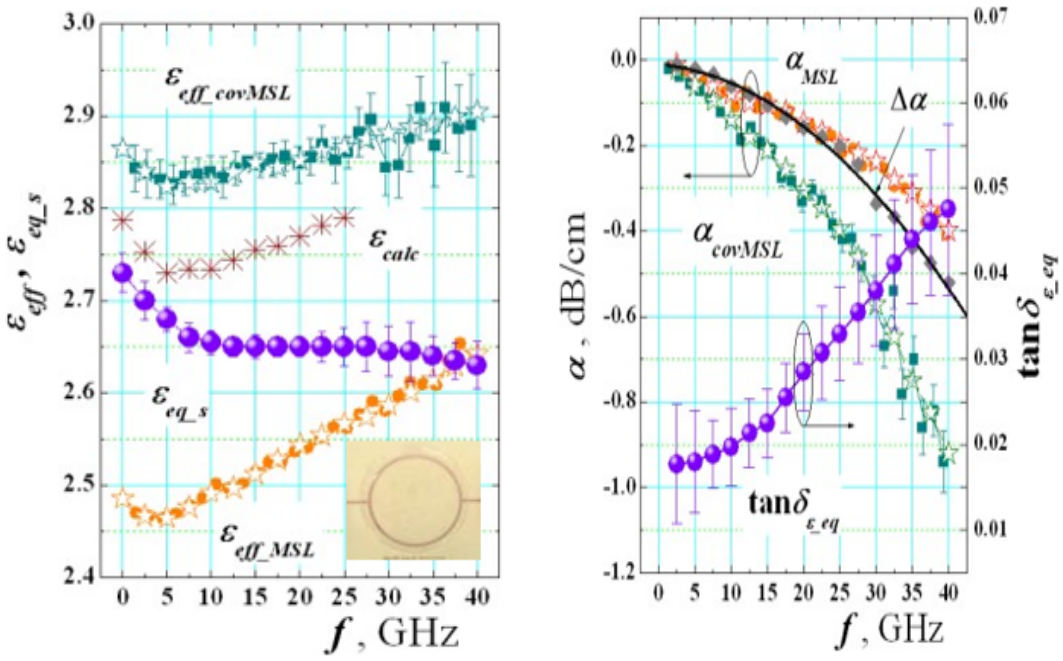

(a) (b)

FIGURE 3.18: Measured effective dielectric constants (a) and attenuation (b) of MSL on substrate Isola Astra 3.0 without and with 0.72-mm thick PDMS sample (inset), $\epsilon_{eff_{MSL}}$, α_{MS} and $\epsilon_{eff_{covMSL}}$, α_{covMSL} respectively. Legend: $\epsilon_{eq_s} = \epsilon_{eq_{PDMS}}$ – extracted dependence of the equivalent dielectric constant of PDMS sample by 3D simulations; $\epsilon_{eq_s} = \epsilon_{eq_{calc}}$ – calculated PDMS constant from Eq.(3.6); $\tan\delta_{\epsilon_{eq}} = \tan\delta_{eq_{PDMS}}$– extracted dependence of the equivalent dielectric loss tangent of PDMS sample by 3D simulations; $\Delta\alpha = \alpha_{covMSL}$-$\alpha_{MSL}$: additional attenuation; stars averaged values used in the simulations.

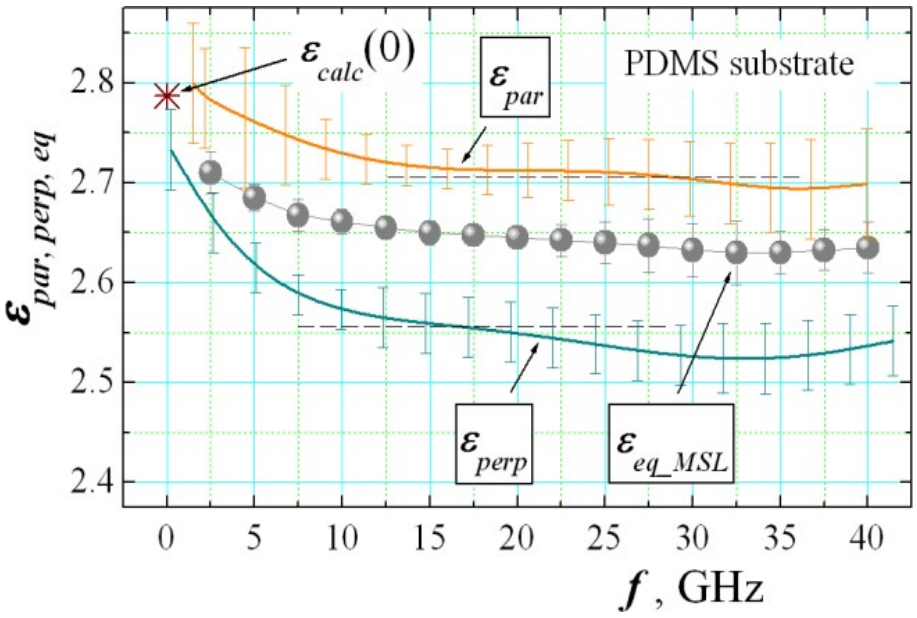

(a)

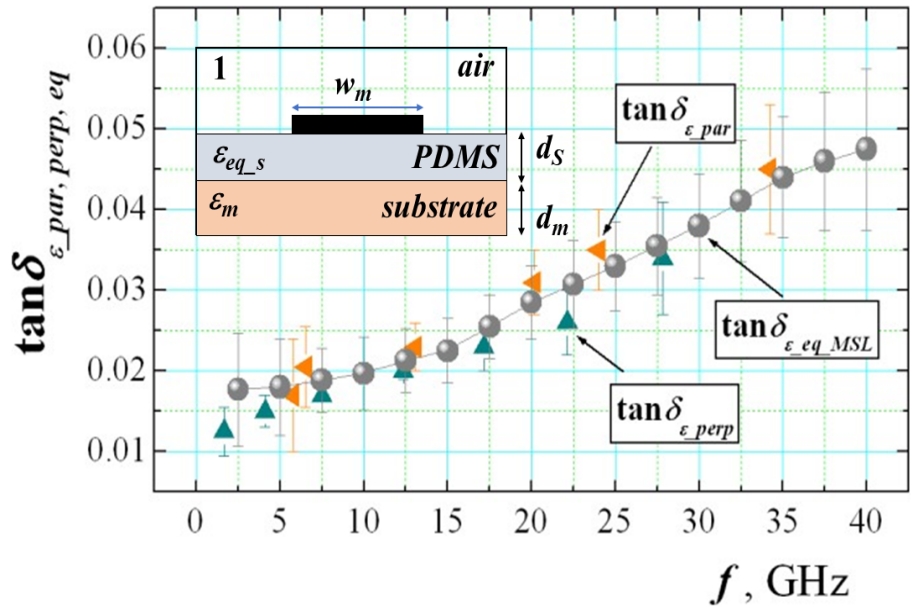

(b)

FIGURE 3.19: Final extracted frequency dependencies of the parameters $\epsilon_{eq_{MSL}}$ (a) and $\tan\delta_{\epsilon_{eq_{MSL}}}$ (b) of PDMS substrates for MSL approach, compared with the corresponding parallel and perpendicular dependencies, ϵ_{par}, ϵ_{perp} from Fig. 3.12 and $\tan\delta_{\epsilon_{par}}$, $\tan\delta_{\epsilon_{perp}}$,$\epsilon_{calc}(0)$ is calculated by Eq.(3.5,3.6) for $f = 0$.

As there are no accurate analytical models for reliably extracting the dielectric parameters of the covering samples from this data, electromagnetic simulations using a commercial 3D simulator are required necessarily (e.g., HFSS). The Transmission-line regime (driven solution, shown in Fig.(3.20)) and Eigen-mode

regime (shown in Fig.(3.22)) are the two options for 3D simulations of the ring resonator.

Transmission-line regime: The S_{21} parameters of the whole structure are computed without and with a PDMS sample in this first option to produce the simulated resonance curves for each TEM mode, which can be compared with the corresponding measured curves. For mode $p = 4$, this possibility is illustrated by Fig. 3.21. As the resonance frequency shift and unloaded Q factor changes for each mode, this is a good option for computing both dielectric parameters of the covering sample (Fig. 3.17 and Table 3.5). The problem associated with this option is that simulation takes a lot of computational time (appropriate meshing of a single frequency and then discrete sweeping in a narrow interval around the resonance frequency). As a result, as illustrated in Fig. 3.20(b) – Model 1 (only modes with even wave number p can be simulated in this case), the proposed 3D model can be split once with appropriate boundary conditions (H-field symmetry on the splitting plane). For each mode, the simulation procedure is as follows:

(i) The ring resonator is simulated without a sample. Usually, the discrepancy between the simulated and measured resonance curves appears; both curves could be made equal by fine-tuning of ϵ_r and $\tan\delta_{\epsilon_r}$ of the substrate under the resonator (Fig. 3.21(a); $p = 4$). The applied procedure is no doubt time consuming, but the close match between the two curves assures that the measuring structure is self-calibrated without the need of a sample; then, the obtained parameters of the substrate under the resonator must have been utilized in the 3D model of the resonator with PDMS sample.

(ii) The next step is to simulate the ring resonator (Model 1) with PDMS samples in a similar way. To begin, the PDMS sample could be presented in the 3D Model 1 in an anisotropic option with averaged parameters taken from the first row of Table 3.3. The derived simulated resonance curve is very close to the measured curve (see dependencies in Fig. 3.21 (b) for $p = 4$). The PDMS sample can now be considered as an isotropic material with equivalent dielectric parameters; now, by tuning only the dielectric parameters of the isotropic PDMS sample, a satisfactory coincidence between the simulated and measured resonance curves of a ring resonator with a sample can be achieved – see Fig. 3.21 (b) for the corresponding

curves. The described procedure is beneficial since it enables for the determination of the covering PDMS sample's own parameters for each mode (typically for p in the interval till 20). However, even for one pair of resonances, the computing time is significant; that's why Table 3.5 only shows the extracted equivalent parameters of the isotropic PDMS sample for mode $p = 4$. The obtained values for, $\epsilon_r = 2.665$ and $\tan\delta_{\epsilon_r} = 0.02$, as anticipated in Table 3.3, are extremely similar.

Eigenmode option: The second option of the ring resonator in the standard radiation box, as shown in Fig. 3.22 (a), allows for faster simulations. The structure can be again split once (Fig. 3.22 (b); Model 2) or twice (Fig. 3.22 (c)); however, not all modes can be simulated in split structures. The procedural steps are quite similar to the previous case:

(i) The ring resonator is simulated without a sample (Model 2), and equivalent dielectric parameters of the substrate under the resonator are determined.

(ii) The ring resonator is simulated with a PDMS sample and equivalent dielectric parameters of the sample are determined. For modes with $p = 2, 4, 6, 8$, and 10, as shown in Fig. 3.23, the simulations are carried out with acceptable results (see the last column in Table 3.5). Now the problem is that in the radiation box of Model 2, a lot of parasitic resonances might arise, which can imitate the right TEM resonances or impact the proper E-field distribution at the high-order resonances as illustrated in Fig. 3.23 for $p = 10$. That's why due to decreased accuracy, simulations for modes with $p > 8$ are not conducted.

The presented method by covered ring resonator is very promising for characterization of such soft polymers as the PDMS material, such research should continue, including the development of other novel methods for extracting the equivalent parameters of the covering sample on microstrip line resonators.

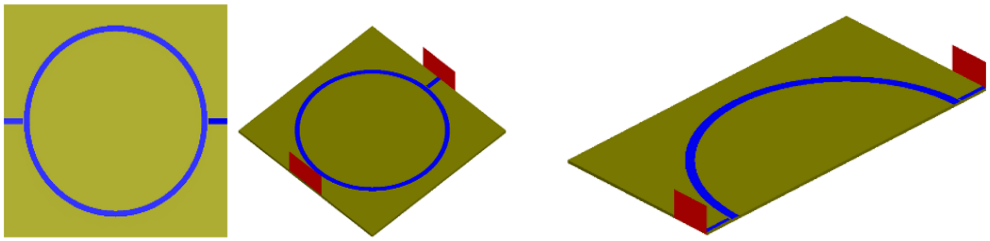

(a) (b)

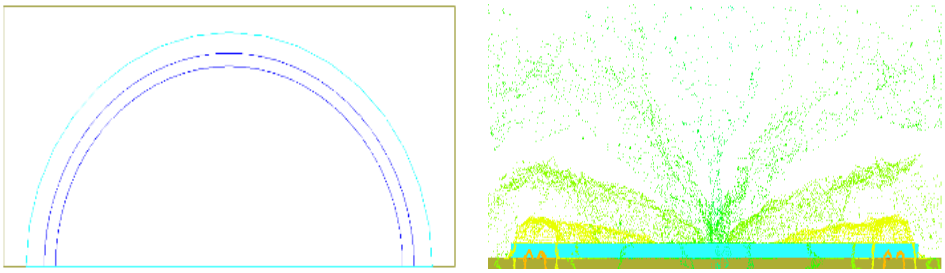

(c) (d)

FIGURE 3.20: 3D models of ring resonators in transmission-line option: (a) whole resonator; (b) Half-splitted resonator (Model 1); (c) Half resonator with covering PDMS sample; (d) electric field distribution in the ring resonator with sample (side view).

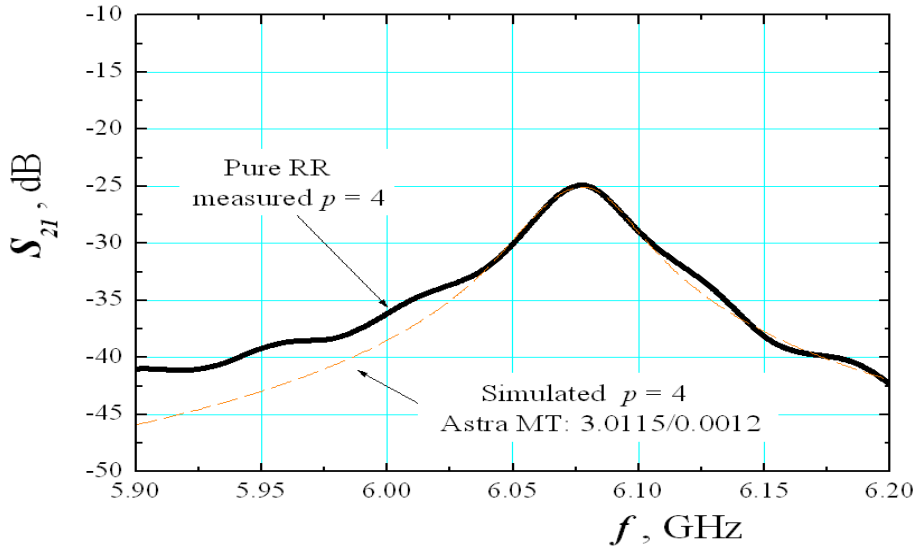

(a)

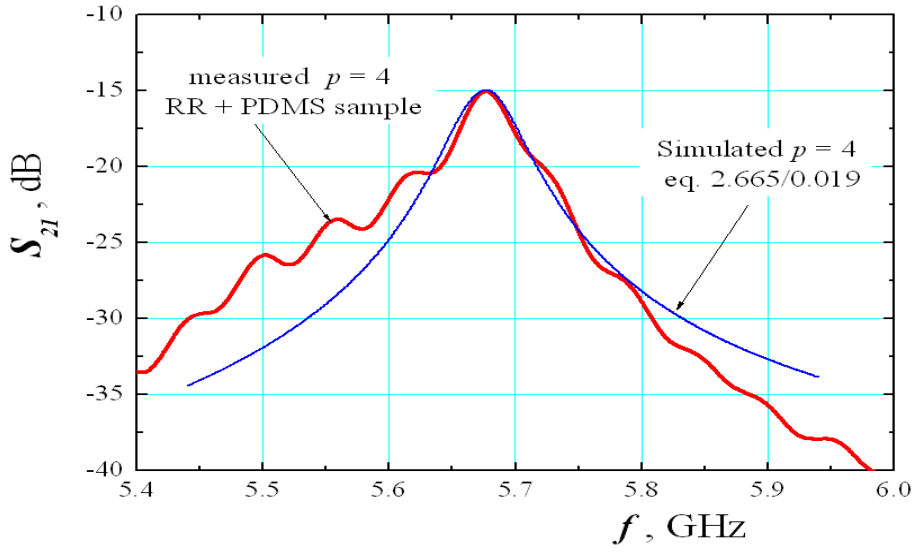

(b)

FIGURE 3.21: Measured and simulated resonance curves for TEM mode with $p = 4$ of microstrip ring resonator on substrate ISOLA Astra MT 3.0 without (a) and with (b) covering PDMS sample.

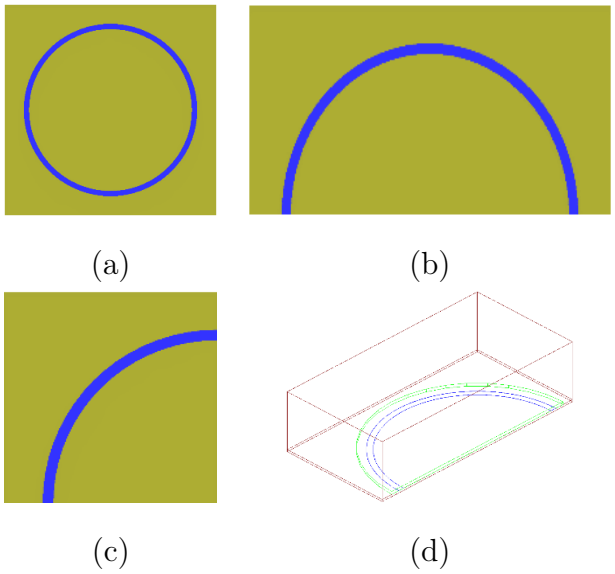

FIGURE 3.22: 3D models of ring resonators in Eigenmode option: (a) whole resonator; (b) half- split resonator (Model 2); (c) quarter-split resonator; (d) 3D Model 2 with covering PDMS sample in standard radiation box in HFSS.

TABLE 3.5: Extracted Equivalent Dielectric Constant and Dielectric Loss Tangent of PDMS Samples by RR Method

p	f_0, GHz	Q_0	f_ϵ, GHz	Q_ϵ	$\epsilon_r/\tan\delta_{\epsilon_r}$ (Model 1)	$\epsilon_r/\tan\delta_{\epsilon_r}$ (Model 2)
1	1.5192	127.4	1.4157	108.3		
2	3.0404	157.3	2.8346	112.8		2.645
3	4.5627	149.1	4.2562	116.8		
4	6.0768	189.5	5.6801	123.2	2.665/0.020	2.640/0.02
5	7.5829	166.4	7.0896	121.1		
6	9.0849	173.8	8.5036	107.0		2.635
7	10.5669	138.7	9.9169	107.0		
8	12.0879	230.5	11.3463	93.0		2.640
9	13.5837	173.7	12.7424	124.3		
10	15.0550	243.5	14.1390	112.2		
11	16.5285	188.0	15.5628	113.2		
12	18.0271	217.7	16.9606	94.7		
13	19.4894	184.5	18.3627	99.8		
14	20.9679	198.8	19.8058	92.2		
15	22.4207	176.1	21.1916	107.3		
16	23.8571	195.3	22.5477	105.3		
17	25.3587	168.6	24.0296	96.0		
18	26.7678	187.3	25.4075	93.3		
19	28.1814	165.4	26.7175	99.1		
20	29.7218	179.3	28.0576	90.1		

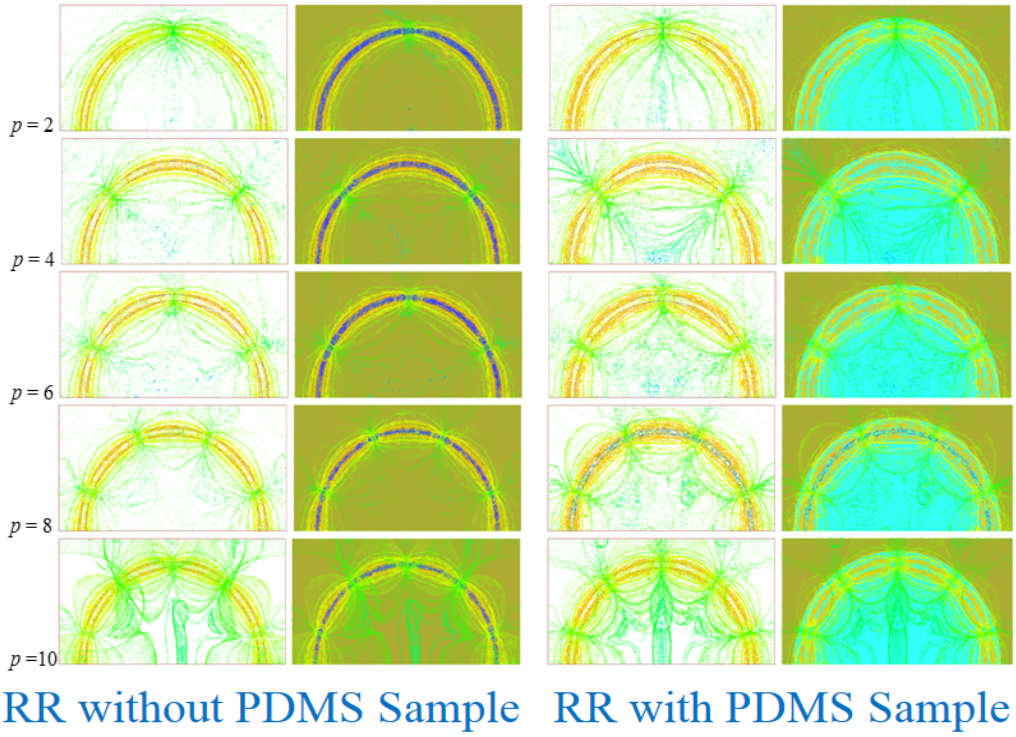

FIGURE 3.23: Electric field distribution of the first even modes ($p = 2, 4, 6, 8, 10$) in the ring resonator without (at left) or with PDMS sample (at right) (top view) using 3D Model 2.

In addition to the methods mentioned above, another simple proposed method can also be applied, which can overcome the ineffectiveness of direct simulations of the RR structure with superstrate in Driven mode or Eigenmode options (if arises). In a classical radiation box (as it is shown in the insets of Fig. 3.18), a short MSL segment of 10 mm can be simulated with selected parameters $\epsilon_{eq_{MSL}}$ and $\tan\delta_{\epsilon_{eq_{MSL}}}$ of the covering sample (superstrate) until a satisfactory coincidence between the numerical and measured parameters $\epsilon_{eff_{covMSL}}$ and $\alpha_{eq_{covMSL}}$ has been achieved. For determining the $\epsilon_{eq_{MSL}}$ the simulation procedure is performed twice; first, for pure MSL to determine the actual RR substrate constant ϵ_m, and then, for MSL with covering sample – to determine $\epsilon_{eq_{MSL}}$. The preliminary determination of the parameter α_{MSL} is not required in the case for evaluating the dielectric loss tangent; the advantage is that $\tan\delta_{\epsilon_{eq_{MSL}}}$ can be directly computed from the $\Delta\alpha$–dependence of the additional attenuation (Fig. 3.18 (b)).

Both extracted curves for $\epsilon_{eq_{MSL}}$ and $\tan\delta_{eq_{MSL}}$ lies between the measured curves ϵ_{par}, ϵ_{perp} and $\tan\delta_{\epsilon_{par}}$, $\tan\delta_{\epsilon_{perp}}$. This is a typical fact for most of the anisotropic

materials [195] and shows that the obtained results are fully compliant. The other important point is the observed weak but measurable frequency dependence of the dielectric constants: $\epsilon_{par} \sim 2.8 - 2.7$; $\epsilon_{perp} \sim$ 2.67-2.52 and $\epsilon_{eq_{MSL}} \sim$ 2.72-2.63 in the frequency range 2-40 GHz. Only one reference [181] presents similar property of the PDMS samples up to 110 GHz and beyond, established by transmission-line measurements of coplanar waveguide (CPW) on this substrate. In fact, the dielectric constant dependence as in [181] coincides with presented in Fig. 3.19 (a) ϵ_{par} dependence. The reason behind this is in the CPW transmission line, the parallel-to-perpendicular E-field ratio is $\sim$ 79 : 21, whereas, in MSL, it is $\sim$ 38 : 62 (for 0.5-0.7 mm thick samples) [204]. As a result, the extracted equivalent dielectric constant from CPW measurements should be close to ϵ_{par}, while the measured $\epsilon_{eq_{MSL}}$ by MSL is a mixed value between ϵ_{par} and ϵ_{perp}. However, at lower frequencies, such as $\tan\delta_{\epsilon} \sim$ 0.07-0.045 in the frequency range 0.1- 40 GHz, the frequency dependence of the dielectric loss tangent reported in [181] is rather implausible; the saturation of 0.045 from 40 to 210 GHz appears to be more feasible. One probable explanation is that the dominant mode of the CPW has a low-frequency cut-off, and measurements below and around this cut-off are in some ways erroneous. The results presented here are $\tan\delta_{\epsilon_{eq_{MSL}}} \sim 0.017 - 0.047$ in the range 2-40 GHz and could be regarded as confirmed data from other PDMS sample measurements [168].

3.4.4 Temperature Behavior of PDMS Dielectric Parameters

The final phase of research presented in this chapter is devoted to temperature measurements of the dielectric parameters of PDMS polymer. No such information does exist in the literature. The temperature response of the PDMS dielectric properties is of apparent importance from the standpoint of wearable/flexible antenna substrates. There are three main circumstances to consider. The first is that this polymer has a relatively high coefficient of thermal expansion (CTE) – typically 300-340 ppm/°C [207] in the temperature interval from –55°C to 150°C. Recent researches have revealed that this coefficient is dependent on the curing temperature;

for example, CTE for the commercial PDMS product Sylgard 184 [208] decreases linearly from 310 ppm/°C at curing temperature 25°C to 240 ppm/°C at curing temperature 135°C [209] (∼ 23%). The observed dielectric anisotropy and the frequency dependence of dielectric characteristics of PDMS samples at room temperature are the other two conditions, and they could be affected by temperature changes.

In this chapter, investigation of the variations of frequency dependencies of parallel, perpendicular, equivalent dielectric parameters of PDMS samples in the temperature range from –40°C to +100°C by two different experimental methods is already applied at room temperature (in section 3.4.2).

With the two-resonator method, the sample anisotropy has been calculated once more, but this time the measuring procedure is performed at each fixed temperature. The temperature measurements are carried out in a commercial Termotron® chamber, which allows for temperature stability in the range of –70°C to +110°C with a ±2°C uncertainty. The chamber contains a temperature gradient, but the working temperature is accepted as a constant in the entire setup (resonator, sample, and VNA adapters – Fig. 3.24 (c)) due to the small size of the resonators and the applied time length of ∼10 min for thermal equalization.

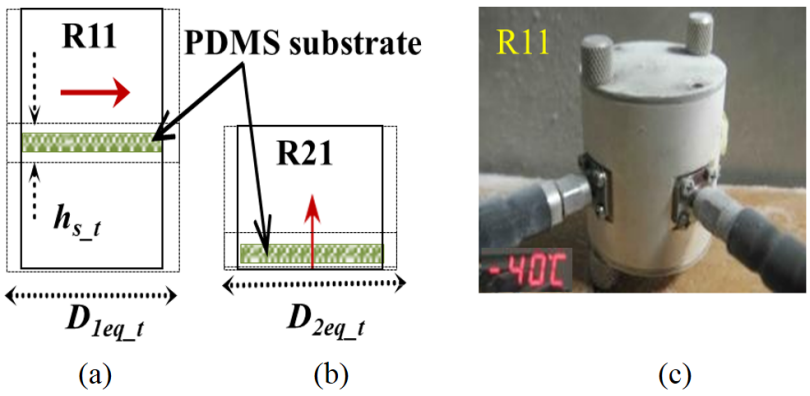

FIGURE 3.24: Schematic view of measuring resonators and samples at room temperature (solid lines) and high temperature (dashed lines): (a) R11; (b) R21; c) resonator R11 in a thermal chamber at –40° .

TABLE 3.6: Parameters of the Silver-Plated Measuring Resonators R11 And R21 and Planar RR in the temperature interval from –40°C to +70°C

t,°C	**Resonator R11** TE_{011}		**Resonator R22** TM_{010} **RR** $(p = 7)$		
	f_{01}, GHz Q_{01}	D_{eq1}, **mm** σ_{eq1}, **S/m**	f_{01}, GHz Q_{01}	D_{eq1}, **mm** σ_{eq1}, **S/m**	ϵ_m **(Isola Astra MT)**
–40	13.1659 16090	30.0182 2.21×10^7	7.6540 7080	29.9822 3.69×10^7	3.092
–20	13.1638 15555	30.0238 2.06×10^7	7.6503 6890	29.9969 3.49×10^7	3.093
0	13.1587 15490	30.0373 2.05×10^7	7.6492 6800	30.0013 3.41×10^7	3.095
+20	13.1555 14950	30.0457 1.91×10^7	7.6469 6573	30.0104 3.18×10^7	3.098
+40	13.1503 14730	30.0598 1.85×10^7	7.6448 6540	30.0186 3.15×10^7	3.102
+70	13.1448 14430	30.0743 1.78×10^7	7.6432 6410	30.0257 3.18×10^7	3.104

The new measurement procedure is as follows (due to the time-consuming and difficult measurements, only the resonators R11 and R21 are used at the lowest-order symmetrical modes TE_{011} and TM_{010}, respectively). To begin, each resonator R11 or R21 must be placed in the thermal chamber without any sample, and the resonance frequency f_0 and unloaded Q_0 factors determined for each temperature of interest. The values of the parameters $f_{0_{1,2}}$ and $Q_{0_{1,2}}$ vary with the temperature due to the linear thermal expansion of the resonator walls and their actual resistivity. Therefore, the actual equivalent diameters $D_{eq_{1,2}}$ (Fig. 3.24 (a), (b)) and equivalent conductivity $\sigma_{eq_{1,2}}$ can be determined. The resonator height has very little influence on the resonance parameters, as mentioned in [23] (see section 3.3.1). As a result, the reliable and accurate determination of $D_{eq_{1,2}}$ and $\sigma_{eq_{1,2}}$ allows to achieve high enough overall accuracy for extraction of the dielectric parameters of the sample at each temperature. The following expressions [203] can be used to determine the equivalent parameters of the empty resonators at each temperature:

$$D_{eq_1} = 356.648 H_1 (f_{0_1}^2 H_1^2 - 22468.9)^{1/2} \tag{3.7}$$

$$D_{eq_2} = \frac{229.48548}{f_{0_2}} \tag{3.8}$$

$$\sigma_{eq_{1,2}} = 3947.842 \frac{f_{0_{1,2}}}{R^2_{s_{1,2}}}, \tag{3.9}$$

where the surface resistances $R_{S_{1,2}}$ are expressed as

$$R_{s_1} = 1.879 \times 10^{-5} H_1 R^2_{eq_1} f^3_{0_1} \left(\frac{1}{Q_{0_1}}\right) \times \left[\frac{0.5H_1}{R_{eq_1}} - 1 + 2.9918 \times 10^{-5} (R_{eq_1} f_{0_1})^2\right]^{-1}, \tag{3.10}$$

$$R_{s_2} = 0.5 H_2 \left(\frac{2.40483}{R_{eq_2}}\right)^2 \left(\frac{1}{Q_{0_2}}\right) \times \left[5.56313 \times 10^{-5} f_{0_2} \left(1 + \frac{H_2}{R_{eq_2}}\right)\right]^{-1}, \tag{3.11}$$

All the geometrical dimensions $D_{eq_{1,2}}$ and $H_{1,2}$ in the expressions Eq. (3.7)-Eq. (3.11) are in mm, $f_{0_{1,2}}$ – in GHz, $R_{S_{1,2}}$ – in Ohms, and $\epsilon_{\sigma_{1,2}}$– in S/m. The actual measured resonance parameters for the used R11 and R21 resonators and equivalent parameters $D_{eq_{1,2}}$ and $\sigma_{eq_{1,2}}$ at different temperatures are presented in Table 3.6. The obtained variations are 5.1×10^{-4} and 4.0×10^{-4} mm/°C for $D_{eq_{1,2}}$ and $-3.9 \times 10^4$and $-4.6 \times 10^4 S/m/^\circ C$ for $\sigma_{eq_{1,2}}$.

The next step in the temperature characterization of PDMS substrate anisotropy is the measurements of the resonance parameters with samples, $f_{\epsilon_{1,2}}$ and $Q_{\epsilon_{1,2}}$, at the same temperatures at which the measurements of the empty resonators are performed. This set of new results allows the extraction of the pairs of dielectric parameters ($\epsilon_{par}/\epsilon_{perp}$ and $\tan\delta_{\epsilon_{par}}/\tan\delta_{\epsilon_{perp}}$) of each PDMS substrate. In this case, the actual sample thickness h_{s_t}, must be calculated as shown in Fig. 3.24 (a), (b). In the extraction procedure for the dielectric parameters (the same as in the case of room temperature), we take into account only the actual calculated thickness h_{s_t} due to thermal expansion along $0z$ (for PDMS sample CTE = 340 ppm/°C is accepted; once cured, the PDMS material keeps its CTE value); any changes in $0xy$ plane are not taken into account because they practically do not influence the final obtained results. The obtained results are presented in Table 3.7; they are averaged for two PDMS samples (instead of for five samples in Table

3.3 at room temperature). For that reason, the results for the room temperature (including anisotropy parameters ΔA_ϵ and $\Delta A_{\tan\delta_\epsilon}$ slightly differ in both tables. However, here to trace the temperature behavior of single sample and consider only relative changes are expected, not the absolute values (however, the pointed uncertainty at room temperature is related to the absolute values). The obtained results are fascinating (for more convenience, the corresponding temperature dependencies for the dielectric parameters are graphically presented in Fig. 3.25 for the frequency range 7-15 GHz). The first important fact is that both pairs of parameters ($\epsilon_{par}/\epsilon_{perp}$ and $\tan\delta_{\epsilon_{par}}/\tan\delta_{\epsilon_{perp}}$) decrease with increasing of t°C.

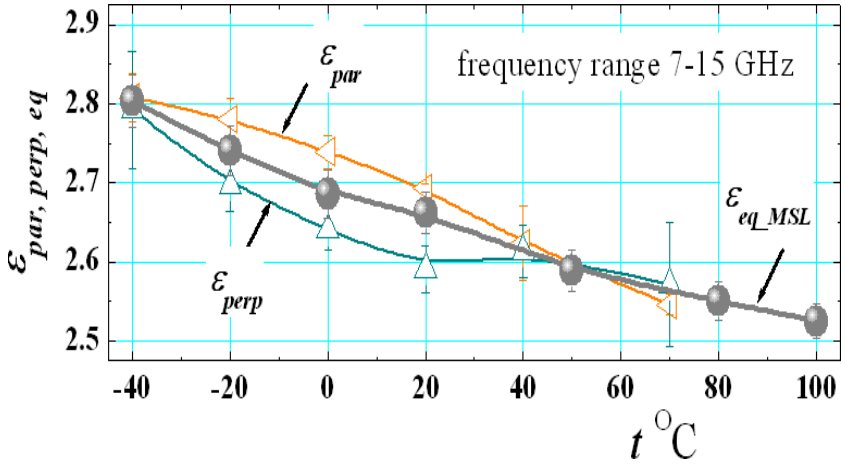

(a)

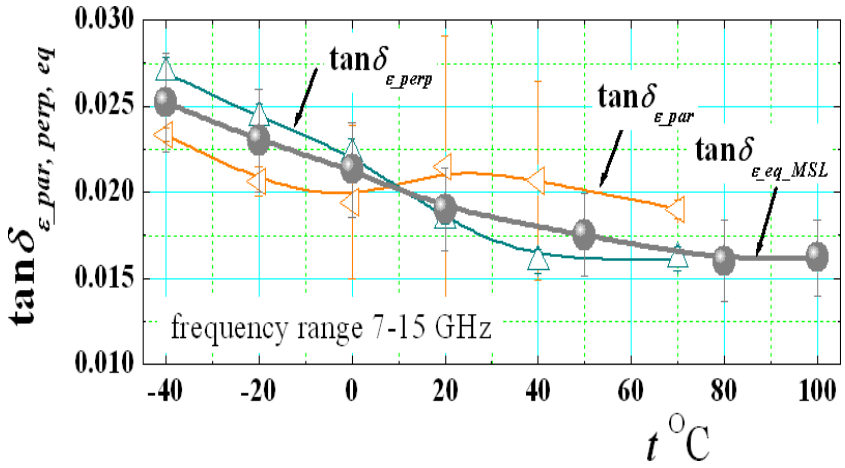

(b)

FIGURE 3.25: Temperature variations of parameters ϵ_{par}, ϵ_{perp} and ϵ_{eq}(MSL) (a) and $\tan\delta_{\epsilon_{par}}$, $\tan\delta_{\epsilon_{perp}}$ and $\tan\delta_{\epsilon_{eq}}$(MSL) (b) of PDMS substrates in the frequency range 7-15 GHz.

Actually, both dielectric constants vary from ∼2.8 at low temperature to ∼2.55 at high temperature (δ_ϵ/ϵ –850 ppm/ $^\circ C$), the values at room temperature are 2.70/2.59. Precisely at these temperatures (below –30°C and above +40°C), the anisotropy becomes negligible and this is a crucial circumstance to understand the origin of the anisotropy of this material. Actually, the observed anisotropy of the PDMS material occurs in the temperature range from –25°C to +30°C. The temperature behavior of the dielectric loss tangents is also very specific – at higher temperatures, it is observed that $\tan\delta_{\epsilon_{par}} > \tan\delta_{\epsilon_{perp}}$,while at lower temperatures – $\tan\delta_{\epsilon_{par}} < \tan\delta_{\epsilon_{perp}}$. This discussion will be continued after the characterization of the temperature behavior of equivalent parameters. As at room temperature, the method of covered ring resonators ($covRR$) is applied to trace the temperature dependencies of the equivalent parameters of PDMS substrate in MSL approximation. Two different setups for the temperature control are applied: in a big thermal chamber –40°C to +70°C and by a small Peltier system (Fig. 3.18(b)), which is powerful enough for the compact RR structure used in the experiments to cover the temperature interval 0-105°C with a single cooling/heating element. The substrate for the RR has been specially selected to be Isola Astra MT (20 mills) [210]. This low-loss substrate has a relatively low dielectric constant ($\epsilon_r \sim 3$), acceptable surface roughness, and little flexibility. Moreover, its CTE values are relatively small in both directions, namely $\text{CTE}_{xy} = 12$ ppm/$^\circ C$ and $\text{CTE}_z = 44.7$ ppm/$^\circ C$ below the glass transition temperature $t_g = 200^\circ C$ of this material.

Fig. 3.26 illustrates the temperature behavior of a resonance curve of selected TEM mode ($p = 18$) excited in RR of diameter 40 mm on substrate Isola Astra MT without and with PDMS sample in temperature range 0°C to +100°C, measured by the setup in Fig. 3.18(c). The corresponding resonance shifts are +0.088 MHz/°C for pure RR and –0.634 MHz/°C for covered RR, and these shifts allow accurate extraction of the frequency dependencies of the corresponding effective dielectric constants, $\epsilon_{eff_{MSL}}$ and $\epsilon_{eff_{covMSL}}$ and attenuations, α_{MSL} and α_{covMSL}, respectively (the results are combined and averaged between the measurements applying both considered methods for the temperature control – in the thermal chamber and by Peltier cooling/heating system). The extraction procedure is absolutely the same as described in detail for the room temperature in the previous section. The procedure

has been again applied twice at each fixed temperature – for uncovered and covered RR. By the measurement of pure RR, the procedure allows extraction of the actual equivalent dielectric constant ϵ_m on the used RR substrate (in this case, Isola Astra MT 3.0 – see the last column in Table 3.6 for TEM mode around 10.6 GHz; the relative shift is small, $\delta_\epsilon/\epsilon \sim +35.2$ ppm/$^\circ C$). The equivalent dielectric loss tangent of this substrate has not been extracted; in fact, the procedure is based on directly applying the results for the additional losses $\Delta\alpha = \alpha_{covMSL} - \alpha_{MSL}$ avoiding the influence of substrate and metallization and this is the vital advantage of the used method.

Fig. 3.28 presents the final results for the extracted frequency dependencies (5-30 GHz) of the equivalent MSL parameters of investigated PDMS samples in a wide temperature interval from –40°C to +70°C, namely $\epsilon_{eq_{MSL}}$ and $\tan\delta_{\epsilon_{eq_{MSL}}}$. The obtained data are reasonably compliant with the temperature dependencies in Fig. 3.25 of the same material for the frequency range 7-15 GHz). Again, it is observed a clearly expressed decrease of both equivalent parameters with the increasing of temperature – relative shifts δ_ϵ/ϵ -661 ppm/$^\circ C$ for $\epsilon_{eq_{MSL}}$ and $\delta\tan\delta/\delta$ –4060 ppm/$^\circ C$ for $\tan\delta_{eq_{MSL}}$ at 10 GHz. These temperature shifts (for the equivalent dielectric parameters, as well as for the parallel and perpendicular parameters) are probably related to the specific porous structure of the PDMS substrates.

We can argue that the higher dielectric constants and dielectric loss tangents at low temperatures result from the more significant influence of the polymer volume fraction of the material and decreased influence of the air gaps, while at higher temperatures, the influence of the air volume fraction increases. A similar approach can satisfactorily explain the observed small dielectric anisotropy of pure PDMS polymer samples and the possible influence of the substrate thickness on the absolute values of the dielectric parameters, which we observed in [21].

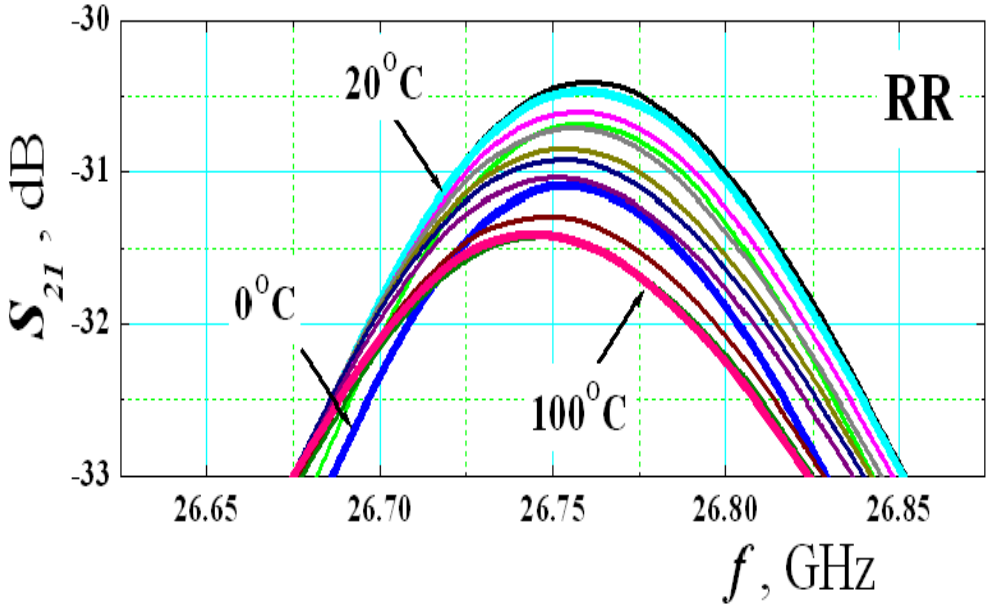

(a)

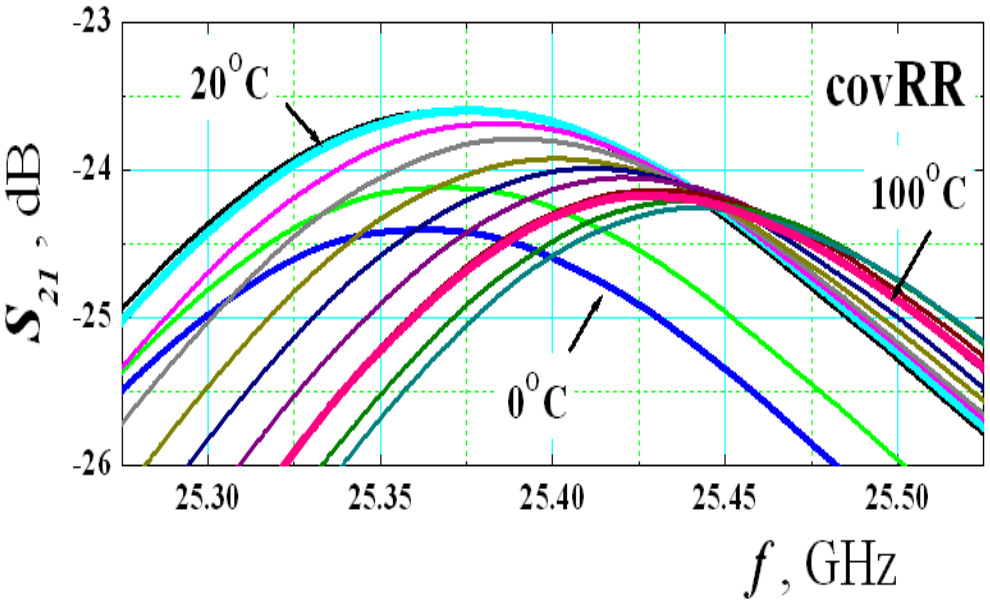

(b)

FIGURE 3.26: Resonance curves of a selected TEM mode (p = 18) excited in RR of diameter 40 mm on substrate Isola Astra MT (20-mills thick) without (a) and with PDMS sample (b) in temperature range 0° C to +100°C with step 10°C.

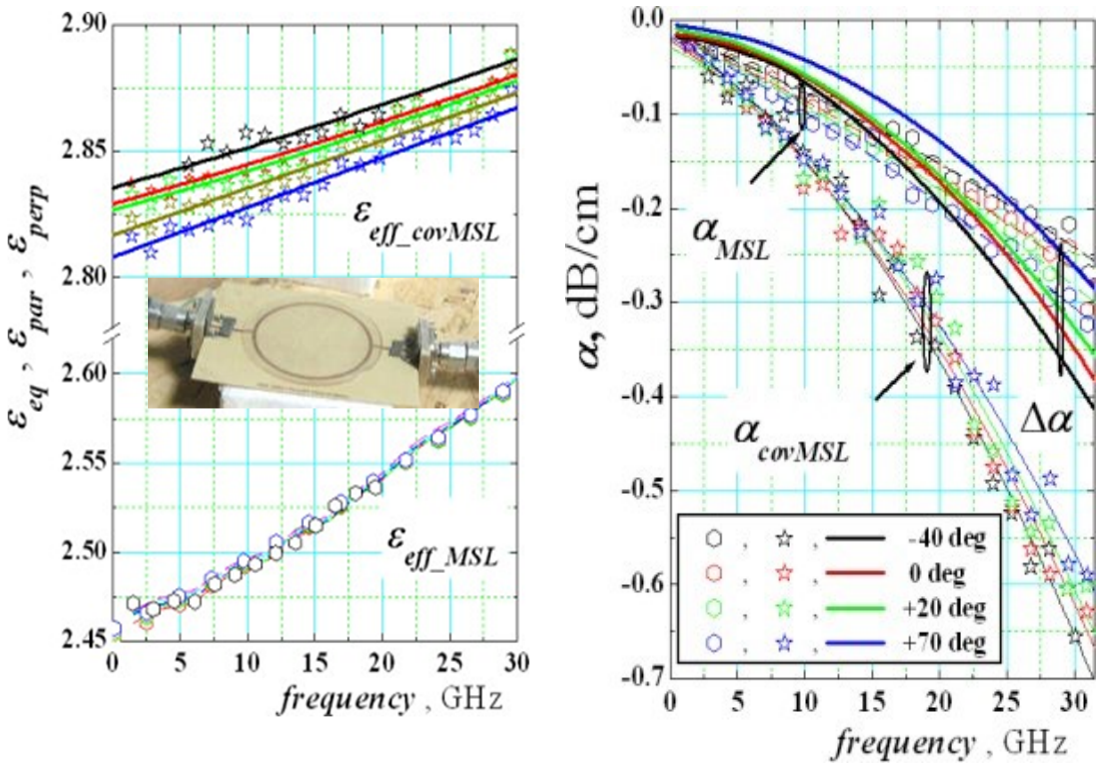

FIGURE 3.27: Measured effective dielectric constants (a) and attenuation (b) of MSL on substrate Isola Astra 3.0 without and with 0.75-mm thick PDMS sample (inset), $\epsilon_{eff_{MSL}}$, α_{MSL} and $\epsilon_{eff_{covMSL}}$, α_{covMSL}, in temperature range from –40° C to +70°C. The legend is the same as in the figure caption of Fig. 3.18

TABLE 3.7: Parallel, Perpendicular and equivalent parameters of PDMS substrates in the temperature range from –40°C to +70°C

$t°$**C**	h_{s_t}, **mm**	ϵ_{par} **(12.5 GHz)**	ϵ_{perp} **(7.5 GHz)**	ϵ_{eq} **(10 GHz)**	$\tan\delta_{\epsilon_{par}}$	$\tan\delta_{\epsilon_{perp}}$	$\tan\delta_{\epsilon_{eq}}$ **(MSL)**	$A_\epsilon; A_{\tan}, \%$
–40	0.730	2.808	2.792	2.803	0.0233	0.0270	0.0252	0.6; –15
–20	0.736	2.781	2.697	2.740	0.0206	0.0243	0.0230	3.1; –17
0	0.743	2.739	2.640	2.686	0.0194	0.0223	0.0213	3.7; –14
+20	0.750± 0.02	2.713 ± 0.010	2.590 ± 0.03	2.662 ± 0.03	0.0215 ± 0.008	0.0184 ± 0.007	0.0190 ± 0.005	4.6; 16
+40	0.760	2.623	2.613	2.589	0.0207	0.0160	0.0175	0.4; 26
+70	0.767	2.545	2.571	2.550	0.0190	0.0161	0.0160	1.0; 17

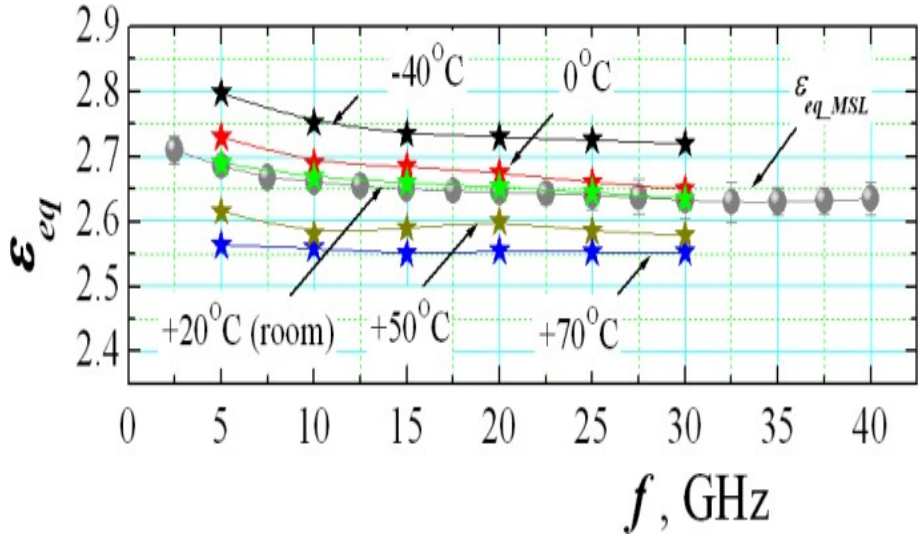

(a)

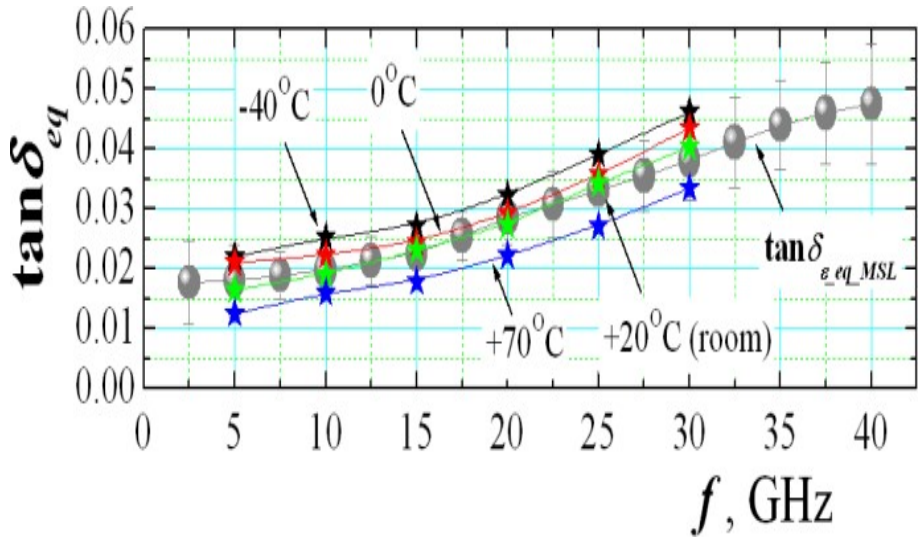

(b)

FIGURE 3.28: Extracted frequency dependencies of the parameters $\epsilon_{eq_{MSL}}$ (a) and $\tan\delta_{\epsilon_{eq_{MSL}}}$ (b) of PDMS substrate for MSL approach in the temperature interval from –40°C to +70°C. The new dependencies are compared with the corresponding averaged dependencies at room temperature (from Fig. 3.19.)

3.5 Conclusion

In this chapter, two experimental methods are applied to characterize the dielectric properties of flexible PDMS substrate. A weak uniaxial anisotropy has been observed for the first time; the parallel dielectric constant is $\sim 5.8\%$ larger than the perpendicular dielectric constant $\epsilon_{par} > \epsilon_{perp}$ mean values $\epsilon_{par} \sim 2.71$ and

$\epsilon_{perp} \sim 2.558$ in the frequency range 6-38 GHz; the corresponding averaged dielectric loss tangents are $\tan\delta_{\epsilon_{par}} \sim 0.027$ and $\tan\delta_{\epsilon_{perp}} \sim 0.0197$ in the same frequency interval. For this popular PDMS polymer which can be considered as a flexible substrate for wearable/flexible antenna and sensor applications, the expressed frequency dependence of the corresponding dielectric parameters ($\epsilon_{par} \sim 2.82 - 2.7$; $\epsilon_{perp} \sim 0.73 - 2.52$) in the frequency range 1-40 GHz have been obtained. The results obtained by the first proposed two-resonator method lie in the range of 6-38 GHz. A set of auxiliary resonance and waveguide methods have been used to extend this interval below 1.6 GHz and over 40 GHz, confirming the obtained results for the measured anisotropy. This is an unusual property for such types of polymers, but comparisons with other organic materials with isotropic behavior support the veracity of the results obtained (the measured "anisotropy" of PTFE is $\sim 1.03\%$, while the near-isotropic Cyclo Olefin polymer has anisotropy of $\sim 1.47\%$). According to obtained results, the measured anisotropy could be partially related to the porous internal structure of the PDMS samples. The first time obtained temperature dependencies on the dielectric constant of PDMS polymer in the temperature interval –40/+70°C validate this notion. They show that measurable uniaxial anisotropy of this material with a large linear temperature coefficient for expansion occurs mainly in the temperature range –30/+40°C and the parameter ϵ_{eq} in Ku band vary from 2.81 at –40°C (where the polymer fraction dominates) to 2.52 at +70°C (where the air-gap effects are stronger).

The second applied method using microstrip ring resonators covered by the sample is well suited for flexible and non-metalized samples. It allows the determination of the equivalent dielectric parameters of the anisotropic sample when it can be considered as an isotropic one. The measured equivalent isotropic dielectric constant for PDMS polymer is $\epsilon_{eq} \sim 2.656$ ($\epsilon_{par} > \epsilon_{eq} > \epsilon_{perp}$) and equivalent dielectric loss tangent $\tan\delta_{eq} \sim 0.023$ in the frequency interval 2-36 GHz. Both of the acquired results are in good compliance with the considered PDMS material. The complete analysis and investigations performed in this chapter demonstrate that PDMS could be a viable choice as a substrate material for flexible/wearable antenna and sensor applications having required dielectric characteristics. The presented methods can also be utilized for the characterization of other similar flexible

substrate materials. Because of the importance of the problem for such widely used polymers, further research in these fields should be pursued in order to apply this effective characterization approach to other polymers and polymer-based materials.

Chapter 4

Bending Effects of Flexible Antenna Substrates

4.1 Introduction

In order to design an efficient flexible antenna, it is important to check the factors that might affect the performance of an antenna when it is used for wearable application. Two important factors, the dielectric parameters and anisotropy of flexible substrates were already discussed in chapter 3. The next crucial factor to be considered is the bending effect (or conformal geometry) of the substrates [211].

Some of the research papers dealing with the design of such antennas using textile or polymer substrates generally consider bending effect at typical radii, compliant with the human body [212–215]. The degree of bending is measured using the curvature radius (R_b), which represents the radius of an imaginary cylinder used to represent the antenna bending [216]. The majority of the research publications just recorded the bending effect on the working frequency and/or frequency bandwidth (typically a decrease of the resonant frequency), and rarely its influence on the gain and radiation pattern is quoted. Many times, unexpected discrepancies are detected between the simulated and measured results because of bending [214] explained by imperfect measurements. Only a few researchers have explained the nature of the bending effect.

To understand the bending effect, it is crucial that the measurements are well performed. For example, in [212] the authors explained that the thickness of the

substrate material is crucial for the degree of the bending influence. The optimal thickness for minimizing the bending effect over the frequency shift is about 6 mm for the flexible substrate as felt with $\epsilon_r = 1.3$ and thickness 0.5–12 mm. In [217], the authors have provided beneficial results to understand the bending effects using a rectangular patch antenna on denim substrate. At 2.4 GHz, the considered parameters of this material with thickness 2 mm are $\tan\delta_{\epsilon_{Denim}} = 0.01$ and $\epsilon_{r_{Denim}} = 1.6$. The authors had shown using simulations that in the rectangular patch antenna, the lowest-order TM_{10} mode's resonance frequency should continuously increase with increasing the bending radius R_b, with a relatively low degree for the width-bent patches and with a higher degree for the length-bent patches. However, the measured results are slightly different from the simulations, as relatively big ripples appeared as the experimental frequency shifts around ±2.5 MHz for width-bent and ±85 MHz for length-bent patches (in comparison to the flat patches resonance frequency ∼2.4 GHz). Moreover, the tendency of increment in the resonance frequency is noticeable. The authors attributed this discrepancy to other physical properties of the conductive textile material that were not accurately replicated in simulations when it was bent.

In [53], the authors have considered both, bending of the flexible substrate and its anisotropy and proposed that they can simultaneously affect the resonant properties of the flexible antennas. They have used rectangular resonators on isotropic substrates to present their result, but the influence of the substrate anisotropy was not separately investigated. Also, except some estimations of the mutual coupling, input impedance, and return losses S_{11} [218, 219] in anisotropic substrate-based cylindrically conformal patch antennas, anisotropy and bending effects are not investigated in parallel in any other research. In this chapter, more deeper investigations of the opposite impacts of the dielectric anisotropy and bending of the flexible substrates on the resonance characteristics of planar radiators are performed.

In this research, in order to avoid any parasitic influence of the feeding lines, patches and antennas with feeds are not considered, but pure resonant structures are examined. The novel results for the frequency shift of the modes in planar rectangular resonators and their modifications are from the performed simulations and measurements, allowing for the separation of the effects of anisotropy and

bending as well as the independent characterization of the degree of these effects.

A methodology has been proposed in this chapter for the accurate measurements of the bending effects on the resonance characteristics of the planar resonator. Then, for separate numerical investigations of the bending and anisotropy as well as both effects together, an effective procedure is introduced for creating suitable 3D models of planar resonators. Data for the measured anisotropy of selected flexible anisotropic and isotropic materials used in this research is calculated using the methods described in chapter 3. The obtained results for the separate and simultaneous influence of the anisotropy and bending for materials with different anisotropy and bent at different radii are described in the results and discussions part of this chapter. Finally, the origins of the considered competing effects on the resonance planar structures are discussed and practically useful conclusions are offered.

4.2 Bending Measurement Procedures for Planar Resonators using Flexible Substrates

To perform the accurate measurements of the bending in the flexible/wearable structures is a challenging task due to the strong mechanical changes during bending, like deformations in the substrates, metal layout and the feeding line, which can affect the resonance behavior of the structure. In order to investigate only pure resonant structures, in this research, coaxial probes are applied in the planar structures to excite the lowest-order resonances. In flat and bent microstrip resonators, the simulated E-field pattern for the first two planar modes is shown in Fig. 4.1. The coaxial probes with a short coaxial pin orientated along the E field (electric type) should be put close to the E-maximums. In this research, more stable coaxial magnetic loops are applied in close vicinity to the magnetic field's H-maximums of the corresponding mode, as shown in Figs. 4.2 (a), (b), and (c) for TM_{10} mode, TM_{01} mode and for both modes, respectively. The vector network analyzer (KEYSIGHT N9928A VNA) performs the measurements in the L and S bands in the transmission regime. During the measurements, the loops' orientation and placement are fine-tuned until the transmission losses S_{21} increase

more than -40 dB. At these conditions, the measured resonance frequencies achieve a satisfactory level of accuracy and practically become independent of the loop proximity.

In the presented research, self-adhesive 0.05-mm thick metal (Al or Cu) folio is applied to form the resonator layout. At first, the measurements are performed in the flat position of the resonator and then measuring the bent resonator with a continuous decrement of the bending radius. The resonator substrates are bent over a set of smooth metallic cylinders with radii R_b from 80 to 12.5 mm. As illustrated in Fig. 4.2, three types of bending are applied: length-(L), width-(W) and diagonal-bent (D) resonators. While bending, special care is taken to ensure that the metallization remains well adhered to the substrate with no detachment. As a result, measurements are performed only for decreasing bending radius and not in reverse order. A new fresh resonator folio is used for the realization of each of these pointed bending types. The results for the ratio between the resonance frequencies for the bent and flat resonators are presented in this research.

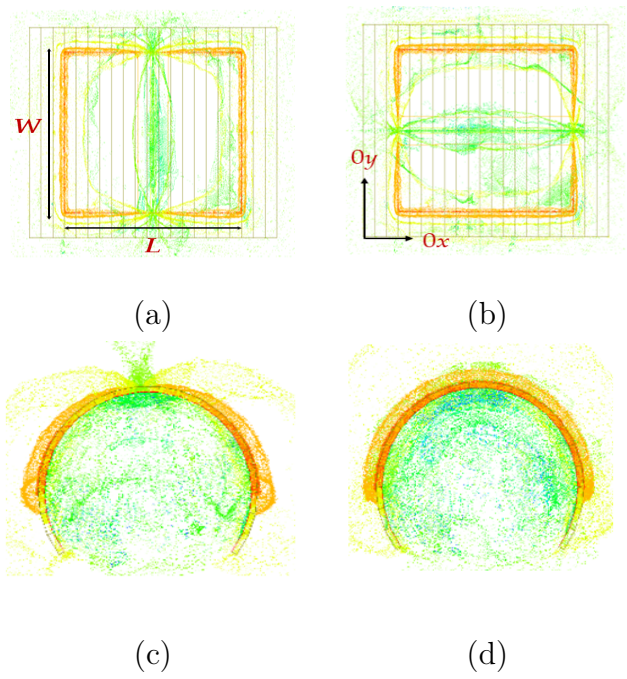

FIGURE 4.1: E-field simulation pattern: (a,b) TM_{10} and TM_{01} in a flat microstrip resonator; (c,d) TM_{10} and TM_{01} in a bent microstrip resonator. Legend: L—length; W—width.

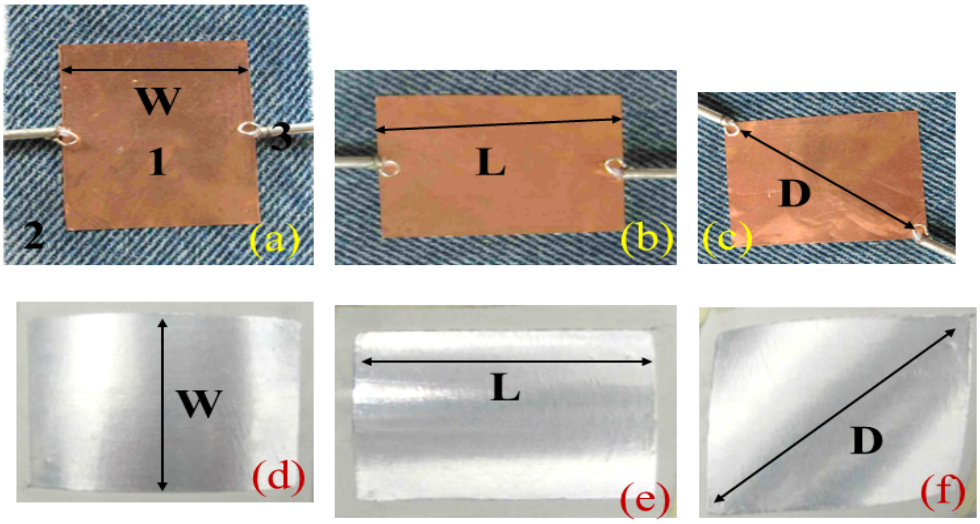

FIGURE 4.2: Planar resonator with a (a–c) pair of magnetic coaxial loops placed on the length (L), width (W), and diagonal (D); (d–f) L-bent, W-bent, and D-bent microstrip resonators (Legend: 1 –resonator; 2—substrate; 3—pair of magnetic coaxial probes).

4.3 Numerical Models for Investigations of Bent Planar Resonators on Anisotropic Substrates

The anisotropic materials can be introduced with the help of available options in most of the modern electromagnetic simulators, but this cannot be easily performed directly for the case of conformal planar structures when the substrate is introduced as a single object and accurate determination of the anisotropy. Therefore, in this research a geometrical approach is preferred.

Several slices in the form of prisms are used to equally divide the anisotropic substrate (having a trapezoidal cross-section view for the bent resonators and rectangular cross-section view for the flat resonators). These slices as the whole substrate have equal anisotropic properties, but the parallel and perpendicular directions are used to determine the uniaxial anisotropic dielectric parameters that can be controlled now for each slice with the change of the bending radius as shown in Fig. 4.3 for the half of structures. The chosen concrete width w_s of the slices is equal to 2 mm in the presented research, however this might be reduced for thicker substrates or smaller bending radii for better fitting of the bent substrate cross-section. The other chosen sizes are height h_s and length $l_s = W_s$. Fig. 4.4 illustrates the 3D

views of flat and bent microstrip resonators on sliced anisotropic substrates. During the bending, the rule to keep the resonator dimensions L and W is satisfied. The ground and slices, on the other hand may undergo some deformations.

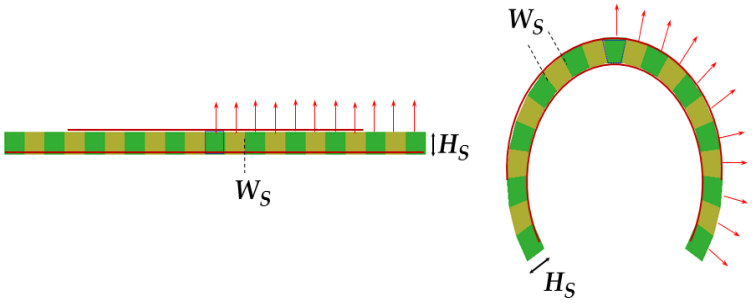

FIGURE 4.3: Microstrip resonators: Flat and bent on substrate constructed by sliced prisms, each with its own anisotropic characteristics. In flat and bent substrates, arrows denote the normal direction in each slice.

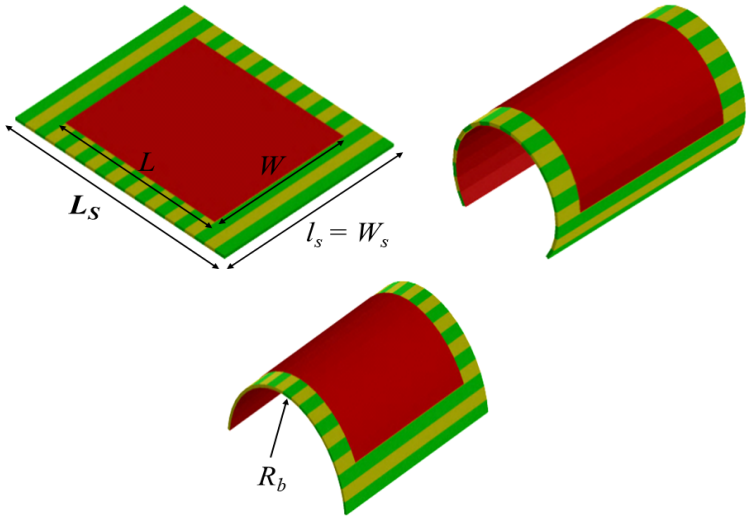

FIGURE 4.4: Flat and bent microstrip resonators (3D view) with width W = 26 mm and length L = 30 mm on sliced substrates having length L_s = 42 and width W_s = 34 mm (bending radius R_b = 14.3 and 9.6 mm in the last two cases).

4.4 Materials Used in the Research

Different isotropic and anisotropic flexible substrate materials as per the requirements of the presented research are selected as shown in table 4.1.

TABLE 4.1: Measured values of dielectric parameters and anisotropy of selected materials for this research (averaged values for the frequency interval 6–13 GHz).

Material	h_s, **mm**	$\epsilon_{par}/\tan\delta_{\epsilon_{par}}$	$\epsilon_{perp}/\tan\delta_{\epsilon_{perp}}$	$\Delta A_\epsilon/\Delta A_{\tan\delta_\epsilon}$; %
Group 1: Textile and polymer samples				
Denim	0.90	1.74/0.048	1.61/0.030	7.8/38
Linen	0.65	1.65/0.043	1.58/0.044	4.3/-2.3
Waterproof fabric with breathability GORE-TEX®	0.20	1.53/0.0057	1.38/0.0043	10.3/28
Polydimethylsiloxane (PDMS)	0.70	2.73/0.022	2.57/0.019	6.00/15
Group 2: Flexible isotropic and near-to-isotropic samples				
Polytetrafluoroethylene (PTFE)	0.45	2.05/0.00027	2.04/0.00026	0.49/3.8
Polycarbonate (PC)	0.50	2.77/0.0056	2.76/0.0055	0.36/1.8
Silicone elastomer	0.90	2.21/0.0010	2.19/0.0008	0.91/22
Ro3003	0.51	3.00/0.0012	2.97/0.0013	1.0/-8
Group 3: Relatively flexible anisotropic reinforces substrates				
Ro4003	0.21	3.67/0.0037	3.38/0.0028	8.2/28
NT9338	0.52	4.02/0.005	3.14/0.0025	24.6/67
Group 4: Relatively flexible anisotropic soft ceramics				
Ro3010	0.645	11.74/0.0025	10.13/0.0038	14.7/-41

These selected materials are divided into four groups, the first group consists of several textile and polymer samples with different degrees of anisotropy (ΔA_ϵ from 4.3 to 10.3), the two-resonator method (described in chapter 3) is applied for the measurements. In Table 4.1 (upper section), the measured values for the pairs of parameters $\epsilon_{perp}/\tan\delta_{\epsilon_{perp}}$ and $\epsilon_{par}/\tan\delta_{\epsilon_{par}}$, as well as for the uniaxial anisotropy $\Delta A_\epsilon/\Delta A_{\tan\delta_\epsilon}$ are presented. The second group consists of different flexible isotropic substrates chosen for measuring the pure bending effect. These materials have very small anisotropy, $\Delta A_\epsilon < 1\%$. The representatives of relatively flexible reinforced substrates and soft artificial ceramics are included in the last two groups. Their anisotropy ΔA_ϵ varies in a large interval- 8.2–24.5%.

4.5 Results and Discussion

In this section, the obtained results are discussed in the corresponding subsections. The first subsection presents the numerical and experimental results for the pure

bending effect in planar resonators on flexible isotropic and near-to-isotropic substrates (4.5.1). In the next subsection, the obtained results are verified using the assumption that the bending effect and substrate anisotropy have opposite effects on the flexible/wearable radiators and sensors (4.5.2).

4.5.1 Bending Effect

The investigated bending effect for different flexible/wearable planar patches and devices, usually masked by certain phenomena (as mentioned in the Introduction section) are usually not considered and addressed in the simulations [214, 215]. Here, in this research, pure resonance structures are used (to minimize the effects of the feeding lines) to address and solve all these issues on the experimentally proven pure flexible isotropic substrates. The accurate measurement procedure described in detail in section 4.2 is followed. In this research a new measurement parameter curvature angle α_C (Fig.4.5), which is the angle between the neighbor slices used to construct the substrate is used to measure the degree of bending. The dependencies of the ratio of resonance frequencies for bent and flat rectangular resonators on pure isotropic substrate f_{bent}/f_{flat} for the lowest-order TM_{10} mode versus the curvature angle α_C, are shown in Fig. 4.6 (a). Fig.4.5 shows the structural geometry and relationship between bending radius R_b and curvature angle α_C (for example, $\alpha_C = 4^\circ$ that corresponds to $R_b = 28.7$ mm; $\alpha_C = 8^\circ$ corresponds to $R_b = 14.3$ mm; $\alpha_C = 12^\circ$ corresponds to $R_b = 9.6$ mm, etc.). The obtained results show the known fact [217] that the resonance frequency of the length (L)-bent resonator increases in comparison to the flat resonator for pure isotropic substrates, but this dependency is not linear exactly. At the same time, the effect of bending is relatively small for width (W)-bent resonators, which is also an expected result. The obtained dependencies correspond to the classical "positive" bending ($\alpha_C > 0$). When the material bends, mechanical deformations occur, for example shrinking at the bottom area (to the ground) and stretching at the top (to the resonator). In the proposed model, this effect is taken into account by changing the cross-section shape of the separate slices from rectangular to trapezoidal, as shown in Figs. 4.3 and 4.5 (a). The narrow side of the trapezoid is oriented to the ground of

the resonance structure. The proposed model thus confirms the assumption that as compared to the geometrical length L (shown by the dashed line in Fig. 4.5 (a)), the electrical length L_E of the L-bent resonator decreases. The increase of the resonance frequency with the increase of curvature angle α_C is explained well by the localization of the standing wave of the lowest order TM_{10} mode exactly along the curvature in the L-bent structures as shown in Fig. 4.1 (a) and (c). The standing wave, on the contrary is located in a perpendicular direction during the W-bending and the bending influence is negligible, especially for thin substrates.

Fig. 4.6 (a) also illustrates the "negative" bending ($\alpha_C < 0$) effect. This effect is just the opposite and it confirms the origin of the bending effect for the flexible and wearable structures. For this case, the narrow side of each slice's trapezoid is orientated to the resonator layout of the resonance structure and in comparison, to the geometrical length L, the effective electrical length L_E of the L-bent resonator increases and the corresponding resonance frequency decreases. This type of bending is very rare so, it is not discussed in detail here.

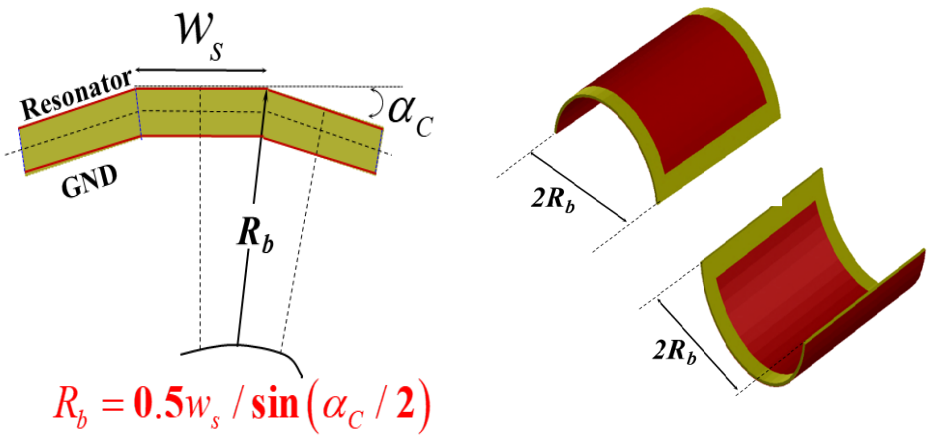

FIGURE 4.5: (a) Relationship between bending radius R_b and curvature angle α_C ; dashed middle line in the resonator substrate represents the formation of the effective electrical length of the resonator; (b) positive ($+\alpha_C$) and negative ($-\alpha_C$) bent substrate resonance structures (the bending radius R_b is always determined to the side of the resonator layout).

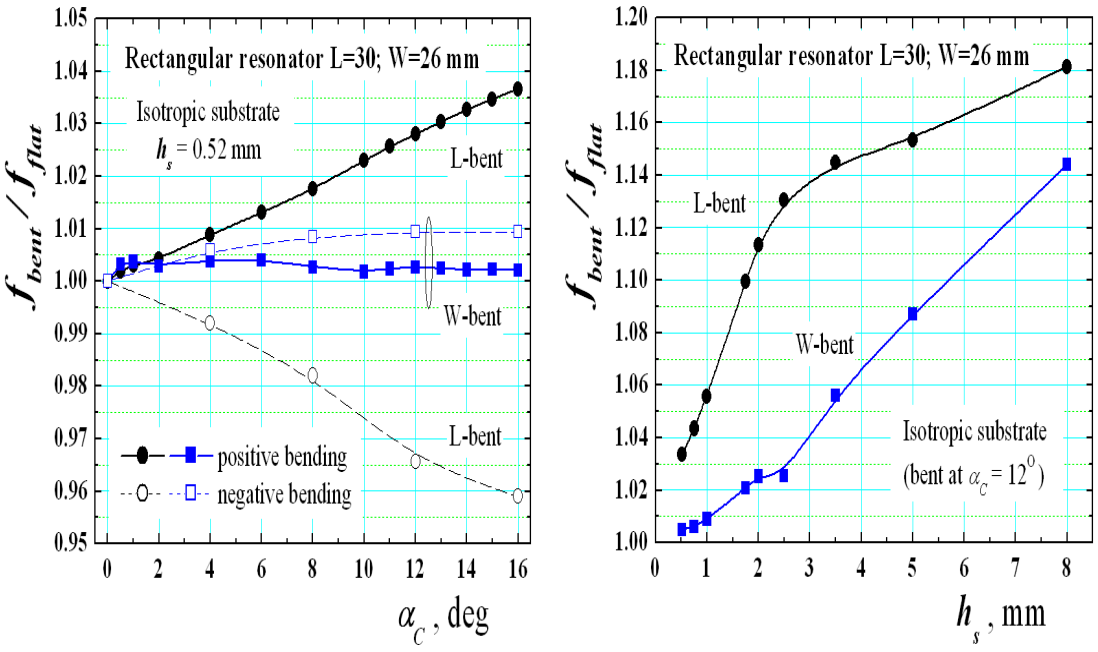

(a) (b)

FIGURE 4.6: Numerical dependencies between (a) the curvature angle α_C between the substrate slices and (b) substrate thickness h_s and the ratio between the bent and flat rectangular resonator on isotropic substrate resonance frequencies f_{bent}/f_{flat} of the lowest-order TM_{10} mode. The isotropic dielectric constant is set to 3.0, but its concrete value has negligible influence. Positive and negative curvature angles are employed.

At last, the variations of the bending effect in substrates with different thicknesses are presented additionally in Fig. 4.6 (b). For a thickness range of 0.5–2.5 mm, the bending effect now increases significantly, and eventually saturation occurs for L-bent structures (a relatively substantial increase is also observed for W-bent structures at more significant thicknesses). However, as shown in [212], the existence of an optimal thickness where the bending effects are minimized cannot be observed.

These tendencies are proved experimentally in this next step. Fig. 4.7 illustrates a set of measurement results for the ratio of resonance frequencies f_{bent}/f_{flat} in bent and flat rectangular resonators of the lowest-order TM_{10} mode on several isotropic substrates versus the bending radius R_b having three types of dependencies- for L, W, and D-bent resonators. All these obtained results resemble closely with the

results obtained from the numerical simulations shown in Fig. 4.6 (a) (D-bent resonators are not simulated). They depend on substrate flexibility and deformations. The best results are obtained for the flexible silicone elastomer ($h_s = 0.9$ mm), as shown in Fig. 4.7 (c). The results obtained by Ro3003 substrate ($h_s = 0.52$ mm) are also good, as shown in Fig. 4.7 (a); on the other hand, for small bending radii, this soft substrate went to technological stretching with a slight decrement in f_{bent}. Better stability is presented by the harder substrate PC ($h_s = 0.5$ mm) at low R_b. The obtained results for the flexible PTFE substrate ($h_s = 1.0$ mm) varies from the theoretical dependencies due to their poor adhesion properties to the metal folio. However, a similar material to PTFE with the commercial mark Polyguide® Polyflon ($h_s = 1.5$ mm) shows a better behavior. For all these presented cases, the curves obtained for D-bent substrate materials (moderate influence) lie in between the curves obtained for L-bent (upper curves; stronger influence) and W-bent substrates (lower curves; smaller influence). It can be deduced from these measurements that the experimental results fully confirm the numerical simulations for the pure bending effect on the isotropic substrate-based planar resonators, taking into account the substrate deformation during the bending at very small radii R_b.

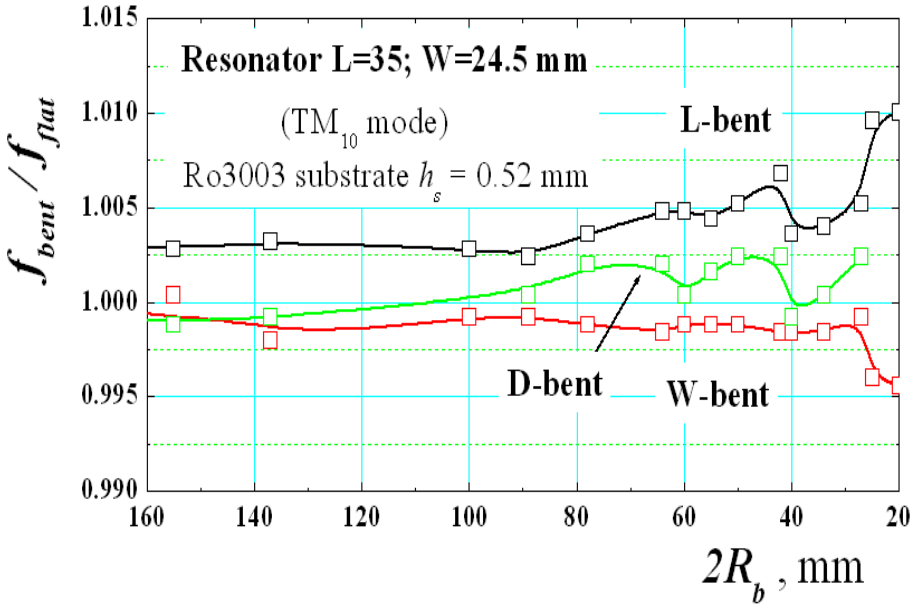

(a)

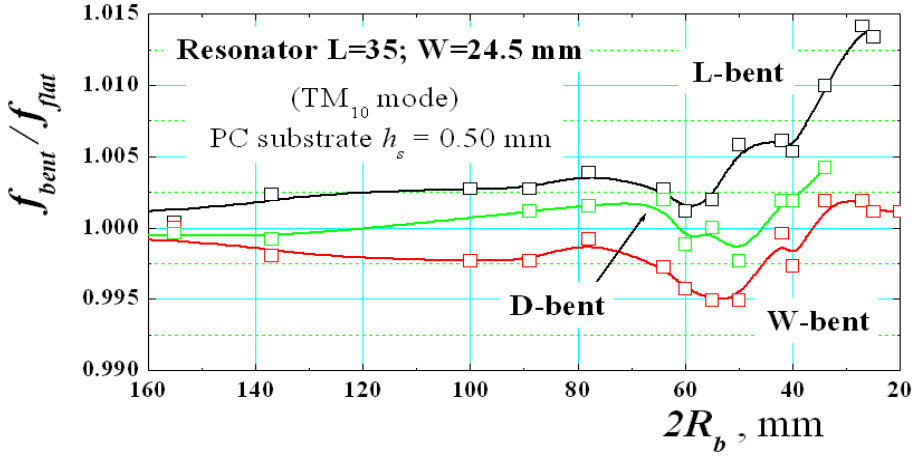

(b)

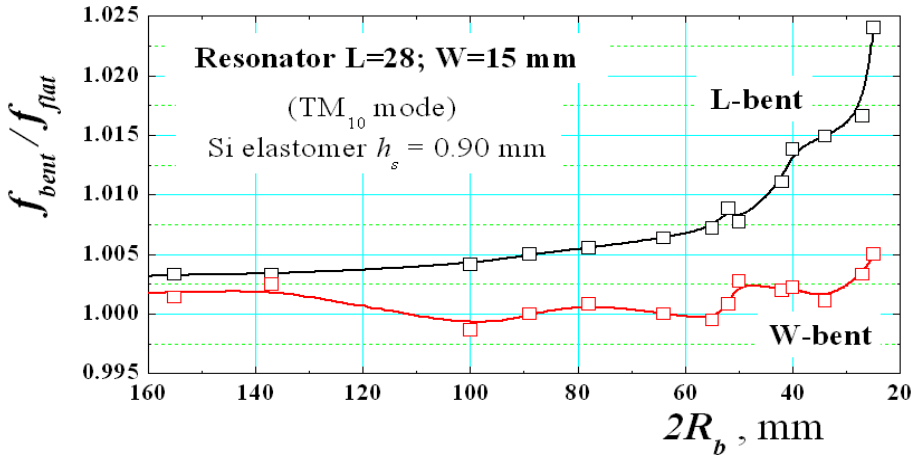

(c)

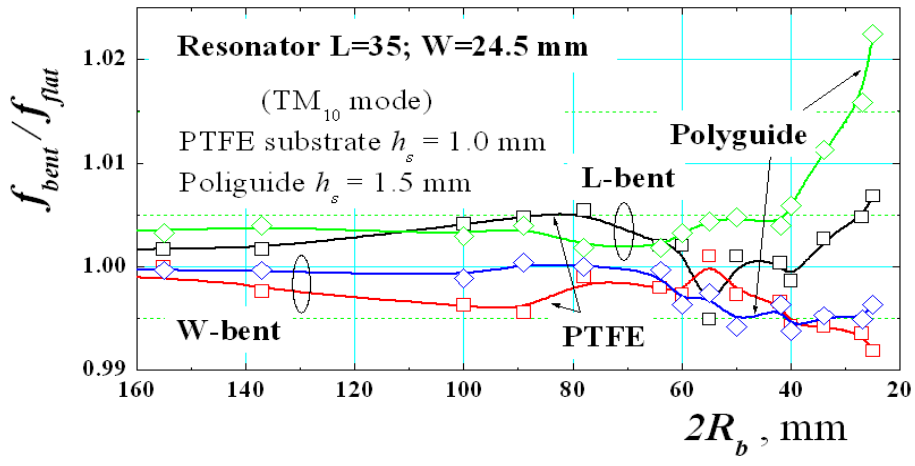

(d)

FIGURE 4.7: Experimental dependencies between ratio of the lowest-order TM_{10} mode's resonance frequencies f_{bent}/f_{flat} and the bending radius R_b for bent and flat rectangular resonators on several isotropic substrates: (a) Rogers (Ro3003); (b) Polycarbonate (PC); (c) commercial silicone elastomer; (d) Polytetrafluoroethylene (PTFE) and Polyguide® Polyflon (ref: http://www.polyflon.com; dielectric parameters 2.05/0.00045).

4.5.2 Investigation of the Simultaneous Effects of Anisotropy and Bending of Planar Resonators

This section presents the analysis of simultaneous effects of anisotropy and bending of planar resonators. It is important to assess the influence of anisotropy in the flat resonators initially. The simulated dependence of the ratio of the resonance frequencies $f_{flat_{aniso}}/f_{flat_{iso}}$ of TM_{10} and TM_{01} modes for flat rectangular resonators on anisotropic ($\Delta A_\epsilon \sim 25\%$) and isotropic substrates versus the substrate thickness h_s are shown in Fig. 4.8 (a). The result is noticeably ineffective. The resonance frequency shift by 1–1.5% due to anisotropy influence only for reasonably thick substrates, which is why this feature is not widely used in patch antenna design. The reason is simple: parallel E fields (which have a noticeable influence of the ϵ_{par} component) emerge only near the edge of such a wide planar structure and in comparison to the microstrip line, the relative effect is essentially non-existent [195].

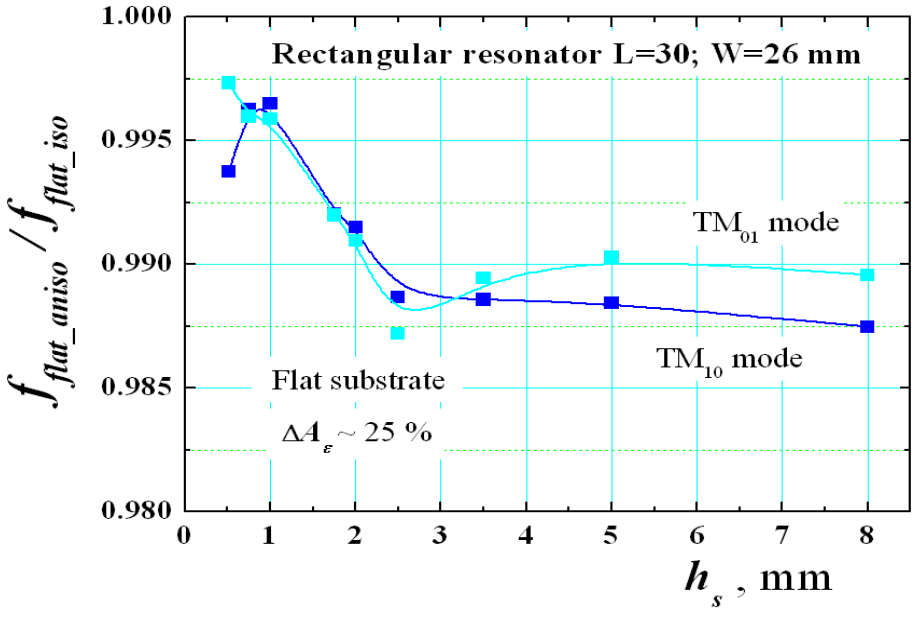

(a)

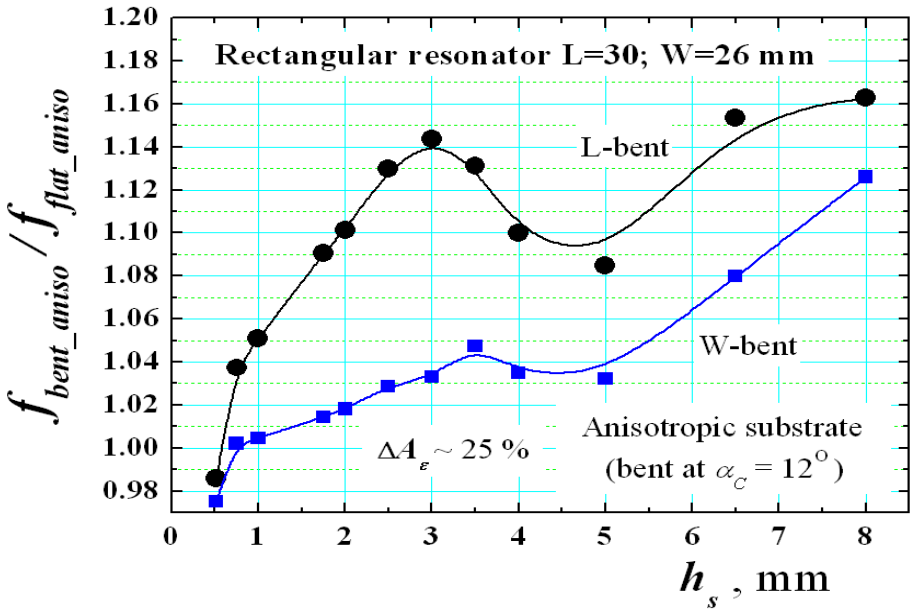

(b)

FIGURE 4.8: (a) Numerical dependencies between the ratio of resonance frequencies $f_{flat_{aniso}}/f_{flat_{iso}}$ of TM_{10} and TM_{01} modes for flat rectangular resonators on anisotropic and isotropic substrate and the substrate thickness h_s . (b) Numerical dependencies between the ratio of resonance frequencies $f_{bent_{aniso}}/f_{flat_{aniso}}$ of TM_{10} mode for bent (L/W) and flat rectangular resonators on anisotropic substrates and the substrate thickness h_s .

However, when the resonators are bent, a stronger effect is expected. In order to perform the more profound research, the 3D models as shown in Figs. 4.3 and 4.4 are used to simulate a set of bent resonators. Fig. 4.9(a) (firstly) shows numerical dependencies between the ratio of resonance frequencies $f_{bent_{aniso}}/f_{bent_{iso}}$ of TM_{10} mode for L-/W-bent rectangular resonators and the curvature angle α_C. The anisotropy ΔA_ϵ of the substrate is chosen to be small (∼3.5%), moderate (∼ 11%), and large (∼ 25%). This ratio is not quantifiable, but it depicts the effect of anisotropy in bent resonators in its purest form. The obtained results reveal, for the first time, that this influence is significantly more than in the flat case (up to -5% moves downward). The effect of substrate anisotropy reduces the resonance frequency compared to the hypothetical case of an isotropic bent substrate, as shown by the provided dependencies. As a result, it can be deduced that the influence of the substrate's anisotropy is the polar opposite of the effect of bending (as is shown in Fig. 4.6(a)). This was the initial hypothesis used in

the presented research, and it can be deemed mathematically validated. Therefore, it can be expected that both effects can strongly change the behavior of these dependencies.

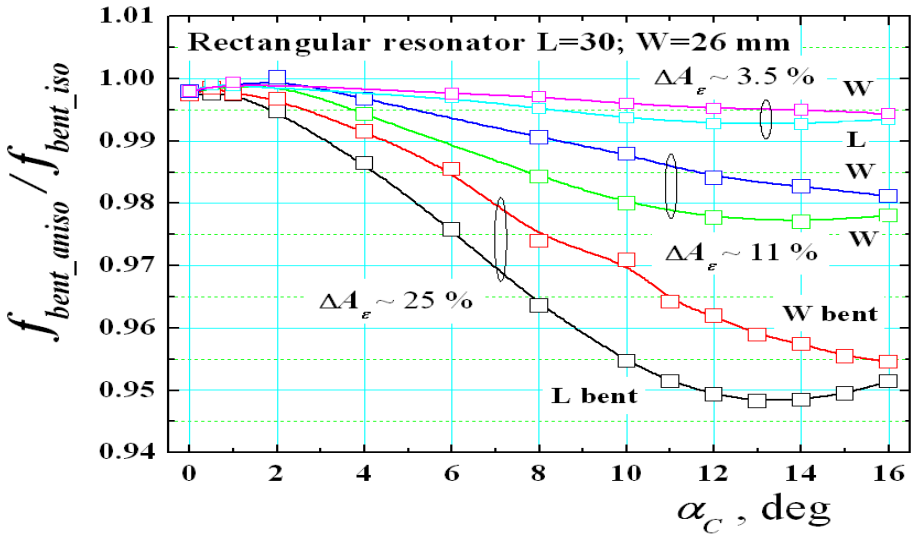

(a)

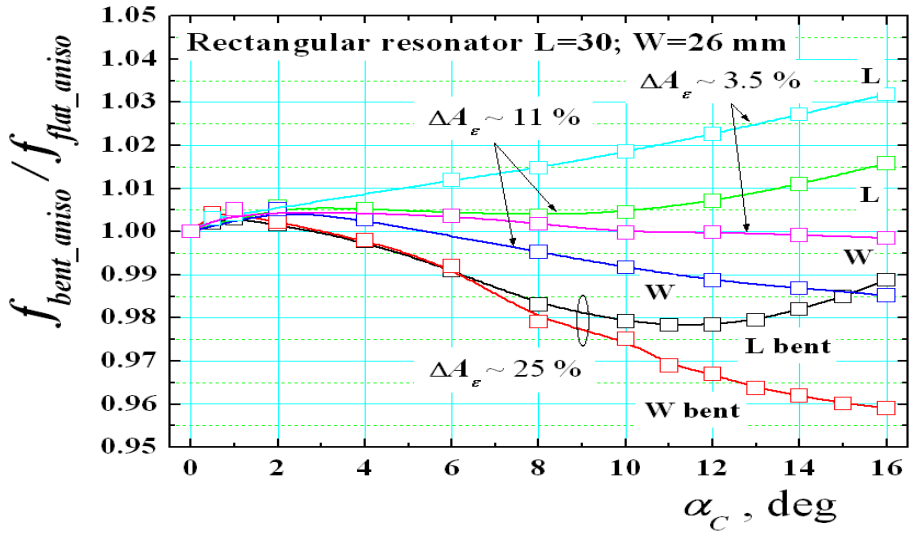

(b)

FIGURE 4.9: (a) Numerical dependencies between the ratio of resonance frequencies $f_{bent_{aniso}}/f_{bent_{iso}}$ of TM_{10} mode in bent (L/W) resonators on anisotropic and isotropic substrates with $h_s = 0.52$ and the curvature angle α_C ; (b) Numerical dependencies between the ratio of resonance frequencies $f_{bent_{aniso}}/f_{bent_{iso}}$ of TM_{10} mode in bent (L/W) and flat rectangular resonators on anisotropic substrates and the curvature angle α_C .

For length (L)/width (W) bent rectangular resonators on anisotropic substrates, the ratio of resonance frequencies $f_{bent_{aniso}}/f_{flat_{aniso}}$ of TM_{10} mode and the curvature angle α_C is shown in Fig. 4.9 (b). This ratio is now quantifiable and can be verified experimentally. The new dependencies reveal that, depending on the actual parameter ΔA_ϵ, the resonance frequency shift in a resonator on realistic (anisotropic) substrates can have both positive and negative values, which is impossible for pure isotropic substrates. The impact of the substrate thickness h_s on the corresponding ratio $f_{bent_{aniso}}/f_{flat_{aniso}}$ is also investigated. The curves for L- and W-bent resonators at curvature angle $\alpha_C = 12°$ are presented in Fig. 4.8 (b). The obtained results show that for thicker substrates, the bending effect can partially compensate for the anisotropy impact. It's worth noting that, like in [212], the influence of anisotropy reduces the bending effect for intermediary thicknesses (named "optimal thickness" in [212]); this trait is likely dependent on the curvature angle α_C and hasn't been well examined.

Now it's time to present some experimental dependencies for bent resonators on anisotropic substrates, which were chosen in section 4.4. Fig. 4.10 shows the measurement findings for the TM_{10} mode ratio of f_{bent}/f_{flat} in the flat and bent rectangular resonators versus the bending radius R_b. They differ from the isotropic substrate dependencies seen in Fig. 4.7. Below the resonance frequencies of the equivalent flat resonators, both L- and W-bent resonators show more or less pronounced ripples in the resonance shifts in the anisotropic case (as in [217]), which is practically impossible in the isotropic case when an accurate measurement procedure is used.

Therefore, all of these cases confirm the simultaneous influence of the anisotropy and bending of the used substrates. The curves for denim, linen, and commercial multilayer GORE-TEX® textile fabrics, as well as for the silicon-based flexible polymer PDMS with a small degree of stretching, are very typical. Three reasonably flexible commercial reinforced substrates, Ro4003, NT9338, and soft ceramic Ro3010, show similar behavior. However, the non-plastic deformation in these substrates, which prevents bending at extremely small radii, also impacts the course of dependences. Of course, due to the difficulties in achieving perfect measurement conditions, especially at small bending radii, all of the presented experimental

curves cannot be directly compared to the theoretical ones in Fig. 4.9 (b), but the trends that reveal the impact of anisotropy combined with the bending effect in wearable structures are apparent.

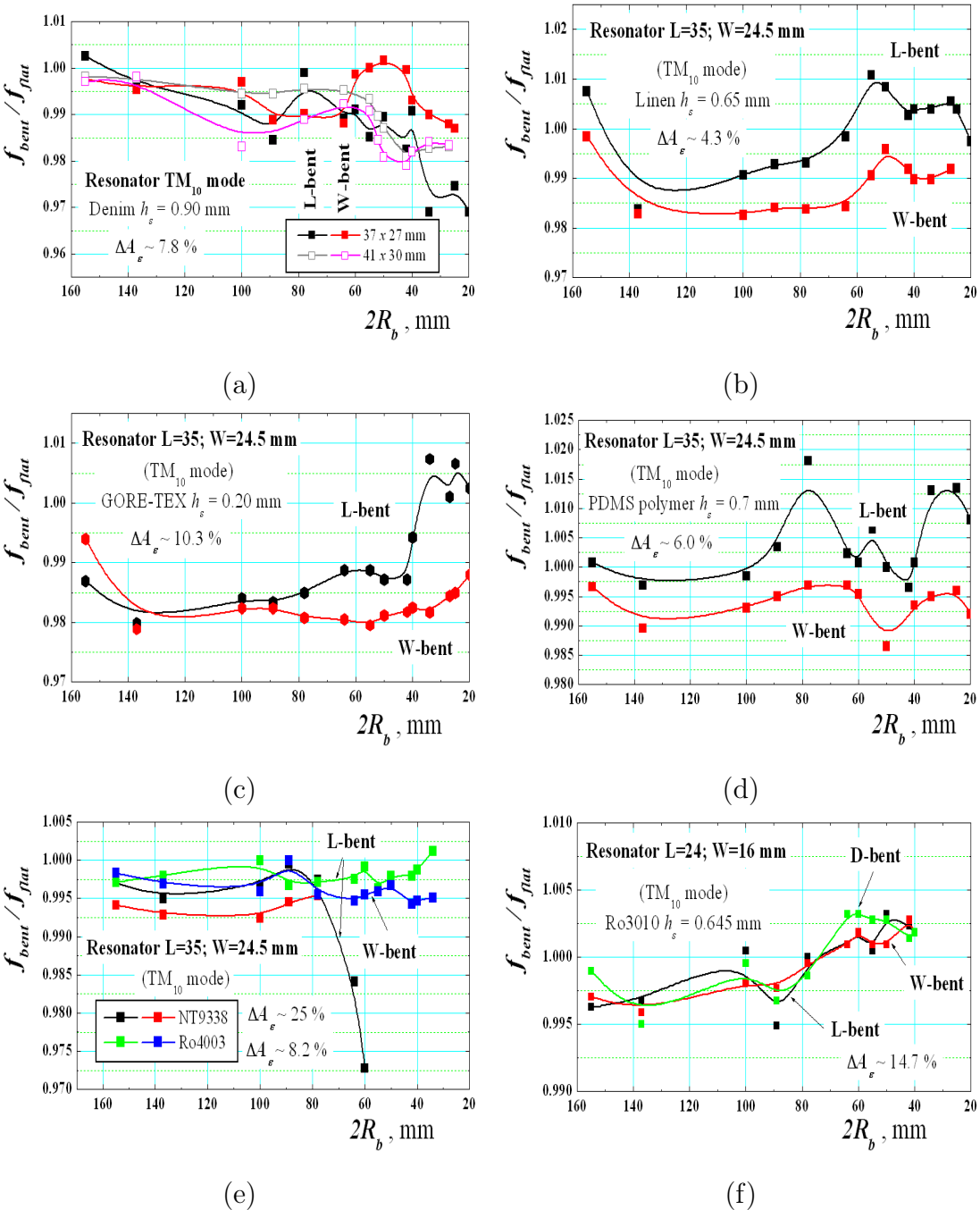

FIGURE 4.10: Experimental dependencies between the ratio of resonance frequencies f_{bent}/f_{flat} of the lowest-order mode TM_{10} for bent and flat rectangular resonators on different anisotropic substrates and the bending radius R_b : (a) Denim substrate; (b) Linen substrate; (c) commercial textile fabrics GORE-TEX ® ; (d) Polydimethylsiloxane (PDMS); (e) NT9338, Ro4003; (f) Ro3010.

4.6 Conclusion

The primary goal of the research presented in this chapter to prove the opposite influence of bending and anisotropy on the resonance characteristics of flexible and wearable structures has been successfully accomplished. The advantage of this research is that these effects have been separated in numerical simulations, allowing the evaluation of the degree and sign of resonance frequency shifts of simple rectangular planar resonators on both anisotropic and isotropic substrates in flat and bent states. All simulations and experimental results reveal that the pure bending effect, which can only be achieved with experimentally validated isotropic substrates, enhances the resonance frequency of bent rectangular resonators in contrast to flat ones, proving the effect's origin in its purest form. In contrast, the numerical analysis shows that anisotropy (the presence of direction-dependent dielectric constants ϵ_{par} and ϵ_{perp}) has the exact opposite effect: the resonance frequency of flat or bent rectangular resonators on anisotropic substrates always decreases (when $\epsilon_{par} > \epsilon_{perp}$) as compared to pure isotropic substrates using same structures. The final effect is not directly quantifiable, but it provides the expected pure effect of substrate anisotropy, depending on the degree of anisotropy ΔA_ϵ and the actual bending radius R_b.

When bent and flat rectangular resonators are considered- as positive as well as negative resonance frequency shifts, the combined effects of anisotropy and bending lead to a more complex behavior of the analyzed resonance structures. These combined effects are now completely measurable. In the L and S bands, the resonance shifts in bent and flat resonance structures are measured using well-selected flexible anisotropic substrates (including textile materials). The obtained dependencies for bending radii R_b ranging from 80 to 10 mm show that the resonance frequencies increase (as for the pure bending effect) and dropping (the last phenomenon is theoretically impossible for pure bending effect). The derived results explain well the observed dependencies by other authors, including the existence of optimal substrate thicknesses where the bending effect (but also anisotropy too) may be minimized. The proposed methods for simultaneous investigation of the effects of bending and anisotropy can also be applied to metasurfaces.

Chapter 5

Comparative Analysis of Polydimethylsiloxane (PDMS) and Denim (Jean) Substrate based Flexible Antenna

5.1 Introduction

With the advent of flexible electronics devices in recent years, flexible antennas have sparked a lot of attention. The implementation of flexible antennas for different applications like In-body, On-body, and Off-body communication is the latest trend in antenna design. A complete review of flexible antennas using various substrates and fabrication technologies is already discussed in Chapter 2. Polymer substrates have surpassed fabric and rigid substrates in popularity for the construction of flexible and wearable antennas, and their merits and downsides have been explored in previous chapters.

Flexible antenna proposed in this chapter is used to compare fabric and polymer substrate-based flexible antennas in order to determine whether the predicted benefits of polymer substrates over fabric substrates are realistic. Denim (Jean) is employed as the fabric substrate and Polydimethylsiloxane (PDMS) is used as polymer substrate in the antenna design.

The proposed antenna is evaluated under various operating situations such as bending, wet condition analysis, and to observe the effect on human body specific absorption rate (SAR) analysis is also performed here.

5.2 Antenna Design

The primary goal of this proposed flexible antenna is to compare the performance of flexible antennas with fabric and polymer substrates under conventional and variable operating circumstances. According to the literature review presented in Chapter 2, polymer-based substrates have certain advantages over rigid and fabric substrates when used to design flexible antennas, like performing better under various operating conditions such as bending and stretching and being less susceptible to environmental variations such as moisture absorption. Therefore, the same antenna is fabricated using both substrates, as shown in Fig. 5.1, to examine all of these theoretical studies in action.

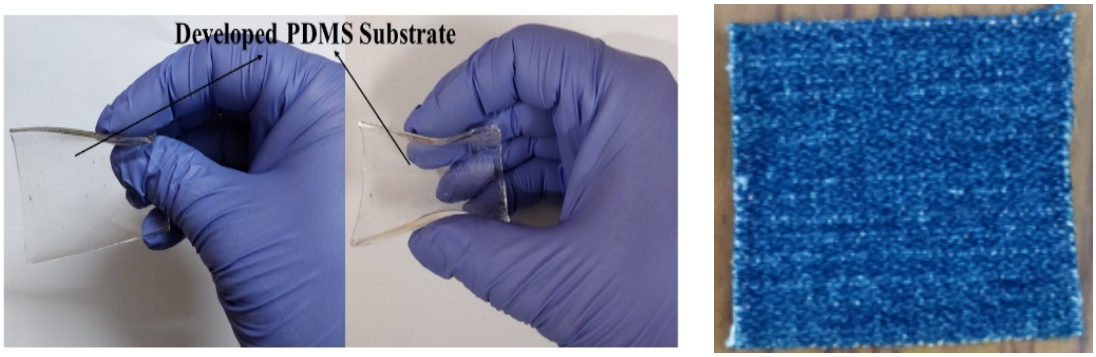

(a) (b)

FIGURE 5.1: Substrates: (a) PDMS developed at BITS- Pilani Lab, and (b) Denim (Jean)

5.2.1 Antenna Geometry

The physical design aspects of this flexible, slotted patch antenna with a defective ground plane for various wireless applications are presented in this section. The proposed antenna's geometry is shown in Fig. 5.2, and its dimensions are listed in Table 5.1. In this proposed design, PDMS is used as a substrate and for the comparison, the same antenna is designed using Jean substrate. The chosen PDMS and Jean substrates have a thickness of 1 mm, and their dielectric properties (dielectric constant, ϵ_r, loss tangent, $\tan\delta_{\epsilon_r}$ values are of 2.65 and 0.02 (PDMS), 1.78 and 0.085 (Jean)) are obtained as described in [21–23, 220] and [221] respectively.

The dimension of the defected ground plane ($L_g \times W_g$) is 8.5 mm × 30.1 mm. Two rectangular slots of 2 mm × 4 mm are cut in the ground plane to give the antenna wideband characteristics. Two staircase steps of size 2 mm × 2 mm are introduced on the lower side of the patch to increase the gain and bandwidth of the proposed antenna. The microstrip feed of size 12 mm × 1.9 mm is used in the proposed design for impedance matching of 50 Ω. The simulation analysis of the proposed antenna is performed using ANSYS® HFSS.

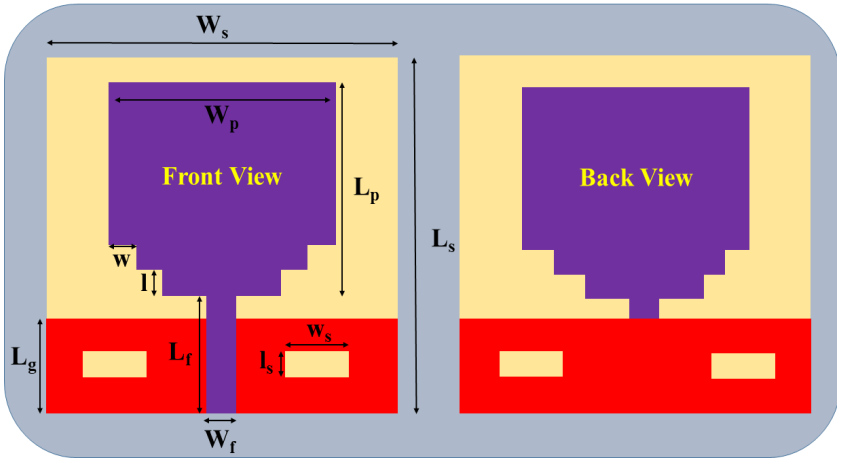

FIGURE 5.2: Antenna Geometry

TABLE 5.1: Antenna Design Parameters with Dimensions

Design Parameters	**Dimensions (mm)**
Substrate Length, L_s	30.1
Substrate Width, W_s	30.1
Substrate Height, h	1
Patch Length, L_p	18.5
Patch Width, W_p	18
Ground Length, L_g	8.5
Ground Width, W_g	30.1
Feed Length, L_f	12
Feed Length, W_f	1.9
Slot Length, l_s	2
Slot Width, w_s	4
Step Length, l	2
Step Width, w	2

5.2.2 Development of Prototype

Fig. 5.3 (a), (b), and Fig. 5.4 (a), (b) shows the fabricated prototypes of the proposed antenna using PDMS and Jean substrates, respectively. In order to develop

the prototypes using PDMS and Jean substrates, first of all, the substrates are cut in the required dimensions of 30.1 mm × 30.1 mm. The radiating patch, ground, and microstrip feed line are made up of copper, constructed using the adhesive copper tape of thickness 0.06 mm. While fabricating the antenna, it is observed that the PDMS substrate, due to its excellent adhesive properties, allowed the use of copper tape more easily than Jean substrate. While attaching the SMA connectors, the soldering was easily performed on PDMS substrate compared to Jean, as it can withstand higher temperatures. The antenna fabricated using the PDMS substrate is highly flexible, stable, adhesive to the material used for constructing the radiating parts, and transparent compared to the antenna fabricated using Jean substrate. A detailed comparison of performance parameters, bending, SAR and wet condition analysis is presented in the later sections of this chapter. To validate the simulated results, the measurements are performed using the KEYSIGHT N9928A vector network analyzer (VNA), as shown in Fig. 5.3 (c) and Fig. 5.4 (c).

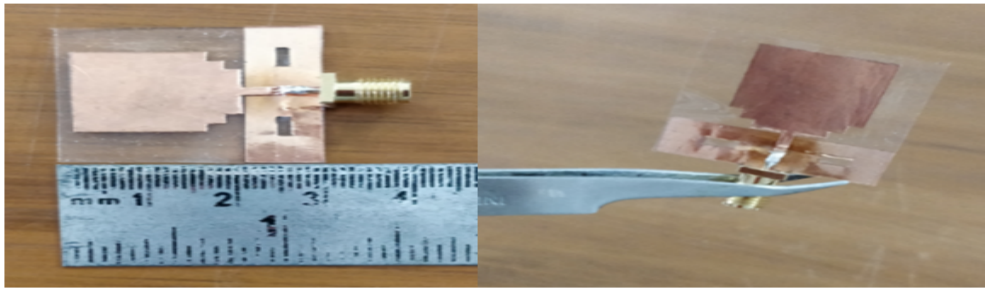

(a)

(b)

(c)

FIGURE 5.3: Fabricated antenna using PDMS substrate, (a) Front view, (b) Back view, and (c) Measurement set-up

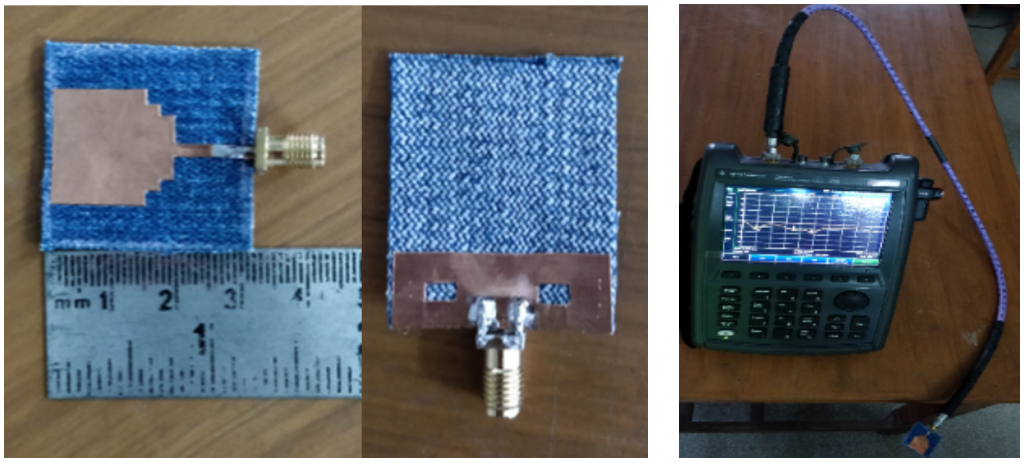

(a) (b)

FIGURE 5.4: Fabricated antenna using Jean substrate, (a) Front view, (b) Back view, and (c) Measurement set-up

5.3 Performance Analysis

This section presents the comparative analysis of simulated and measured results for the proposed antenna design using PDMS and Jean substrate. From Fig. 5.5, it can be observed that the simulated antenna using PDMS substrate shows a broad impedance bandwidth from 2.7 GHz to 13.4 GHz (10.7 GHz), which is 132.9 %, and the simulated antenna using Jean substrate also reveals a wide bandwidth of 2.4 GHz to 12 GHz (9.6 GHz) which is 133.3%. The measured results show that the impedance bandwidth using PDMS and Jean substrate is 2.5-12.2 GHz (9.7 GHz, 131.9%) and 1.9-9.7 GHz (7.7 GHz, 132%), respectively. The difference between simulated and measured bandwidth for PDMS substrate antenna is 1%, and for Jean substrate antenna is 1.3%. The difference between the measured and simulated results can be ascribed to the fabrication, soldering exactness, and measurement conditions.

The proposed antenna design using the PDMS substrate shows the maximum resonance in simulation at 5.7 GHz, having a S_{11} value of -46.32 dB, and at 7.3 GHz, the S_{11} value is -43.29 dB with a VSWR value of 0.08 and 0.11, respectively. In the measured results, the maximum resonance is obtained at 5.4 GHz having the S_{11} value of -30.04 dB, and at 7.1 GHz, the S_{11} value is -27.9 dB with a VSWR value of 1.01 and 1.20, respectively, as shown in Fig. 5.5 and Fig. 5.6. The simulated

results with the exact antenna dimensions using Jean substrate show the maximum resonance at 9.2 GHz with a S_{11} value of -26.21 dB and a VSWR value of 0.85 dB. At all other frequencies, the VSWR values are greater than 2; that's why they are not considered here. The measured results show the maximum resonance at 9.3 GHz with a S_{11} value of -21.32 dB and VSWR of 2.2 dB. The total gain of the proposed antenna when simulated at 6.5 GHz using PDMS substrate is 3.53 dBi, and using Jean substrate is 3.13 dBi, as shown in Fig. 5.7 (a) and (b), respectively. Fig. 5.8 shows the gain vs. frequency plot of the presented design using PDMS and Jean substrate. It is observed that a peak gain of 6.4 dBi at 3.7 GHz and 7.8 dBi at 9.8 GHz is obtained when the antenna is simulated using PDMS and Jean substrate respectively. The peak gain of the antenna using Jean substrate is higher than the PDMS substrate due to low surface waves as the dielectric constant of the Jean is less than PDMS.

Fig. 5.9 and 5.10 shows the good agreement between simulated and measured radiation patterns at E and H planes at different resonance frequencies of the presented antenna using PDMS and Jean substrate, respectively. The radiation patterns of the proposed design using PDMS substrate at different resonating frequencies, i.e., 5.7 GHz, 6.5 GHz is omnidirectional, and it is taking quasi-omnidirectional shape as moving towards the higher frequency at 7.3 GHz. For the same antenna design using the Jean substrate, the radiation patterns at resonating frequencies of 2.9 GHz and 5.8 GHz are also omnidirectional. It is quasi-omnidirectional as moving towards the higher frequencies of 6.5 GHz and 9.2 GHz. The antenna's radiation patterns using the PDMS substrate are also omnidirectional as Jean substrate, which signifies the better transmission and reception of signals from all directions in both the presented antennas.

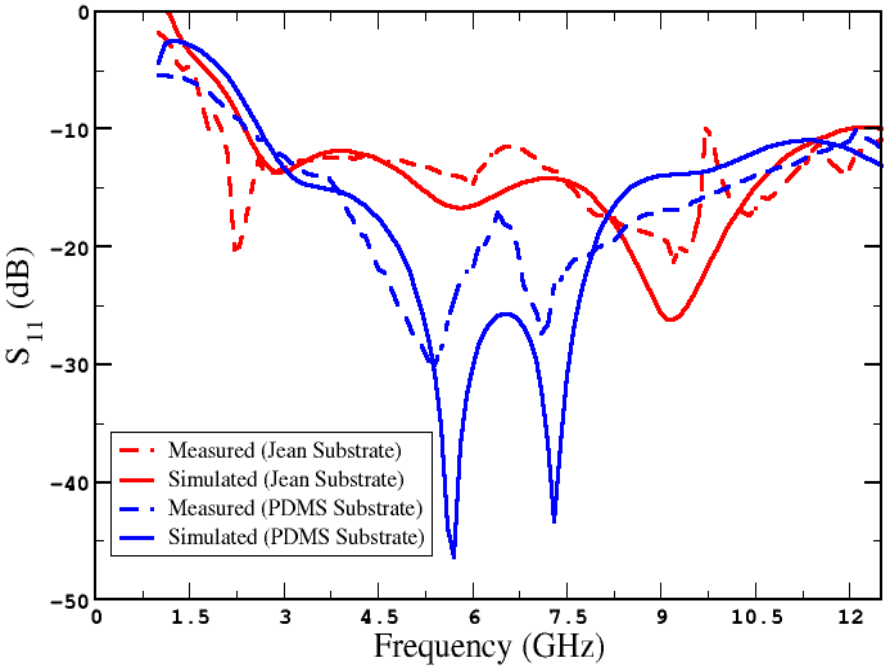

FIGURE 5.5: Simulated and Measured S_{11} vs. frequency curve for proposed antenna using PDMS and Jean substrate

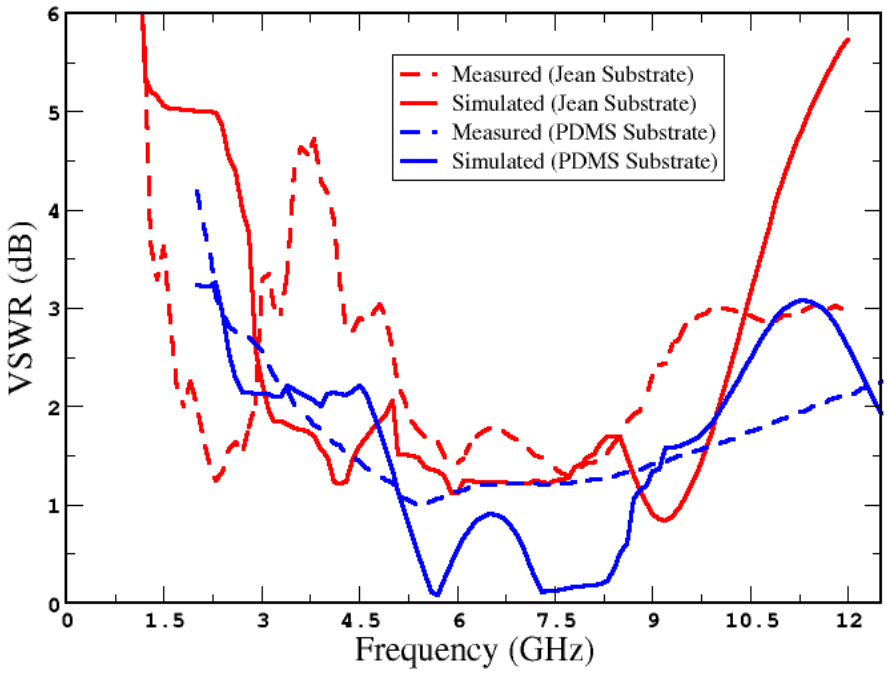

FIGURE 5.6: Simulated and Measured VSWR vs. frequency curve for proposed antenna using PDMS and Jean substrate

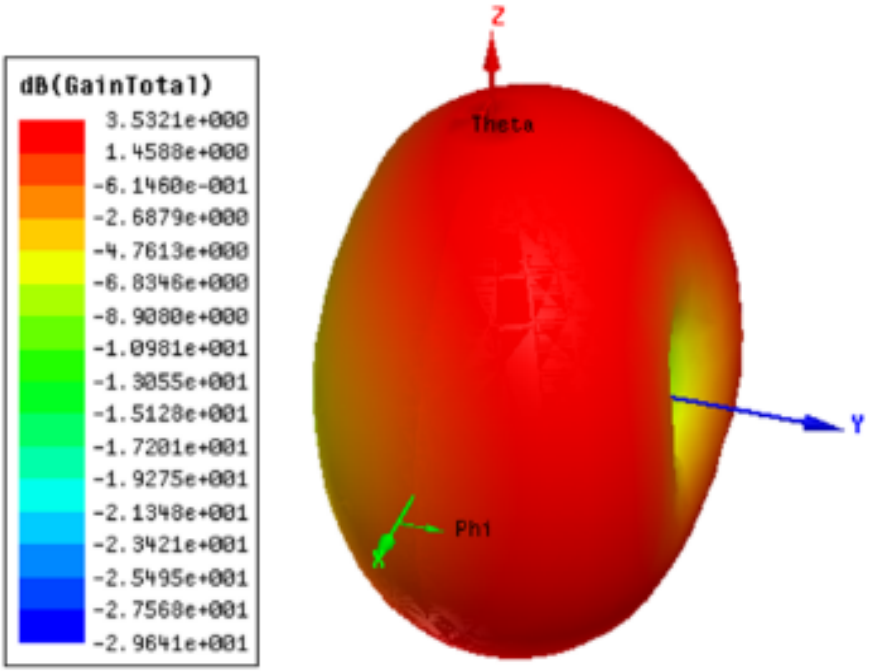

(a)

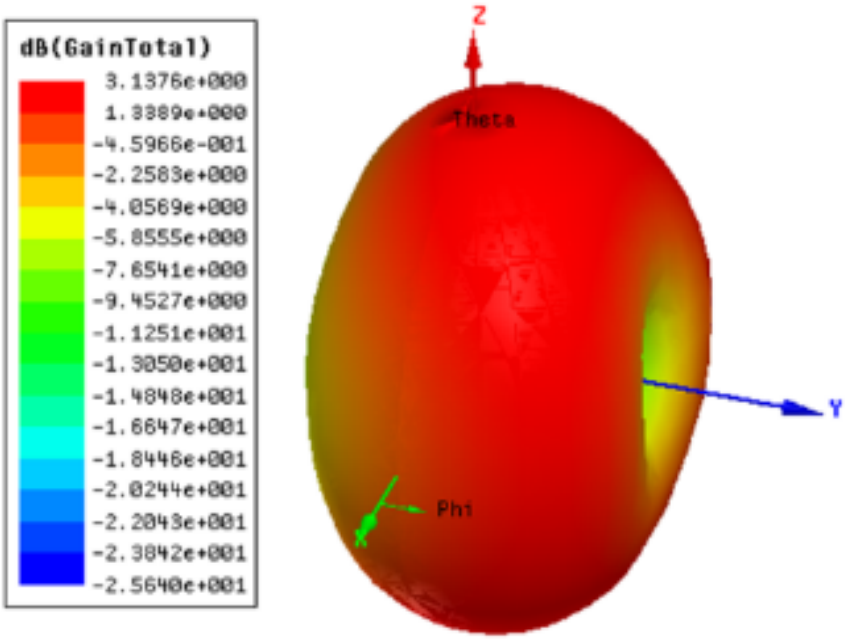

(b)

FIGURE 5.7: Total Gain for the proposed antenna using PDMS substrate (a), and Jean substrate (b) at 6.5 GHz.

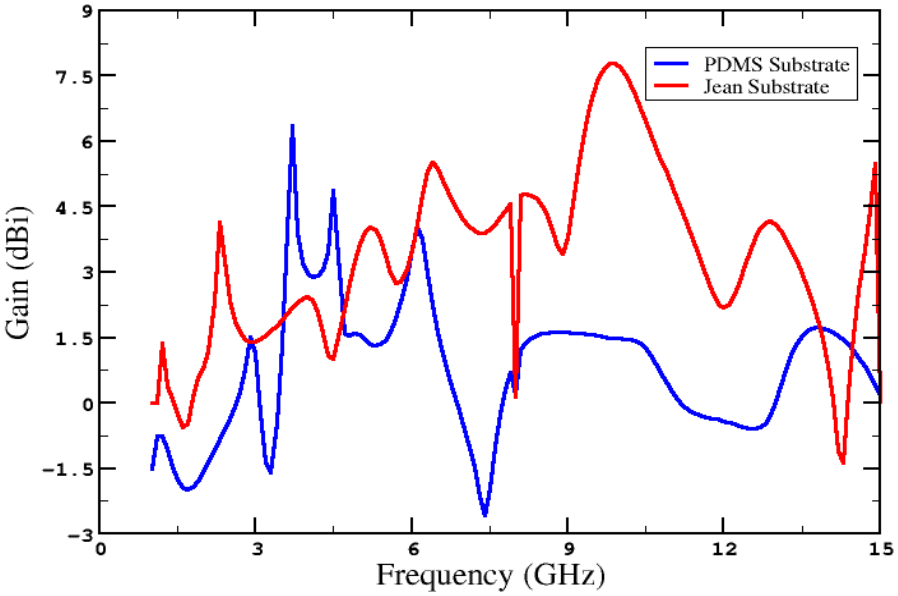

FIGURE 5.8: Simulated Gain vs. frequency curve for proposed antenna, using PDMS, and Jean substrate

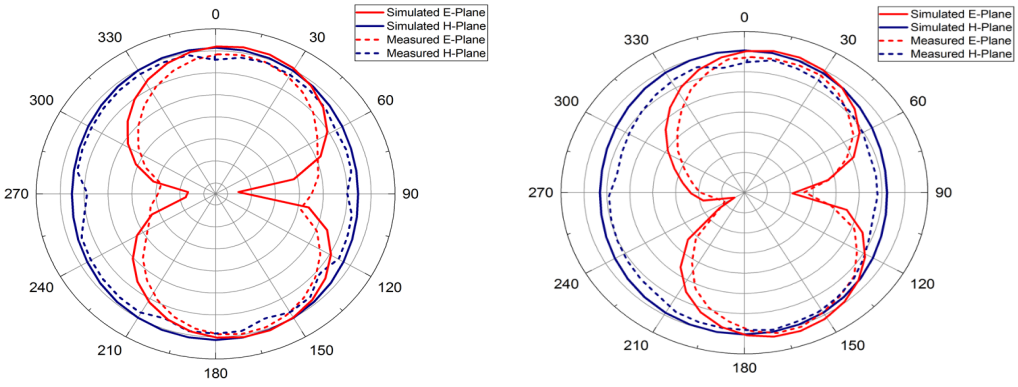

(a) 5.7 GHz

(b) 6.5 GHz

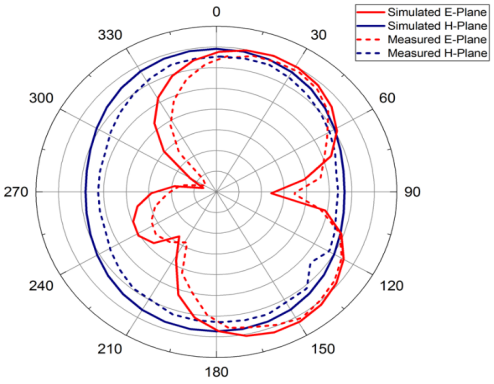

(c) 7.3 GHz

FIGURE 5.9: E and H plane curves for various resonance frequencies for the proposed antenna using PDMS substrate

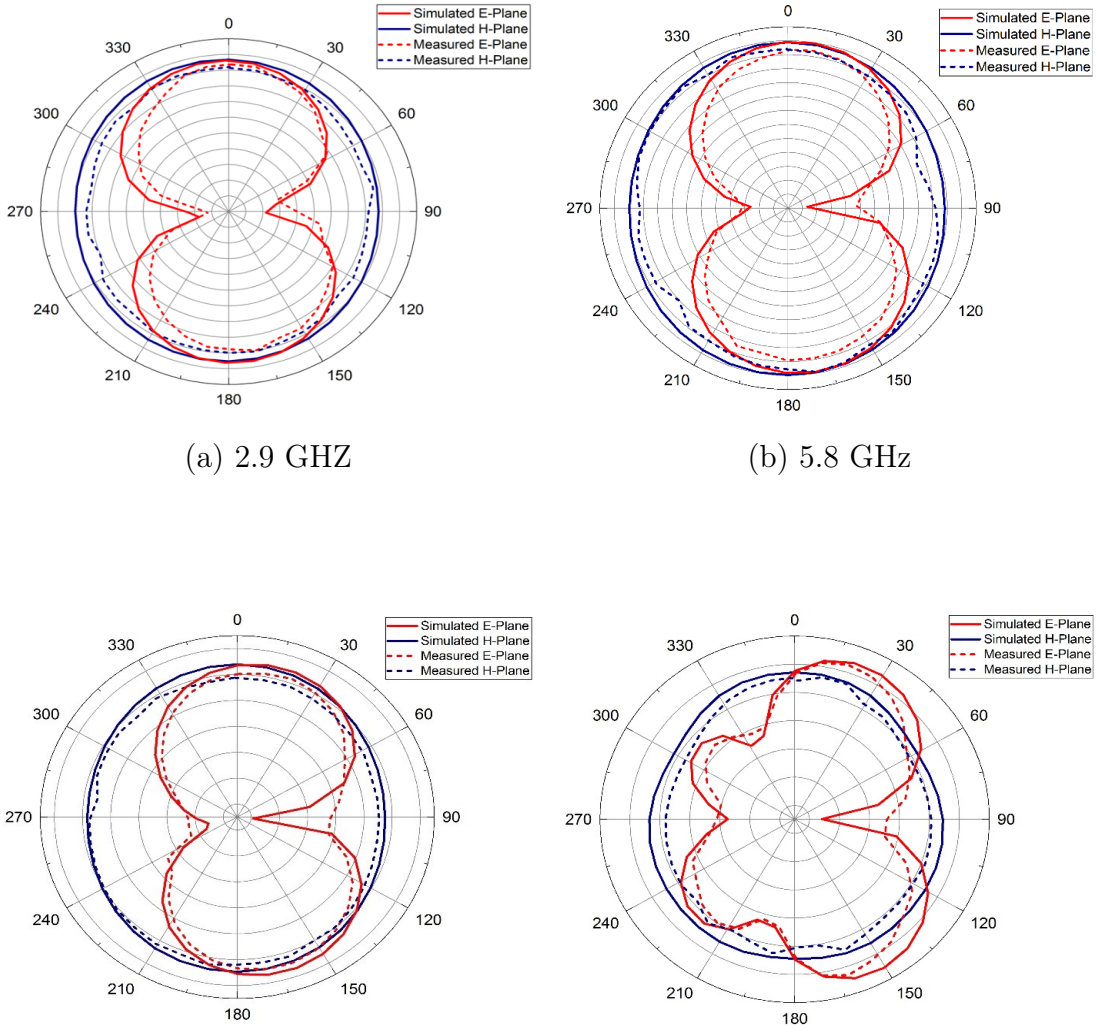

(a) 2.9 GHZ

(b) 5.8 GHz

(c) 6.5 GHz

(d) 9.2 GHz

FIGURE 5.10: E and H plane curves for various resonance frequencies for the proposed antenna using Jean substrate

A comparative analysis of both simulated and measured performance parameters for the proposed antenna design using PDMS and Jean substrate is summarized in Table 5.2.

TABLE 5.2: Comparison of performance parameters of the proposed antenna using PDMS and Jean substrate

Performance Parameters	**PDMS Substrate**	**Jean Substrate**
Impedance Bandwidth	Simulated: 10.7 GHz, 132.9% Measured: 9.7 GHz, 131.9 % Difference: 1%	Simulated: 9.6 GHz, 133.3% Measured: 7.7 GHz, 132% Difference: 1.3%
Maximum Resonance	Simulated: 5.7 GHz, 7.3 GHz Measured: 5.4 GHz, 7.1 GHz	Simulated: 9.2 GHz Measured: 9.3 GHz
S_{11} Values	Simulated: -46.32 dB, -43.29 dB Measured: -30.04 dB, -27.9 dB	Simulated: -26.21dB Measured: -21.32 dB
VSWR	Simulated: 0.08 dB, 0.11 dB Measured: 1.01 dB, 1.20 dB	Simulated: 0.85 dB Measured: 2.2 dB
Peak Gain	6.4 dBi at 3.7 GHz	7.8 dBi at 9.8 GHz

5.4 Testing Under Bending

In order to analyze the effect of bending on the radiation characteristics of the antenna, the developed antenna is tested under bending conditions. To observe its effect, two different conditions are selected; in the first case, the antenna's performance is measured on the human hand at 10° bend, and in the second case, two different cylinders of the radius 3 cm and 4 cm are used for the measurements. The above two conditions are applied to the presented antenna design using both Jean and PDMS substrates. Fig. 5.11 shows the measurement set-up on the human hand and two different cylinders for these antennas.

(a) (b)

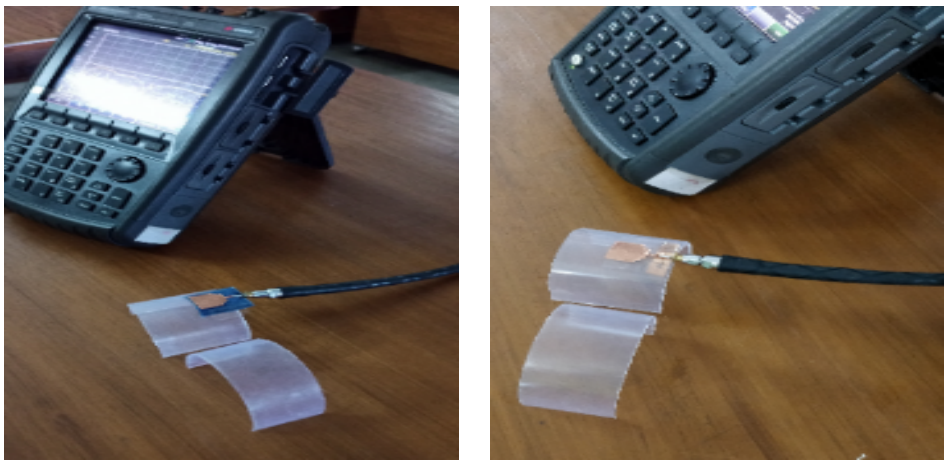

(c) (d)

FIGURE 5.11: Measurement Set-up for antenna test under bending, (a) On human hand (using Jean substrate), (b) On human hand (using PDMS substrate), (c) Using 3 cm and 4 cm cylinders (using Jean substrate), and (d) Using 3 cm and 4 cm cylinders (using PDMS substrate)

Case-I: One of the major requirements of a flexible/wearable antenna is to perform well when placed on the human body, which is the limitation of rigid substrate-based antennas. When the antenna is placed on the human hand for measurements, as shown in Fig. 5.11 (a) and (b), it acts as a lossy medium due to the presence of human tissues, which may absorb some amount of energy. This leads to the change in the proposed antenna's S-parameter values in both PDMS and Jean substrate based antennas as shown in Fig. 5.12 (a).

Due to the low value of dielectric constants for both flexible substrates, the surface waves' effect is suppressed, and proper impedance matching can be achieved. ***Case-II***: In order to further analyze the bending effect on the performance parameters of the antenna, the proposed fabricated antennas are placed on the two cylinders of radius 3 cm and 4 cm, as shown in Fig. 5.11 (c) and (d), respectively. As illustrated in Fig. 5.12, the measured result shows that the bandwidth of the proposed antenna using PDMS substrate on 4 cm radius cylinder is 2.7-11.9 GHz (9.2 GHz, 126.0 %) and on 3 cm radius cylinder is 2.9-11.5 GHz (8.6 GHz, 119.4 %) as compared to the measured bandwidth of 2.5-12.2 GHz (9.7 GHz, 131.9%) under no bend condition (as shown in Fig. 5.12 (b)). Similarly, Fig. 5.12 (c) shows that the measured bandwidth using Jean substrate on 4 cm cylinder is 2.2-9.8

GHz (7.6 GHz, 126.6%) and on 3 cm cylinder is 2.7-10.1 GHz (7.4 GHz, 115.6%) as compared to 1.9-9.7 GHz (7.7 GHz, 132%) under no bend condition. Hence, decreasing the bending surface radius from 4 cm to 3 cm, an increment in the S_{11} value and decrement in the bandwidth are observed. Overall comparison between the antennas fabricated on PDMS and Jean substrate shows that the antenna designed using PDMS substrate shows better results in terms of S_{11} values and bandwidth under bending conditions.

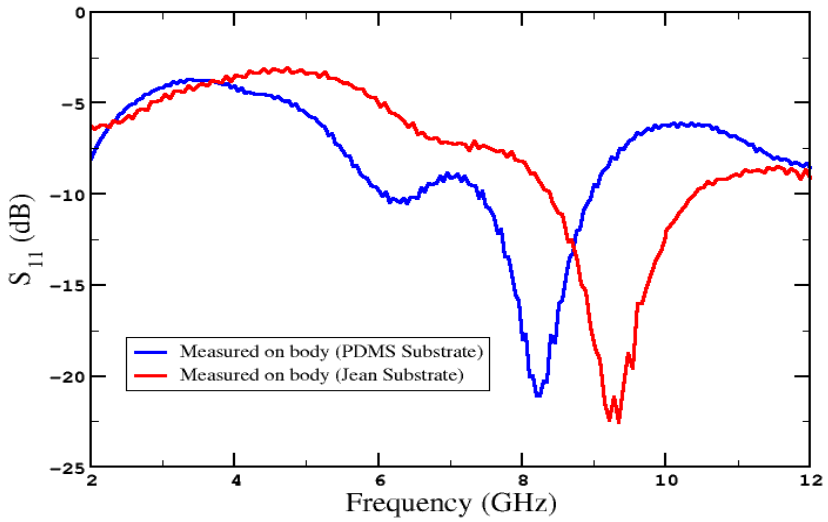

(a)

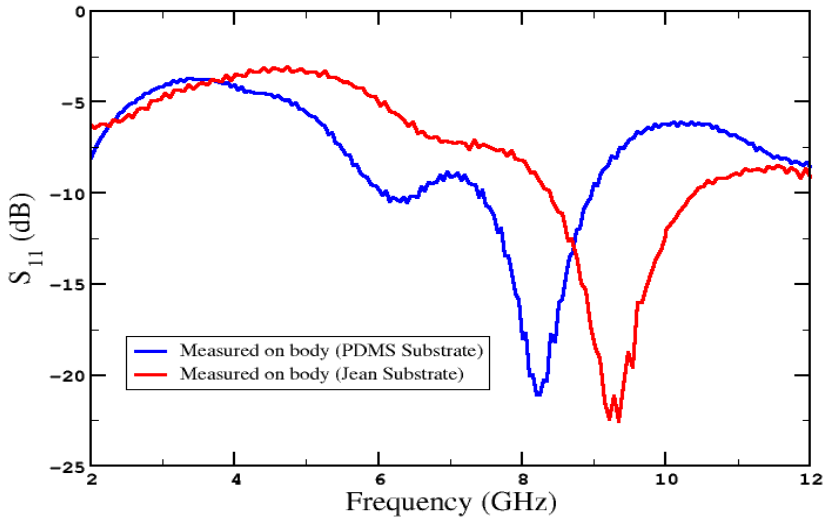

(b)

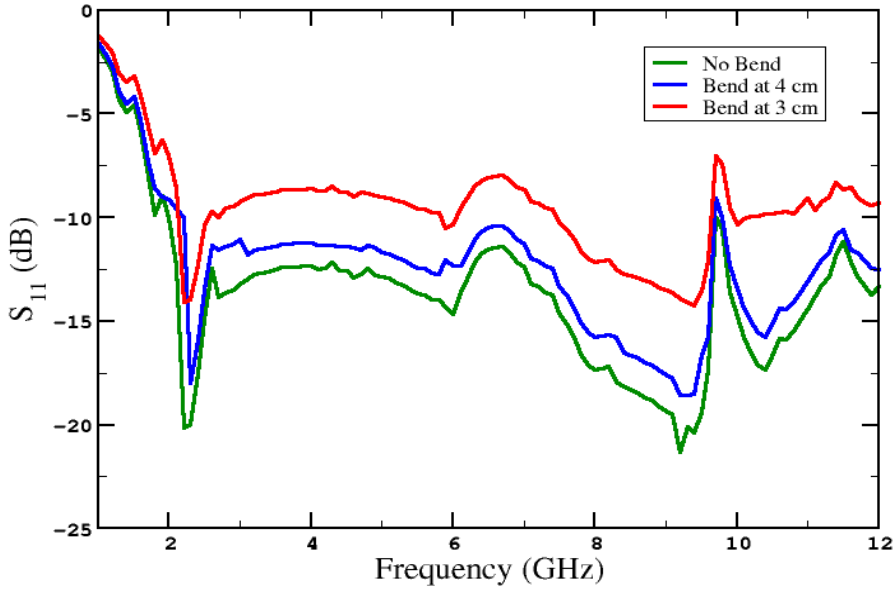

(c)

FIGURE 5.12: Measured S_{11} values under different bending conditions, (a) At 10° (on human hand), and (b) Bend at 3 cm and 4 cm cylinder using PDMS substrate and (c) Bend at 3 cm and 4 cm cylinder using Jean substrate

5.5 SAR Analysis

The specific absorption rate (SAR) analysis is also performed for the presented antenna design for Jean and PDMS substrates using the simulation model to observe the antenna's effect on the human body. The SAR simulation model is a three-layered structure where the top layer is the skin layer, the middle layer is the fat layer, and the lower layer is the muscle layer [222]. The properties of the human tissues are taken from [223–225].

The mathematical expression to evaluate the value of the SAR is as follows:

$$\text{SAR} = \frac{\sigma|\text{E}|^2}{\rho} \tag{5.1}$$

where σ is conductivity (S/m) of the sample under test, E represents the electric field (V/m), and ρ is the human tissue's mass density (kg/m^3). Fig. 5.13 (a) and (b) show that the SAR values (by simulation model using HFSS at 6.5 GHz) of the proposed antenna using PDMS and Jean substrate are 1.60 and 1.89, respectively. As per the European standard, SAR should be lower than 2 W/kg for 10 grams

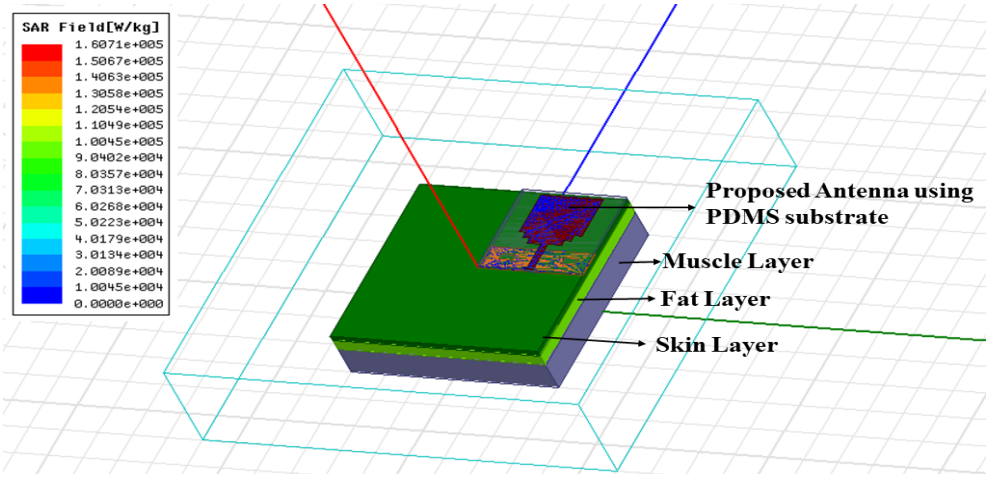

(a)

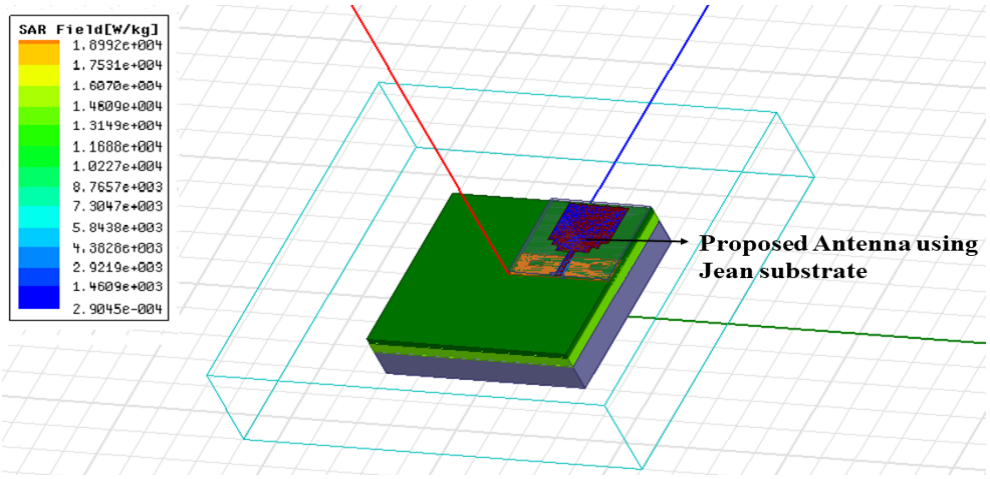

(b)

FIGURE 5.13: Simulation model of SAR analysis of proposed antenna using (a) PDMS substrate, and (b) Jean substrate

of an average mass of human tissue. The obtained SAR values for the proposed antenna using both substrates satisfy these criteria.

5.6 Testing under Wet Conditions

The fabric substrate-based (like Jean) antennas are more prone to environmental conditions because they absorb moisture, which badly impacts the antenna's radiation characteristics. While the polymer substrate (like PDMS) based antennas overcome this limitation due to their physical and chemical properties. To prove this, the proposed (fabricated) antenna is also tested under wet conditions

by inserting it in water and letting it dry for 10 minutes. Fig. 5.14 shows the measurement setup to test both the antennas under wet conditions. Fig. 5.15 shows the S_{11} values and impedance bandwidth for these antennas under wet conditions. A very slight change in the frequencies and the corresponding S_{11} values with the measured bandwidth is observed for the PDMS-based antenna as compared to the Jean-based antenna, where this shift is colossal.

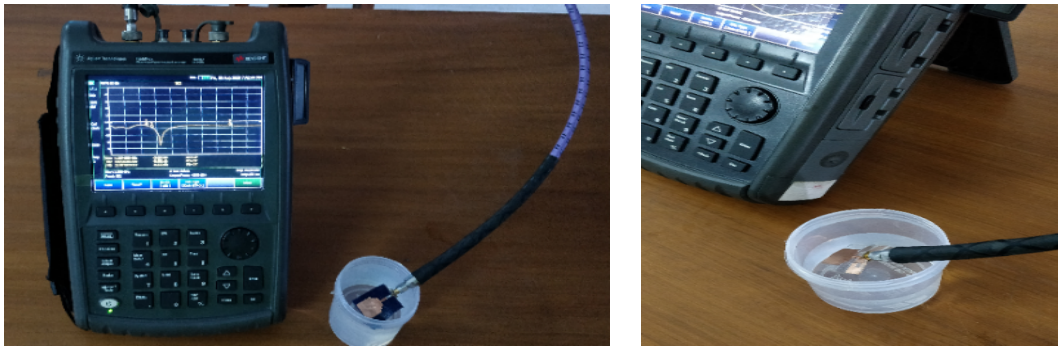

(a) (b)

FIGURE 5.14: Measurement Set-up for wet condition, (a) Proposed antenna using Jean substrate, and (b) Proposed antenna using PDMS substrate

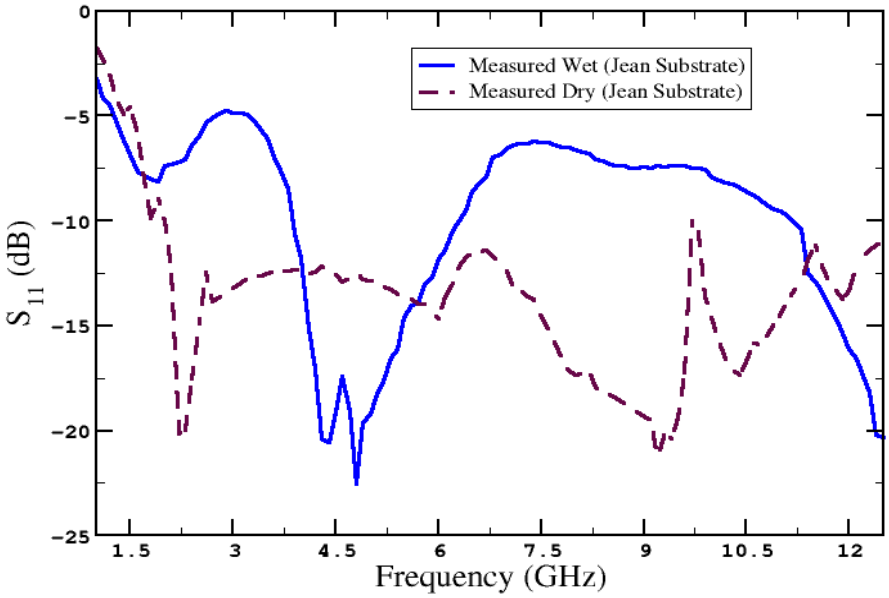

(a)

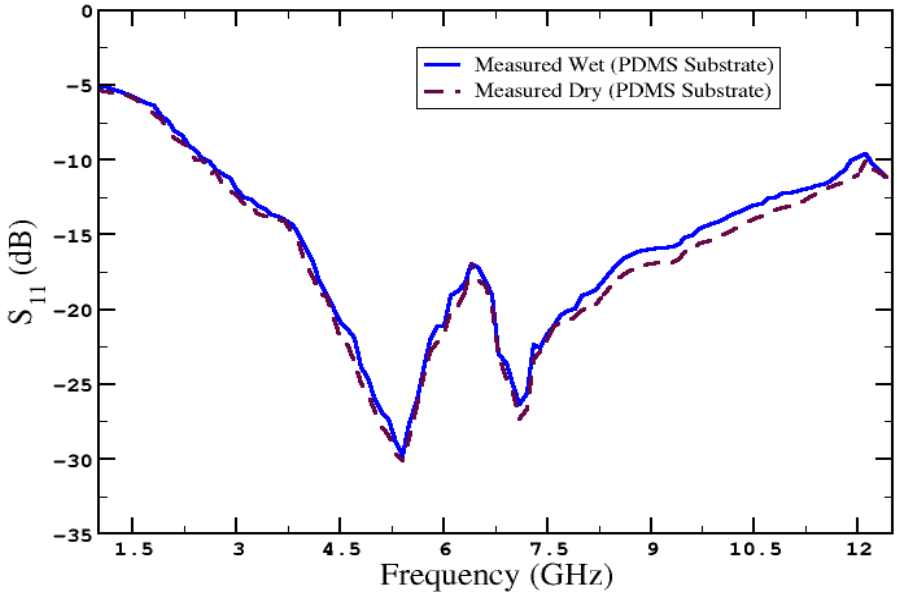

(b)

FIGURE 5.15: Measured S_{11} values of proposed antenna under wet condition, (a) Using Jean substrate, and (b) Using PDMS substrate

The comparison of the proposed antenna using Jean and PDMS substrate with the previous works is presented in Table 5.3. From this table it can be observed that the presented antenna design performs better in terms of gain and bandwidth as compared to previous research.

TABLE 5.3: Comparison of Proposed Flexible Antenna (PA) with Previous Works

Substrate Used	**Antenna Size (mm3)**	**Gain (dBi)**	**Impedance Bandwidth (GHz)**	**Test for Bending and Wet conditions**	**Ref. No.**
Polyamide	40×30×0.15	2	3.1-4.8	Not Performed	[226]
Liquid Crystalline Polymer (LCP)	26×16×0.05	2- 3	3.1-4.5 & 6-11	Bending Test: Performed, Wet condition Test: Not Performed	[74]
Cotton Cloth	40×30×0.75	2- 4	3-10.6	Bending Test: Performed, Wet condition Test: Not Performed	[227]
Liquid Crystalline Polymer (LCP)	40×22×0.1	4.2	2.5-11	Bending Test: Performed, Wet condition Test: Not Performed	[228]
Cotton	70×60×1.6	6.17	1.6-11.2	Bending Test: Performed, Wet condition Test: Not Performed	[229]
Composite Laminate	40.5×40.0×0.3	3.1	3.3-12	Bending Test: Performed, Wet condition Test: Not Performed	[230]
RT/Duroid 5880	30×25×0.8	5.15	2.9-3.95 GHz, 10.5-12.9 GHz	Bending Test: Performed, Wet condition Test: Not Performed	[231]
Jean	**30.1×30.1×1**	**7.8**	**2.4-12**	**Bending and Wet condition Test: Performed**	**PA**
PDMS	**30.×30.1×1**	**6.4**	**2.7-13.4**	**Bending and Wet condition Test: Performed**	**PA**

5.7 Conclusion

A comparative analysis of the flexible antenna designed using PDMS and Jean substrate is presented in this chapter. This antenna can be used for various wireless applications like ultra-wideband (UWB), WLAN and WBAN. The antenna designed using the PDMS substrate shows a better performance in terms of S-parameters and VSWR as compared to the Jean substrate. The peak gain of the Jean substrate-based proposed antenna is higher than the PDMS antenna due to its

low dielectric constant value. The difference between the simulated and measured results of the presented antenna using the PDMS substrate is also significantly less than the Jean substrate. The proposed antenna's radiation patterns using PDMS substrate are more omnidirectional than the Jean substrate. Under the bending conditions, the PDMS based antenna shows stable results compared to the Jean substrate-based antenna. Under wet conditions, the PDMS substrate-based antenna shows a negligible difference in the measured results compared to the Jean substrate-based antenna. Therefore, it can be concluded that the PDMS is a better substrate for the design of the flexible antennas as compared to the Jean substrate.

Chapter 6

Metamaterial Inspired Flexible Antenna

6.1 Introduction

As it was presented in chapter 2 that the use of metamaterial in antenna design improves its performance, so the concept of metamaterial is introduced in the proposed flexible antenna using PDMS substrate. A single circular split-ring resonator (SRR) structure is used on the same side of the patch. It provides the required frequency notched characteristics for the targeted frequency bands, compactness, minimize losses, and backward radiation when used in close proximity to the human body.

This proposed flexible antenna is designed for WLAN (Wireless Local area networks) and WBAN (Wireless body area networks) applications [232–235]. The WBAN has a wide range of applications in today's wireless communication environment, including medical sector like health monitoring systems, industrial, scientific, and medical (ISM) band applications [236] for body-centric wireless applications [237, 238].

The proposed antenna is also tested in a variety of operating conditions. Bending analysis, wet condition analysis, and specific absorption rate (SAR) analysis is also done to study the performance of flexible antenna.

6.2 Antenna Design

This section presents a 50×40 mm^2 CPW-fed triple-band flexible antenna operating at 5 GHz, 5.8 GHz, and 6.6 GHz for WLAN and WBAN applications. In this

proposed design, Polydimethylsiloxane (PDMS) is employed as a substrate with a dielectric constant ϵ_r of 2.65 and a loss tangent $\tan\delta_{\epsilon_r}$ of 0.02. To improve the performance of the proposed antenna, a single split ring resonator structure with a slotted ground plane is loaded on the same side of the patch.

6.2.1 Metamaterial Cell Analysis

A single circular split-ring resonator structure (SRR) is used in this proposed design to enhance the antenna radiation properties, reduce overall size, and provide multiband notched frequencies. These properties are required to overcome the issues of frequency overlapping for narrowband applications like WLAN and WBAN with the neighboring frequency bands. These significant issues are highlighted in our previous research [239], in which a flexible antenna was proposed for wireless applications without SRR loading. The circular SRR position and dimensions are optimized and offset to give the presented antenna triple-band notch characteristics.

The loaded SRR consists of two concentric rings with an opening at opposite ends, which act as capacitive reactance and help in regulating the resonant characteristics of this structure. The structure and dimensions of circular SRR are shown in Fig. 6.1 (a). The equivalent circuit of the proposed SRR is an LC-tank circuit, as shown in Fig. 6.1 (b). The total inductance due to both the rings is L_{Total}, distributed capacitances of both the rings are C_{d1} and C_{d2}, which divide the whole structure of the unit cell into two parts above and below the split gaps. Due to these split gaps between inner and outer rings, two-gap capacitances, as C_{gap1} and C_{gap2}, are also considered in the equivalent circuit.

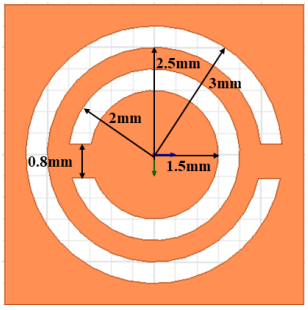

(a)

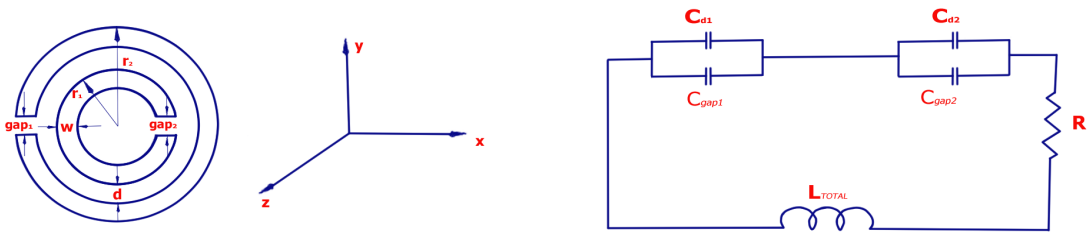

(b)

FIGURE 6.1: Circular SRR structure: (a) Dimensions, and (b) Equivalent Circuit

The resonant frequency of the circular SRR is given as:

$$f_{rCircular-SRR} = \frac{1}{2\pi}\sqrt{\frac{1}{L_{Total}C_{Total}}} \tag{6.1}$$

where C_{Total} is the total equivalent capacitance of the unit cell structure and is calculated as:

$$C_{Total} = \frac{(C_{d1} + C_{gap1})(C_{d2} + C_{gap2})}{(C_{d1} + C_{gap1}) + (C_{d2} + C_{gap2})} \tag{6.2}$$

As the split gaps are of identical dimensions, $g_{gap1} = g_{gap2} = g$, so $C_{gap1} = C_{gap2} = C_{gap}$ and the distributed capacitances, $C_{d1} = C_{d2} = C_d$. As a result, the Eq. (6.2) may be written as:

$$C_{Total} = \frac{(C_d + C_{gap})}{2} \tag{6.3}$$

The gap capacitances $C_{gap1} = C_{gap2} = C$ gap can be expressed as:

$$C_{gap} = \frac{\epsilon_0 wt}{g} \tag{6.4}$$

where w and t are the width and thickness of the circular SRR rings, respectively, and ϵ_0 is the free space permittivity.

The distributed capacitances C_{d1} and C_{d2} are also dependent on the split gap dimensions $g_{gap1} = g_{gap2} = g$ and is expressed as:

$$C_d = (\pi r_a - g)C_{pl} \tag{6.5}$$

where r_a is the average ring radius and C_{pl} is the capacitance per unit length, and are expressed as:

$$r_a = r_2 - w - \frac{d}{2} \tag{6.6}$$

where radius of the outer ring is r_2 , and d is the inner and outer ring separation.

$$C_{pl} = \frac{\sqrt{\epsilon_{eff}}}{cZ_o} \tag{6.7}$$

where ϵ_{eff} is the effective permittivity of the medium, Z_o is the characteristics impedance of the line, and c is the velocity of the light $(3 \times 10^8\, m/sec)$.

Therefore, by putting all the values from the above equations in Eq. (6.1), the resonant frequency of the circular SRR can be calculated as:

$$f_{rCircular-SRR} = \frac{1}{2\pi\sqrt{L_{Total}C_{Total}}} = \frac{1}{2\pi\sqrt{L_{total}}\left[\frac{(\pi r_a - g)C_{pl}}{2} + \frac{\epsilon_0 wt}{2g}\right]} \tag{6.8}$$

where total equivalent inductance L_{Total} can be expressed as [240]:

$$L_{Total} = 0.0002l\left(2.303\log_{10}\frac{4l}{t} - \gamma\right)\mu H \tag{6.9}$$

where l is the length of finite rectangular cross-section wire and can be calculated by considering a single loop with r_2 as radius, γ is constant of wire loop geometry and is equal to 2.451. All of the parameters in the equations above are in millimetres.

The analysis of SRR structure is performed using the HFSS software by placing it in a waveguide medium. It's required S-parameters; reflection coefficient (S_{11}) and transmission coefficient (S_{21}) values are extracted as illustrated in Fig. 6.2. The perfect electric conductor (PEC) is allocated to the top and bottom walls of the medium, and perfect magnetic conductor (PMC) is assigned to the front and rear walls and two wave ports, port 1 and port 2, are utilized for the excitation at opposite faces of the medium. Using the values of the extracted S- parameters, the required parameters like permittivity (ϵ) and permeability (μ) are evaluated. Fig. 6.3 shows the variation of the ϵ and μ as a function of frequency. It has been

observed that the negative permeability and permittivity values exist over most of the desired band of operation, which confirms its property as a SRR.

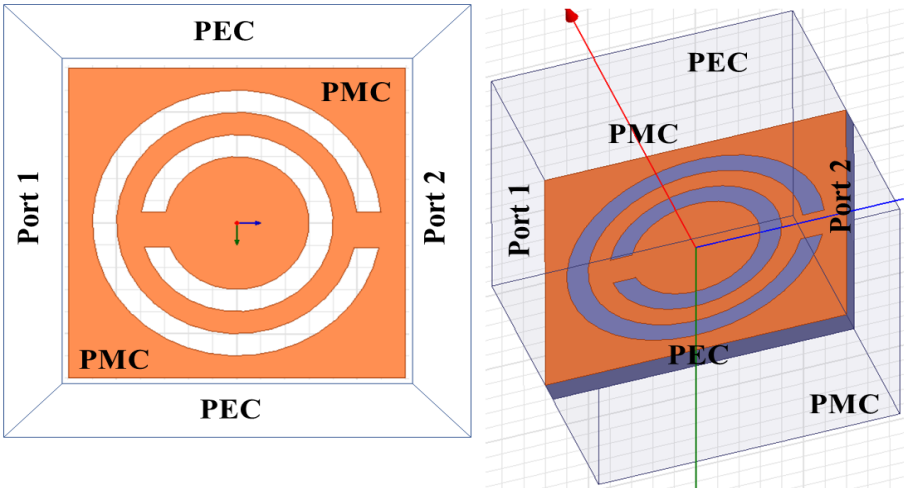

FIGURE 6.2: Circular SRR Analysis for the extraction of the S-parameters

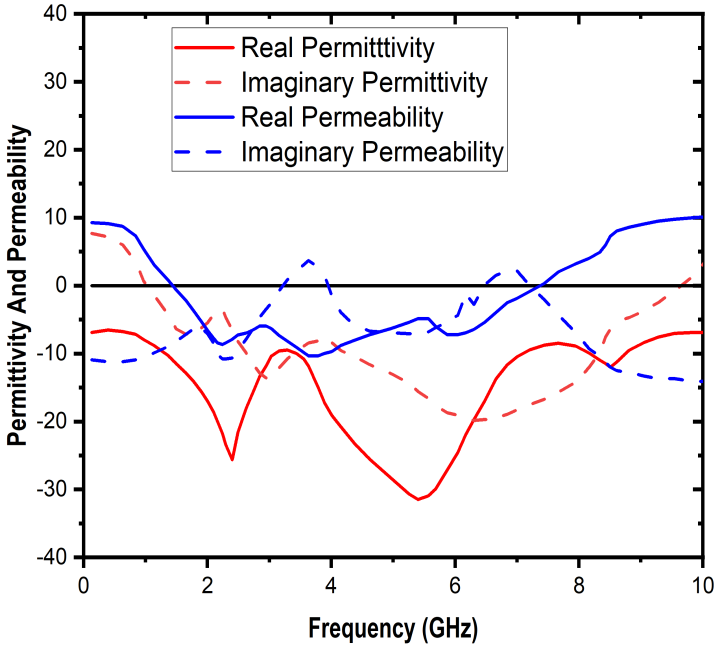

FIGURE 6.3: Variation of permittivity and permeability as a function of frequency for Circular SRR

6.2.2 Antenna Geometry

This chapter presents a flexible circular SRR loaded CPW fed antenna of 50 mm × 40 mm size. The proposed antenna geometry is shown in Fig. 6.4, and its dimensions are listed in Table 6.1. In this proposed design, PDMS having a thickness of 1 mm is used as a substrate. A 50 Ω co-planar waveguide (CPW) feed is preferred here to minimize losses and backward radiation. This antenna has a two-layered structure; another ground plane is also used at the backside of the patch, having a rectangular slot to give the antenna a multiple band characteristic so that the presented antenna resonates at the required frequencies. As described in the previous section, a single SRR ring is inserted in the circular patch to improve its performance parameters and give antenna multi-notched frequency band behavior. All the dimensions of the presented design are carefully optimized to obtain the required characteristics using the HFSS.

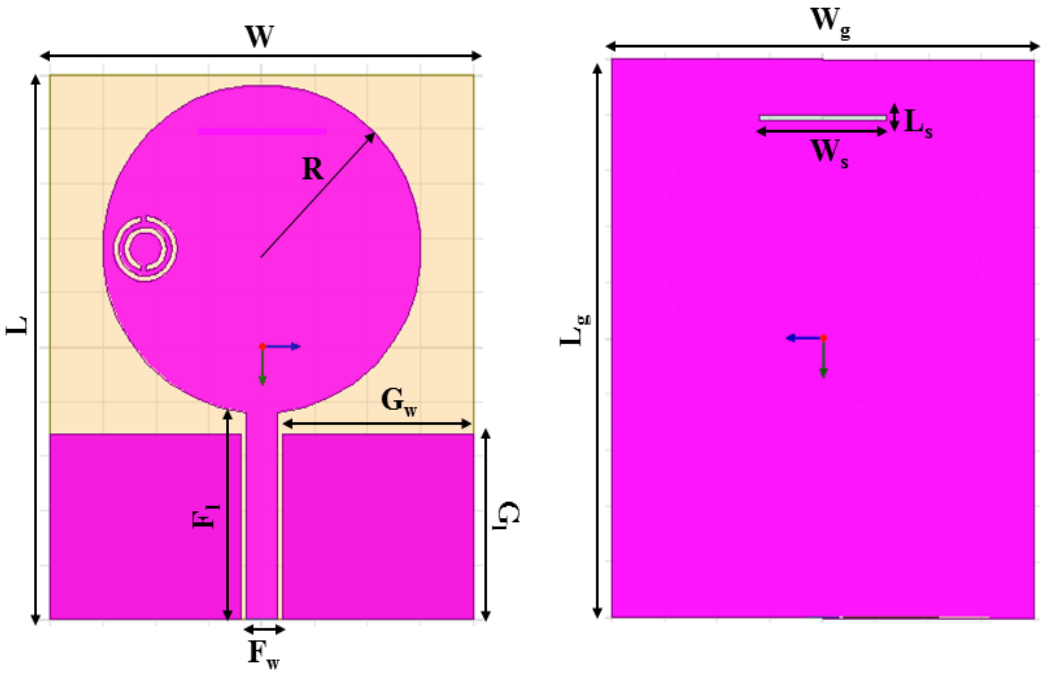

FIGURE 6.4: Antenna Geometery

TABLE 6.1: Antenna Design Parameters with Dimensions

Parameters	**Dimensions (in mm)**
Substrate Length (L)	50
Substrate Width (W)	40
Patch Radius (R)	15
Feed Length (F_l)	17
Feed Width (F_w)	18
Ground-1 Length (G_l)	19
Ground-1 Width (G_w)	3
Ground-2 Length (L_g)	50
Ground- 2 Width (W_g)	40
Slot Length (L_s)	12
Slot Width (W_s)	0.5

6.2.3 Development of Prototype

In order to validate the obtained simulation results, the presented antenna is fabricated, and measurements are performed using the KEYSIGHT N9928A vector network analyzer (VNA), as shown in Fig. 6.5 (c). PDMS substrate is cut in the required dimensions of 50 mm × 40 mm for fabricating the antenna. The radiating patch, ground, and feed are made up of copper constructed using the adhesive copper tape of thickness 0.06 mm. As PDMS substrate possesses excellent adhesive properties, the copper tape sticks more easily on the substrate. The antenna fabricated using the PDMS substrate is highly flexible, stable, adhesive to the material used for constructing the radiating parts, and transparent. A detailed analysis of performance parameters, bending, SAR, and wet condition analysis are presented in the next section.

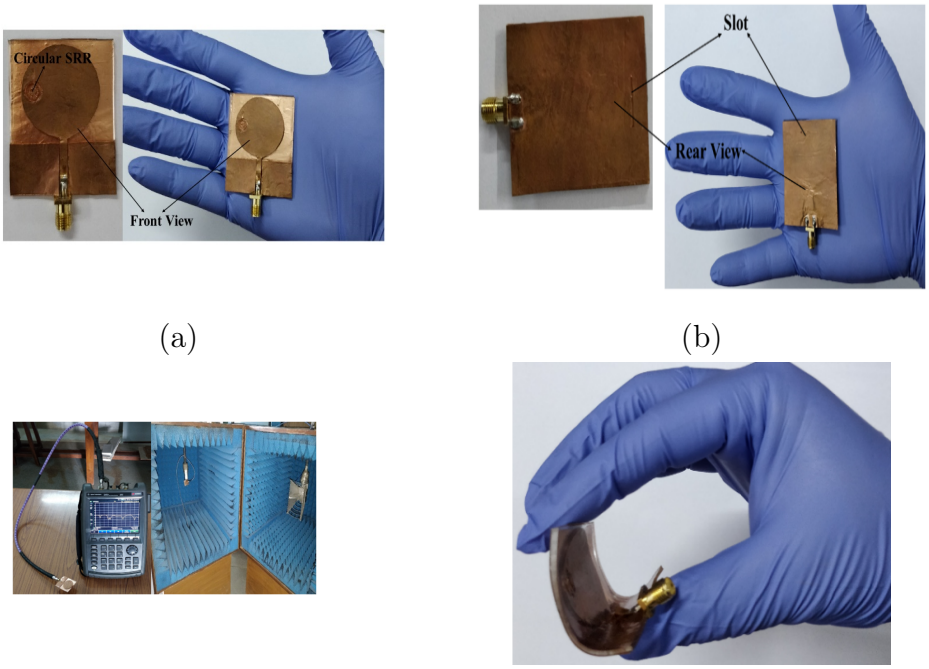

FIGURE 6.5: Fabricated Antenna: (a) Front-view, (b) Rear-view, (c) Measurement set-up, and (d) Developed Flexible antenna

6.3 Performance Analysis

This section presents the comparative analysis of simulated and measured results for the proposed antenna. The proposed antenna has triple band-notched characteristics, as shown in Fig. 6.6 and it is operating at 5 GHz (as per the IEEE 802.11ac requirements) for WLAN applications, introduced in recent years to overcome the traffic-related issues for the 2.4 GHz band; 5.8 GHz (as per the IEEE 802.16d requirements) for high-speed WiMAX and WBAN applications and 6.6 GHz (as per the IEEE 802.11ax requirements) which is the new 6 GHz band introduced only in 2020 for high speed and data rates for WLAN applications.

The impedance bandwidth (-10 dB) of 820 MHz (4.42 GHz- 5.24 GHz) at 5 GHz, 640 MHz (5.53 GHz- 6.17 GHz) at 5.8 GHz and 520 MHz (6.23 GHz- 6.75 GHz) at 6.6 GHz is observed in the simulated results and 780 MHz (4.70 GHz- 5.48 GHz) at 5.2 GHz, 560 MHz (5.61 GHz- 6.17 GHz) at 5.9 GHz and 510 MHz (6.42 GHz- 6.93 GHz) at 6.8 GHz is observed in the measured results. The corresponding reflection coefficient (S_{11}) and VSWR values (Fig. 6.7, $<$2 dB VSWR is observed)

across these resonating frequencies are listed in Table 6.2. The discrepancy in measured and simulated results may be due to the fabrication, soldering exactness, and measurement conditions.

The peak gain observed in the simulation at 5.0 GHz is 6.2 dBi, 5.8 GHz is 4.2 dBi, and at 6.6 GHz is 2.3 dBi which is quite comparable with the measured peak gains of 6.0 dBi at 5.2 GHz, 4.1 dBi at 5.9 GHz, and 2.1 dBi at 6.8 GHz, as illustrated in Fig. 6.8. Fig. 6.9 shows the good agreement between simulated and measured radiation patterns at E and H planes at different resonant frequencies of the presented antenna. The proposed antenna exhibits a typical monopole behavior having an omnidirectional radiation pattern at lower frequencies. It is nearly omnidirectional at higher frequencies of 6.6 GHz and 6.8 GHz in simulated and measured results, respectively.

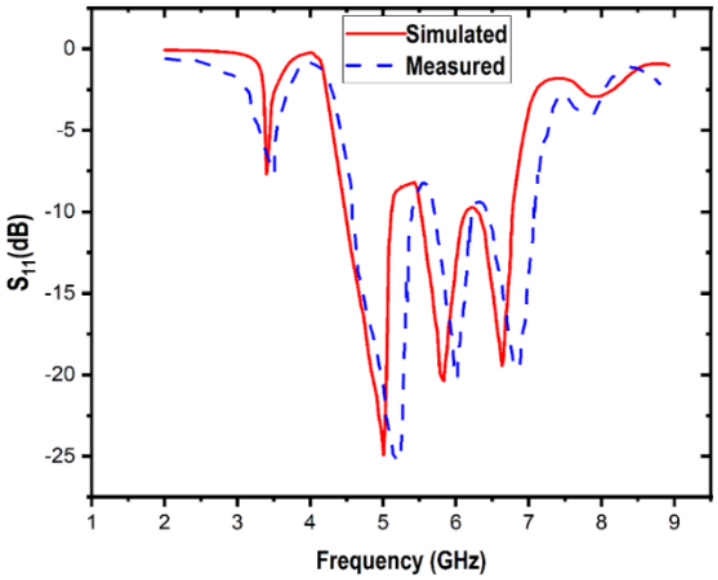

FIGURE 6.6: Simulated and Measured S_{11} vs. frequency curve for proposed flexible antenna

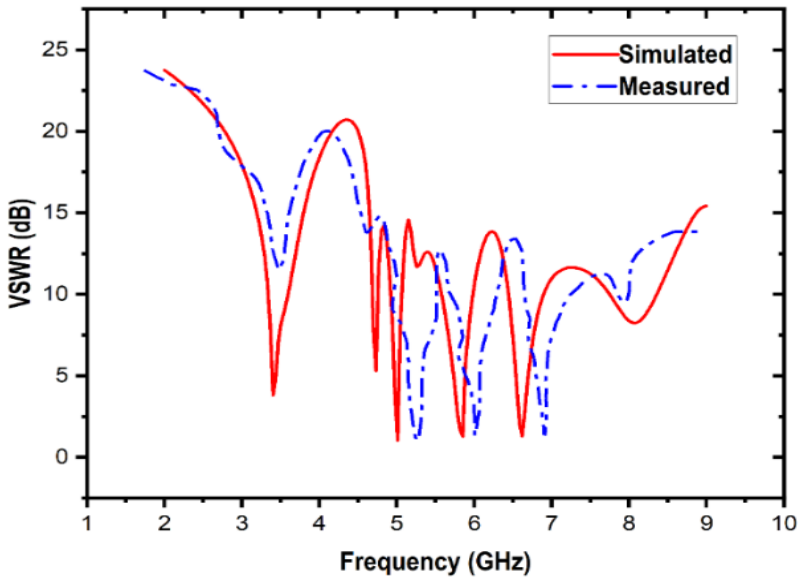

FIGURE 6.7: Simulated and Measured VSWR vs. frequency curve for proposed flexible antenna

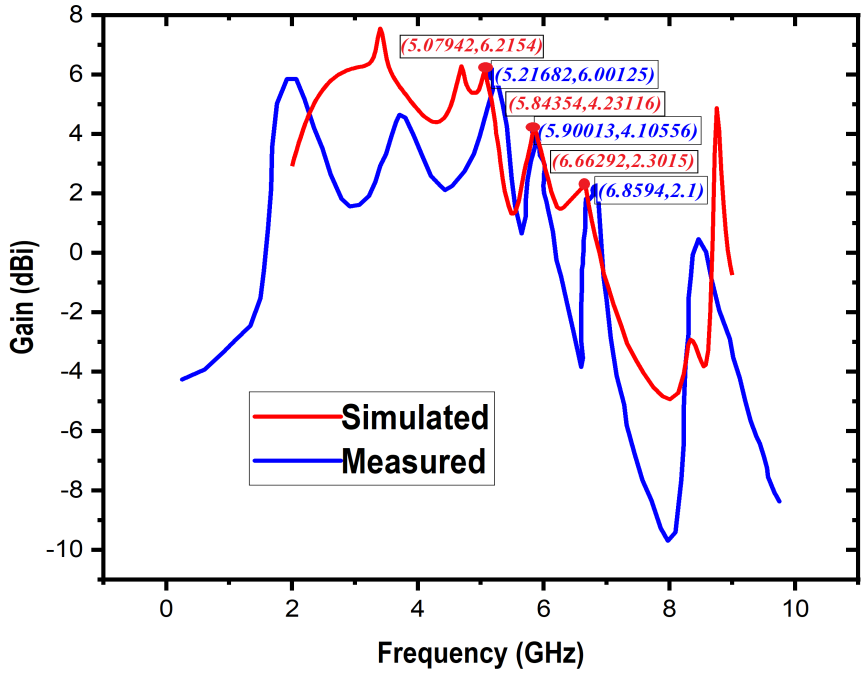

FIGURE 6.8: Simulated and Measured Gain vs. frequency curve for proposed flexible antenna

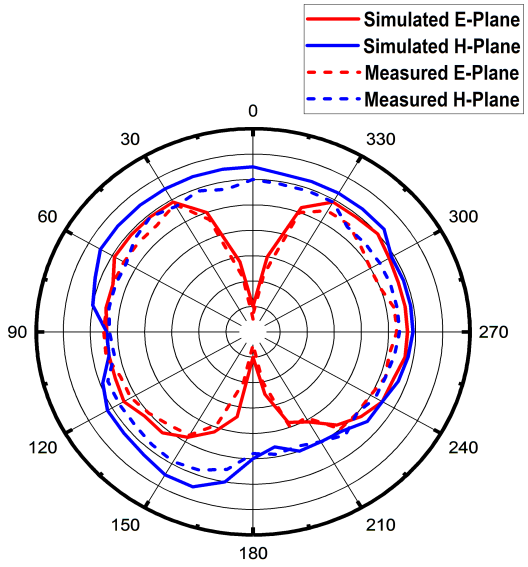

(a) 5 GHz

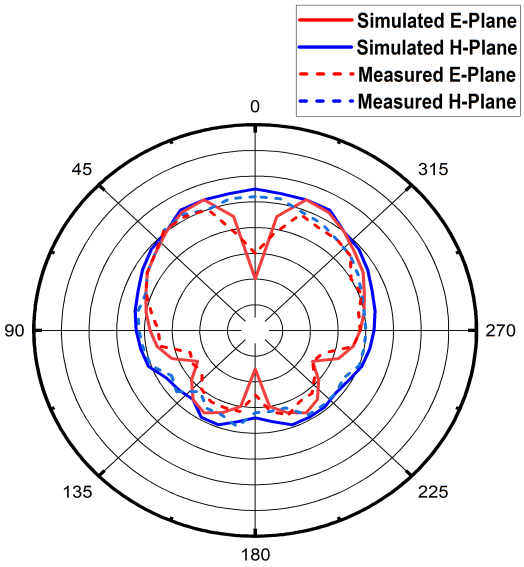

(b) 5.8 GHz

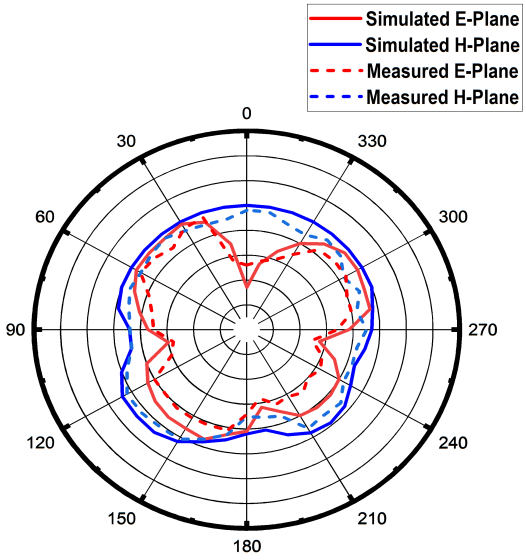

(c) 6.6 GHz

FIGURE 6.9: E and H plane curves for various resonance frequencies for the proposed flexible antenna

TABLE 6.2: Comparison of Simulated and Measured Results

Performance Parameters	**Simulated**	**Measured**
Impedance Bandwidth	5.0 GHz: 4.42-5.24 GHz = 820 MHz 5.8 GHz: 5.53-6.17 GHz = 640 MHz 6.6 GHz: 6.23-6.75 GHz = 520 MHz	5.2 GHz: 4.70-5.48 GHz = 780 MHz 5.9 GHz: 5.61-6.17 GHz = 560 MHz 6.8 GHz: 6.42-6.93 GHz = 510 MHz
S_{11}	5 GHz: -24.9 dB 5.8 GHz: -20.2 dB 6.6 GHz: -19.4 dB	5.2 GHz: -23.5 dB 5.9 GHz: -18.3 dB 6.8 GHz: - 17.8 dB
VSWR	5 GHz: 1.03dB 5.8 GHz: 1.6dB 6.6 GHz: 1.2dB	5.2 GHz: 1.3 dB 5.9 GHz: 1.9 dB 6.8 GHz: 1.9 dB
Gain	5 GHz: 6.2 dBi 5.8 GHz: 4.2 dBi 6.6 GHz: 2.3 dBi	5.2 GHz: 6.0 dBi 5.9 GHz: 4.1 dBi 6.8 GHz: 2.1 dBi

6.4 Bending Analysis

In order to analyze the effect of bending on the radiation characteristics of the antenna, the developed antenna is tested under bending conditions. To observe its effect, two different conditions are selected; in the first case, the antenna's performance is measured on the human hand at 10° bend, and in the second case, two different cylinders of the radius 3 cm and 4 cm are used for the measurements. Fig. 6.10 shows the measurement set-up on the human hand and two different cylinders for the presented antenna.

Case-I: When the antenna is placed on the human hand for measurements, as shown in Fig. 6.10 (a), it acts as a lossy medium due to the presence of human tissues, which may absorb some amount of energy. This leads to the change in the proposed antenna's S-parameters values, and shifting in the resonating frequencies can also be observed, as illustrated in Fig. 6.11 (a). However, it is observed that the presented antenna continues to operate in the required frequency bands and has triple-band characteristics. The dielectric properties of substrate play an important role here, as the dielectric constant of PDMS is relatively low. Hence, it helps in suppressing the surface waves for the proper impedance matching.

Case-II: To further analyze the bending effect on the antenna's performance, the proposed fabricated antenna is mounted on the two cylinders of radius 3 cm and 4 cm, as shown in Fig. 6.10 (b). A slight shift in the resonant frequencies and

corresponding S_{11} values are noticed. However, the antenna continues to operate in the required triple frequency bands delivering the notched features, as illustrated in Fig. 6.11 (b). In a recent study [52], we examined the influence of substrate anisotropy and bending on the performance characteristics of the flexible antenna. So, based on our previous research and the results of the current experimental analysis, it can be deduced that with the increase in the bending (decreasing the bending surface radius from 4 cm to 3 cm), the resonating frequencies increases and bandwidth decreases. However, because this difference isn't considerable here (compared to no-bend conditions), the proposed antenna still performs effectively in the bending environment.

(a)

(b)

FIGURE 6.10: Measurement Set-up for bending, (a) On human hand (10° bend), and (b) Using 3 cm and 4 cm cylinders

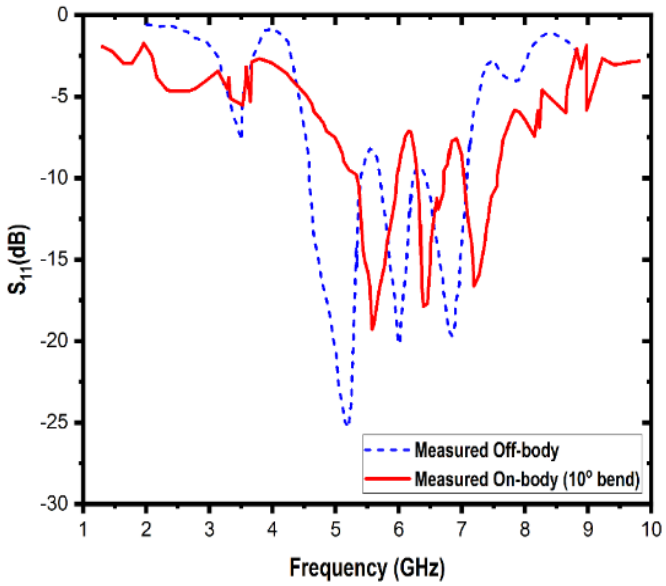

(a)

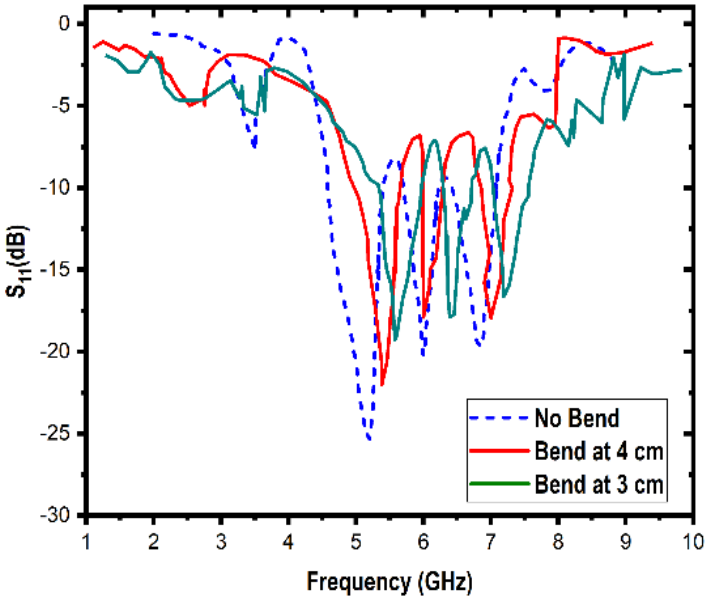

(b)

FIGURE 6.11: Measured S_{11} values under different bending conditions, (a) At 10° (on human hand), and (b) Bend at 3 cm and 4 cm cylinder

6.5 SAR Analysis

In order to check the effect of the antenna on human body, the specific absorption rate (SAR) analysis is performed using the three-layered simulation model as shown

in Fig. 6.12 (a). Fig. 6.12 (b), (c), and (d) show that the SAR values obtained by applying simulation model using HFSS at 5, 5.8 GHz, and 6.6 GHz are 1.601 W/kg, 1.607 W/kg, and 1.9 W/kg, respectively. As per the European standard, SAR should be lower than 2 W/kg for 10 grams of an average mass of human tissue. The obtained SAR values for the proposed antenna at all the resonating frequencies satisfy these criteria.

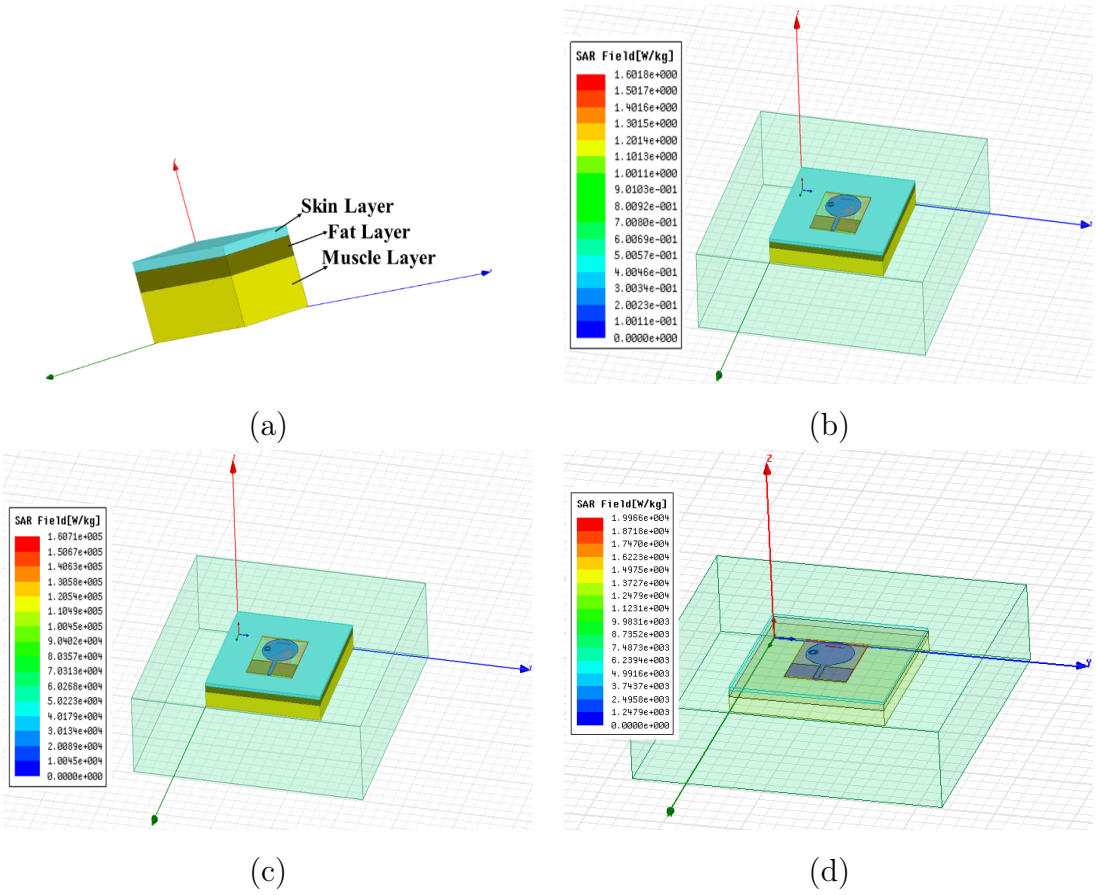

FIGURE 6.12: SAR analysis: (a) Simulation model, (b) At 5.0 GHz and, (c) At 5.8 GHz, and (d) At 6.6 GHz

6.6 Testing under Wet Conditions

Various fabric substrate-based flexible antennas reported in previous studies are more susceptible to environmental conditions due to moisture absorption (as shown in the previous design) and temperature variations, which negatively affect the antenna's radiating characteristics. Because of physical and chemical properties,

polymer substrates like PDMS-based antennas transcend this barrier. To demonstrate this, the developed antenna is further tested under wet settings by immersing it in water, after that dried for ten minutes and analysis is done for its performance.

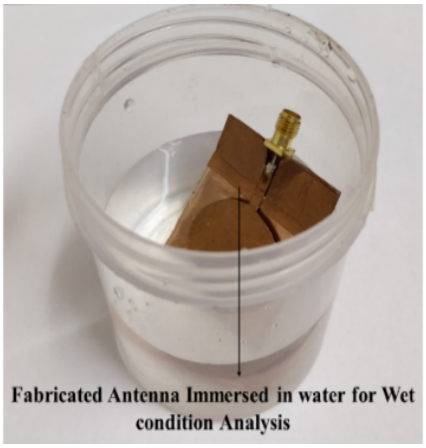

(a)

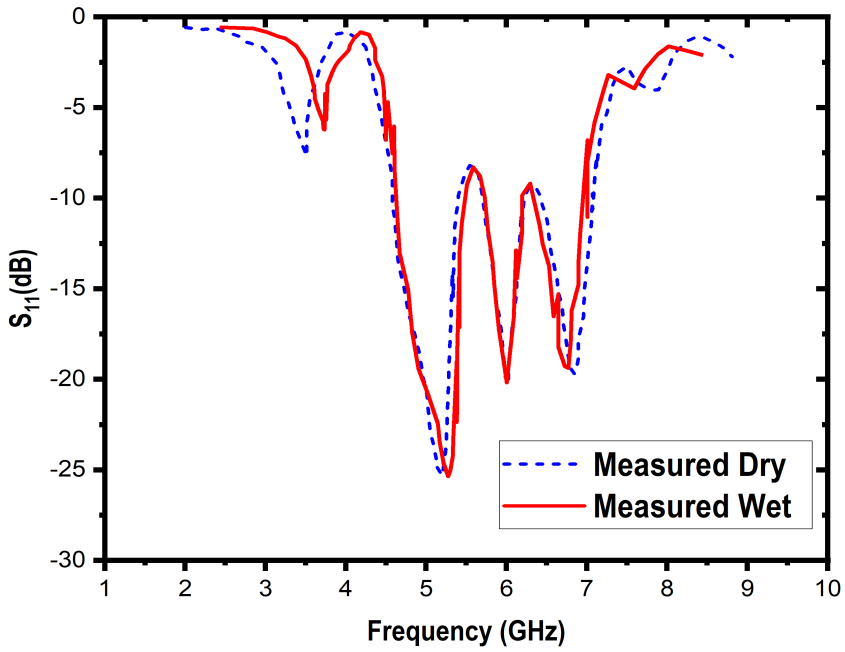

(b)

FIGURE 6.13: Wet condition analysis: (a) Measurement Set-up, (b) Measured S_{11} values of the proposed flexible antenna under wet condition

Fig. 6.13 (a) and (b) shows the measurement set-up of wet condition analysis and variation of S_{11} parameters. A very slight change in the resonating frequencies

and their S_{11} values is observed for PDMS-based antenna compared to the fabric substrate-based antenna [239], having a gigantic shift in these parameters.

TABLE 6.3: Comparison of Proposed Flexible Antenna (PA) with Previous Works

Substrate Used	**Antenna Size (mm^2)**	**Gain (dBi)**	**Frequency Bands/ Applications**	**Metamaterial loading**	**Test in different operating conditions**	**Ref.**
Liquid Crystalline Polymer (LCP)	40×22	4.2	7.5 GHz, UWB band	Not used	Bending Test: Performed; Wet condition Test: Not Performed SAR Analysis: Not Performed	[228]
Cotton	70x60	6.1	UWB band applications	Not used	Bending Test: Performed; Wet condition Test: Not Performed SAR Analysis: Not Performed	[229]
Cotton	94.4 × 113	5.72	2.4 GHz, wearable applications	Mushroom, slotted, and spiral EBG structures	Bending Test: Performed, Wet condition Test: Not Performed SAR Analysis: Performed	[153]
Viscose-wool felt	33 × 30	4.8	UWB band applications	CSRR	Bending Test: Not Performed; Wet condition Test: Not Performed SAR Analysis: Not Performed	[154]
Jean	60 × 60	1.6, 5	2.3/5.5 GHz, WLAN and WiMAX applications	Square SRR	Bending Test: Performed; Wet condition Test: Not Performed SAR Analysis: Performed	[158]
Liquid crystal polymer (LCP)	38 × 32	2	3.5/5.8 GHz, WLAN and WiMAX applications	Circular SRR	Bending Test: Performed; Wet condition Test: Not Performed SAR Analysis: Not Performed	[103]

Continued on next page

Table 6.3– Continued from previous page

Substrate Used	**Antenna Size (mm^2)**	**Gain (dBi)**	**Frequency Bands/ Applications**	**Metamaterial loading**	**Test in different operating conditions**	**Ref.**
PDMS	70 (Diameter)	4.16	2.45/5.8 GHz, ISM band	not used	Bending Test: Performed, Wet condition Test: Not Performed SAR Analysis: Performed	[87]
PDMS	22 x 22	2.25	2.4/3.1 GHz, wearable applications	Not used	Bending Test: Performed, Wet condition Test: Not Performed SAR Analysis: Not Performed	[241]
PDMS	**50×40**	**6.2**	**5.0/5.8/6.6 GHz WLAN/WBAN applications**	**Single circular SRR**	**Bending Test: Performed, Wet condition Test: Performed SAR Analysis: Performed**	**PA**

A comparison of the presented antenna with the previous works is illustrated in Table 6.3. The presented table shows that the proposed flexible antenna is advantageous in terms of gain, multiple frequency bands, and design complexity with reduced size.

6.7 Conclusion

A triple-band CPW-fed flexible antenna using PDMS substrate is presented in this chapter. The proposed antenna resonates at 5 GHz, 5.8 GHz, and 6.6 GHz for WLAN and WBAN applications. To impart the desired notched characteristics, reduce losses and overall size, a single circular SRR ring structure is employed on the same side of the patch with a rectangular slot at the back side. The performance of the presented antennas is also assessed in a variety of operating conditions, such as open space, bending, and wet conditions. The SAR analysis conducted in this research investigates the influence of antenna on the human body. The SAR values obtained using a three-layered simulation model for both proposed designs are less than 2, which are in compliance with the European criteria. The simulated and measured results are found to be in good agreement. The developed flexible antenna is well suited for the intended applications due to its compact structure,

simple and cost-effective fabrication process, flexibility, and consistent performance under diverse operating situations.

Chapter 7

Conclusion and Future Scope

Microwave antennas have been a focus of study, research, and development for a long time. The field of flexible and wearable antennas has also taken a leap into the futuristic vision of achieving high-speed and efficient communication systems, especially with the development of flexible electronics. Rigid substrate-based antennas were not only extensively researched, but they were also widely used in commercial applications. However, as the working environments of antennas for various application requirements, such as body-centric wireless communication, changed, these antennas were unable to meet the requisite performance. Flexible antennas, on the other hand, meet these criteria and operate well in a variety of operational environments. There is a variety of conducting and substrate material choices available in the literature, however in most cases, dielectric characterization of these substrates is either not done, or the values of the dielectric parameters vary, and some of them fail to perform in a variety of operating conditions. Since the substrate's dielectric characteristics affect the antenna's performance, a proper characterization of the substrate is also necessary with the parametric analysis of the antenna.

Thus, the objective of this thesis was to design, characterize, and analyze polydimethylsiloxane (PDMS) based flexible antenna. In order to achieve this research goal, some specific objectives were made, which include development and dielectric characterization of the flexible antenna substrate, investigation of the dielectric anisotropy and bending effect of the flexible substrates, design, simulation and analysis of the antenna on the developed flexible substrate and fabrication and testing of the developed antenna under various operating conditions.

Two prototypes of flexible antennas were designed and their performance was experimentally validated in this research. The initial prototype was developed to experimentally verify the benefits of using polymer substrate (PDMS) over fabric substrate (Denim). The metamaterial-inspired prototype, which was loaded with a single SRR flexible antenna on a PDMS substrate, was the second proposed prototype. This prototype was intended to facilitate the most recent WLAN and WBAN applications. According to IEEE 802.11ac, 802.16d, and 802.11ax specifications, the given antenna has triple band-notched characteristics and operates at 5 GHz, 5.8 GHz, and 6.6 GHz. Both fabricated prototypes were put through their paces in a variety of operating scenarios, with the simulated data demonstrating reasonable agreement.

7.1 Thesis Highlights

The main highlights of the research work presented in this thesis are mentioned below:

The research started with a comprehensive review of the flexible antennas from their inception to the current state of the art. This forms chapters 1 and 2 of this thesis. The first chapter provides a brief introduction of flexible antennas and also addresses the critical problems in developing and deploying flexible antennas for diverse applications in the current context. The research motivation and objectives were also presented in this chapter. In Chapter 2, a detailed study of flexible antennas was conducted to explain their adaptability for various wireless applications as well as their capacity to operate exceptionally well in a typical operating situations. Fundamental concepts, theory, and a detailed review of the different types of conducting and substrate materials, fabrication techniques, and also the usage of metamaterial to enhance the performance of flexible antennas were presented in this chapter.

Polymer substrates were favored over other types of substrates for the flexible antenna design in this research after analyzing different substrate choices available for the development of flexible antennas from the literature review presented

in chapter 2. Because of its numerous advantages for diverse applications, Polydimethylsiloxane (PDMS) was chosen as a substrate. However, researchers have employed different dielectric parameter values, and this material has small but measurable anisotropy, so this laid the groundwork for chapter 3. The development process used at the BITS-Pilani lab for PDMS, primarily as a flexible antenna substrate, was described in Chapter 3. In this chapter, two experimental methods for PDMS dielectric characterization were described. The first method presented was based on resonance measurements, whereas the second method proposed was based on the use of planar structures. These approaches have been used to determine the dielectric properties of PDMS in both parallel and perpendicular directions. The temperature and frequency dependencies of dielectric parameters have also been investigated in this chapter. It is the necessity of a flexible antenna that it should operate well under different conformal conditions, so in chapter 4, the effect of bending and anisotropy have been experimentally and numerically investigated for flexible substrates. Both of these phenomena have been found to have opposing impacts on the resonance characteristics of flexible antennas.

The two prototypes were finally presented in Chapters 5 and 6, after a thorough investigation of all of the PDMS properties. The first prototype was designed to accomplish a comparison investigation of fabric (Denim) and polymer (PDMS) substrates in order to experimentally verify the advantages of polymer substrates over fabric-based substrates based on theoretical observations. The second prototype, which uses PDMS as a substrate, was created for the most recent WLAN and WBAN applications. The proposed design also included a single split-ring resonator (SRR) structure to improve its performance. Both the presented antenna designs were tested for different operating conditions, including bending and damp situations. SAR analysis was carried out on both prototypes to check the effect of the antenna on the human body. The SAR was found to be within the European standard's limits. All of the simulated and experimental results for both prototypes were in good agreement with one another, indicating that the planned applications were met. Despite the fact that all of the research objectives were met, there are still areas that need further investigation.

7.2 Future Scope of Work

In order to continue and improve the work presented in the thesis, the following improvements as future scope of the work are recommended:

- Different experimental methods proposed to characterize the dielectric properties of Polydimethylsiloxane (PDMS) in chapter 3 can be applied to evaluate the dielectric properties of other polymer and paper substrates.
- The dielectric properties of Polydimethylsiloxane (PDMS) can be further modified by adding different dopants like graphene.
- The proposed experimental and numerical methods in chapter 4 for investigating the bending and anisotropy influence can be extended to more complex structures such as metasurfaces.
- To make PDMS more flexible, ultra-thin metallic nanowires can be inserted on the surface as a micro-crack prevention technique.
- In the proposed metamaterial inspired flexible antenna, only a single split ring resonator structure (SRR) is used, but further improvement in the radiation properties of the antenna can be possible by using an array of SRRs.
- Future work could involve investigating novel flexible antenna designs with other flexible substrates using different fabrication techniques.

Bibliography

[1] D. Siegel and S. Shivakumar, *The Flexible Electronics Opportunity.* National Academies Press, 2014.

[2] P. Salonen, L. Sydanheimo, M. Keskilammi, and M. Kivikoski, "A small planar inverted-F antenna for wearable applications," in *Digest of Papers. Third International Symposium on Wearable Computers*, 1999, pp. 95–100.

[3] P. Massey, "Mobile phone fabric antennas integrated within clothing," in *2001 Eleventh International Conference on Antennas and Propagation,(IEE Conf. Publ. No. 480)*, vol. 1. IET, 2001, pp. 344–347.

[4] P. Salonen and L. Sydanheimo, "Development of an S-band flexible antenna for smart clothing," in *IEEE Antennas and Propagation Society International Symposium (IEEE Cat. No. 02CH37313)*, vol. 3. IEEE, 2002, pp. 6–9.

[5] C. Cibin, P. Leuchtmann, M. Gimersky, R. Vahldieck, and S. Moscibroda, "A flexible wearable antenna," in *IEEE Antennas and Propagation Society Symposium, 2004.*, vol. 4. IEEE, 2004, pp. 3589–3592.

[6] A. Jafargholi, "VHF-LB vest antenna design," in *2007 International workshop on Antenna Technology: Small and Smart Antennas Metamaterials and Applications.* IEEE, 2007, pp. 247–250.

[7] M. L. Scarpello, D. V. Ginste, and H. Rogier, "Design of a low-cost steerable textile antenna array operating in varying relative humidity conditions," *Microwave and Optical Technology Letters*, vol. 54, no. 1, pp. 40–44, 2012.

[8] P. Sethi and S. R. Sarangi, "Internet of things: Architectures," *Protocols, and Applications.[(accessed on 16 April 2018)].*

[9] W. Gao, Y. Zhu, Y. Wang, G. Yuan, and J.-M. Liu, "A review of flexible perovskite oxide ferroelectric films and their application," *Journal of Materiomics*, vol. 6, no. 1, pp. 1–16, 2020.

[10] S. F. Jilani, Q. H. Abbasi, and A. Alomainy, "Inkjet-printed millimetre-wave pet-based flexible antenna for 5G wireless applications," in *2018 IEEE MTT-S International Microwave Workshop Series on 5G Hardware and System Technologies (IMWS-5G).* IEEE, 2018, pp. 1–3.

[11] S. Huang, Y. Liu, Y. Zhao, Z. Ren, and C. F. Guo, "Flexible electronics: stretchable electrodes and their future," *Advanced Functional Materials*, vol. 29, no. 6, p. 1805924, 2019.

[12] I. Gagnadre, C. Gagnadre, and J. Fenelon, "Circular patch antenna sensor for moisture content measurement on dielectric material," *Electronics Letters*, vol. 31, no. 14, pp. 1167–1168, 1995.

[13] A. Denoth, "The monopole-antenna: A practical snow and soil wetness sensor," *IEEE transactions on geoscience and remote sensing*, vol. 35, no. 5, pp. 1371–1375, 1997.

[14] M. P. McGrath, R. N. Sabouni, and A.-V. H. Pham, "Development of nanobased resonator gas sensors for wireless sensing systems," in *Nanosensing: Materials and Devices*, vol. 5593. International Society for Optics and Photonics, 2004, pp. 62–72.

[15] M. T. Islam, F. B. Ashraf, T. Alam, N. Misran, and K. B. Mat, "A compact ultrawideband antenna based on hexagonal split-ring resonator for ph sensor application," *Sensors*, vol. 18, no. 9, p. 2959, 2018.

[16] K. Chang, Y.-H. Kim, Y.-J. Kim, and Y. J. Yoon, "Patch antenna using synthesized polyimide for RFID sensing," in *2006 European Conference on Wireless Technology*. IEEE, 2006, pp. 83–86.

[17] K. You, J. Salleh, Z. Abbas, and L. You, "A rectangular patch antenna technique for the determination of moisture content in soil," *Progress in Electromagnetics Research C*, pp. 850–854, 2010.

[18] D. B. Rodrigues, P. F. Maccarini, S. Salahi, T. R. Oliveira, P. J. Pereira, P. Limão-Vieira, B. W. Snow, D. Reudink, and P. R. Stauffer, "Design and optimization of an ultra wideband and compact microwave antenna for radiometric monitoring of brain temperature," *IEEE transactions on biomedical engineering*, vol. 61, no. 7, pp. 2154–2160, 2014.

[19] T. Padmavathy, D. Bhargava, P. Venkatesh, and N. Sivakumar, "Design and development of microstrip patch antenna with circular and rectangular slot for structural health monitoring," *Personal and Ubiquitous Computing*, vol. 22, no. 5, pp. 883–893, 2018.

[20] F. M. Tchafa and H. Huang, "Microstrip patch antenna for simultaneous strain and temperature sensing," *Smart Materials and Structures*, vol. 27, no. 6, p. 065019, 2018.

[21] P. K. Sharma, N. Gupta, and P. I. Dankov, "Characterization of polydimethylsiloxane (pdms) as a wearable antenna substrate using resonance and planar structure methods," *AEU-International Journal of Electronics and Communications*, vol. 127, p. 153455, 2020.

[22] P. K. Sharma, N. Gupta, and P. Dankov, "Wideband transmission line characterization of polydimethylsiloxane (pdms) as a wearable antenna substrate," 2020.

[23] P. Sharma, N. Gupta, and P. Dankov, "Analysis of dielectric properties of polydimethylsiloxane (pdms) as a flexible substrate for sensors and antenna applications," *IEEE Sensors Journal*, 2021.

[24] T. Kaufmann, A. Verma, S. F. Al-Sarawi, V.-T. Truong, and C. Fumeaux, "Comparison of two planar elliptical ultra-wideband ppy conductive polymer antennas," in *Proceedings of the 2012 IEEE International Symposium on Antennas and Propagation*. IEEE, 2012, pp. 1–2.

[25] A. Ghasemi and E. S. Sousa, "Spectrum sensing in cognitive radio networks: requirements, challenges and design trade-offs," *IEEE Communications magazine*, vol. 46, no. 4, pp. 32–39, 2008.

[26] H. Zahir, J.-L. Wojkiewicz, P. Alexander, L. Kone, B. Belkacem, S. Bergheul, and T. Lasri, "Design fabrication and characterisation of polyaniline and multiwall carbon nanotubes composites-based patch antenna," *IET Microwaves, Antennas & Propagation*, vol. 10, no. 1, pp. 88–93, 2016.

[27] K.-Y. Shin, S. Cho, and J. Jang, "Graphene/polyaniline/poly (4-styrenesulfonate) hybrid film with uniform surface resistance and its flexible dipole tag antenna application," *small*, vol. 9, no. 22, pp. 3792–3798, 2013.

[28] K. Ankireddy, T. Druffel, S. Vunnam, G. Filipič, R. Dharmadasa, and D. A. Amos, "Seed mediated copper nanoparticle synthesis for fabricating oxidation free interdigitated electrodes using intense pulse light sintering for flexible printed chemical sensors," *Journal of Materials Chemistry C*, vol. 5, no. 42, pp. 11 128–11 137, 2017.

[29] J. S. Lee, M. Kim, J. Oh, J. Kim, S. Cho, J. Jun, and J. Jang, "Platinum-decorated carbon nanoparticle/polyaniline hybrid paste for flexible wideband dipole tag-antenna application," *Journal of Materials Chemistry A*, vol. 3, no. 13, pp. 7029–7035, 2015.

[30] A. M. Al-Sadi, F. A. Al-Oweisi, S. G. Edwards, H. Al-Nadabi, and A. M. Al-Fahdi, "Genetic analysis reveals diversity and genetic relationship among trichoderma isolates from potting media, cultivated soil and uncultivated soil," *BMC microbiology*, vol. 15, no. 1, pp. 1–11, 2015.

[31] Y. Zare and K. Y. Rhee, "Calculation of the electrical conductivity of polymer nanocomposites assuming the interphase layer surrounding carbon nanotubes," *Polymers*, vol. 12, no. 2, p. 404, 2020.

[32] Z. Hamouda, J.-L. Wojkiewicz, A. A. Pud, L. Koné, S. Bergheul, and T. Lasri, "Magnetodielectric nanocomposite polymer-based dual-band flexible antenna for wearable applications," *IEEE Transactions on Antennas and Propagation*, vol. 66, no. 7, pp. 3271–3277, 2018.

[33] K. Guerchouche, E. Herth, L. E. Calvet, N. Roland, and C. Loyez, "Conductive polymer based antenna for wireless green sensors applications," *Microelectronic Engineering*, vol. 182, pp. 46–52, 2017.

[34] P. Kopyt, B. Salski, M. Olszewska-Placha, D. Janczak, M. Sloma, T. Kurkus, M. Jakubowska, and W. Gwarek, "Graphene-based dipole antenna for a UHF RFID tag," *IEEE Transactions on Antennas and Propagation*, vol. 64, no. 7, pp. 2862–2868, 2016.

[35] W. Dang, V. Vinciguerra, L. Lorenzelli, and R. Dahiya, "Printable stretchable interconnects," *Flexible and Printed Electronics*, vol. 2, no. 1, p. 013003, 2017.

[36] L. Song, A. C. Myers, J. J. Adams, and Y. Zhu, "Stretchable and reversibly deformable radio frequency antennas based on silver nanowires," *ACS applied materials & interfaces*, vol. 6, no. 6, pp. 4248–4253, 2014.

[37] M. Park, J. Im, M. Shin, Y. Min, J. Park, H. Cho, S. Park, M.-B. Shim, S. Jeon, D.-Y. Chung *et al.*, "Highly stretchable electric circuits from a composite material of silver nanoparticles and elastomeric fibres," *Nature nanotechnology*, vol. 7, no. 12, pp. 803–809, 2012.

[38] S. G. Kirtania, A. W. Elger, M. Hasan, A. Wisniewska, K. Sekhar, T. Karacolak, P. K. Sekhar *et al.*, "Flexible antennas: a review," *Micromachines*, vol. 11, no. 9, p. 847, 2020.

[39] W. S. Wong and A. Salleo, *Flexible electronics: materials and applications*. Springer Science & Business Media, 2009, vol. 11.

[40] Y. Kim, J. Zhu, B. Yeom, M. Di Prima, X. Su, J.-G. Kim, S. J. Yoo, C. Uher, and N. A. Kotov, "Stretchable nanoparticle conductors with self-organized conductive pathways," *Nature*, vol. 500, no. 7460, pp. 59–63, 2013.

[41] S. Khan, L. Lorenzelli, and R. S. Dahiya, "Technologies for printing sensors and electronics over large flexible substrates: a review," *IEEE Sensors Journal*, vol. 15, no. 6, pp. 3164–3185, 2014.

[42] W. A. MacDonald, M. Looney, D. MacKerron, R. Eveson, R. Adam, K. Hashimoto, and K. Rakos, "Latest advances in substrates for flexible electronics," *Journal of the Society for Information Display*, vol. 15, no. 12, pp. 1075–1083, 2007.

[43] R. A. Liyakath, A. Takshi, and G. Mumcu, "Multilayer stretchable conductors on polymer substrates for conformal and reconfigurable antennas," *IEEE Antennas and Wireless Propagation Letters*, vol. 12, pp. 603–606, 2013.

[44] H. Subbaraman, D. T. Pham, X. Xu, M. Y. Chen, A. Hosseini, X. Lu, and R. T. Chen, "Inkjet-printed two-dimensional phased-array antenna on a flexible substrate," *IEEE Antennas and Wireless Propagation Letters*, vol. 12, pp. 170–173, 2013.

[45] A. R. Ravindran, C. Feng, S. Huang, Y. Wang, Z. Zhao, and J. Yang, "Effects of graphene nanoplatelet size and surface area on the ac electrical conductivity and dielectric constant of epoxy nanocomposites," *Polymers*, vol. 10, no. 5, p. 477, 2018.

[46] A. Kumar, H. Saghlatoon, T.-G. La, M. M. Honari, H. Charaya, H. A. Damis, R. Mirzavand, P. Mousavi, and H.-J. Chung, "A highly deformable conducting traces for printed antennas and interconnects: Silver/fluoropolymer composite amalgamated by triethanolamine," *Flexible and Printed Electronics*, vol. 2, no. 4, p. 045001, 2017.

[47] J.-H. So, J. Thelen, A. Qusba, G. J. Hayes, G. Lazzi, and M. D. Dickey, "Reversibly deformable and mechanically tunable fluidic antennas," *Advanced Functional Materials*, vol. 19, no. 22, pp. 3632–3637, 2009.

[48] R. B. Simorangkir, Y. Yang, R. M. Hashmi, T. Björninen, K. P. Esselle, and L. Ukkonen, "Polydimethylsiloxane-embedded conductive fabric: Characterization and application for realization of robust passive and active flexible wearable antennas," *IEEE Access*, vol. 6, pp. 48 102–48 112, 2018.

[49] O. M. Sanusi, F. A. Ghaffar, A. Shamim, M. Vaseem, Y. Wang, and L. Roy, "Development of a 2.45 GHz antenna for flexible compact radiation dosimeter tags," *IEEE Transactions on Antennas and Propagation*, vol. 67, no. 8, pp. 5063–5072, 2019.

[50] K. S. Kwak, M. Ameen, D. Kwak, C. Lee, and H. Lee, "A study on proposed ieee 802.15 WBAN MAC protocols," in *2009 9th International Symposium on Communications and Information Technology*. IEEE, 2009, pp. 834–840.

[51] I. Locher, M. Klemm, T. Kirstein, and G. Troster, "Design and characterization of purely textile patch antennas," *IEEE Transactions on advanced packaging*, vol. 29, no. 4, pp. 777–788, 2006.

[52] P. I. Dankov, P. K. Sharma, and N. Gupta, "Numerical and experimental investigation of the opposite influence of dielectric anisotropy and substrate bending on planar radiators and sensors," *Sensors*, vol. 21, no. 1, p. 16, 2021.

[53] P. I. Dankov, V. P. Levcheva, and P. K. Sharma, "Influence of dielectric anisotropy and bending on wearable textile antenna properties," in *2020 International Workshop on Antenna Technology (iWAT)*. IEEE, 2020, pp. 1–4.

[54] P. Salonen and L. Hurme, "A novel fabric wlan antenna for wearable applications," in *IEEE Antennas and Propagation Society International Symposium. Digest. Held in conjunction with: USNC/CNC/URSI North American Radio Sci. Meeting (Cat. No. 03CH37450)*, vol. 2. IEEE, 2003, pp. 700–703.

[55] C. Loss, R. Gonçalves, C. Lopes, P. Pinho, and R. Salvado, "Smart coat with a fully-embedded textile antenna for IoT applications," *Sensors*, vol. 16, no. 6, p. 938, 2016.

[56] S. B. Roshni, M. Jayakrishnan, P. Mohanan, and K. P. Surendran, "Design and fabrication of an e-shaped wearable textile antenna on pvb-coated hydrophobic polyester fabric," *Smart Materials and Structures*, vol. 26, no. 10, p. 105011, 2017.

[57] M. Joler and M. Boljkovac, "A sleeve-badge circularly polarized textile antenna," *IEEE Transactions on Antennas and Propagation*, vol. 66, no. 3, pp. 1576–1579, 2018.

[58] S. M. H. Varkiani and M. Afsahi, "Compact and ultra-wideband cpw-fed square slot antenna for wearable applications," *AEU-International Journal of Electronics and Communications*, vol. 106, pp. 108–115, 2019.

[59] M. Pandimadevi, R. Tamilselvi, and M. Parisa Beham, "Design and simulation of flexible jute antenna with performance validation on bending and soaking conditions," *Textile Research Journal*, vol. 91, no. 1-2, pp. 219–231, 2021.

[60] P. Salonen, M. Keskilammi, J. Rantanen, and L. Sydanheimo, "A novel bluetooth antenna on flexible substrate for smart clothing," in *2001 IEEE International Conference on Systems, Man and Cybernetics. e-Systems and e-Man for Cybernetics in Cyberspace (Cat. No. 01CH37236)*, vol. 2. IEEE, 2001, pp. 789–794.

[61] P. Salonen, Y. Rahmat-Samii, M. Schaffrath, and M. Kivikoski, "Effect of textile materials on wearable antenna performance: A case study of gps antennas," in *IEEE Antennas and Propagation Society Symposium, 2004.*, vol. 1. IEEE, 2004, pp. 459–462.

[62] A. Tronquo, H. Rogier, C. Hertleer, and L. Van Langenhove, "Applying textile materials for the design of antennas for wireless body area networks," in *2006 First European Conference on Antennas and Propagation*. IEEE, 2006, pp. 1–5.

[63] S. Zhu and R. Langley, "Dual-band wearable antennas over EBG substrate," *Electronics Letters*, vol. 43, no. 3, pp. 141–142, 2007.

[64] L. Vallozzi, P. Van Torre, C. Hertleer, H. Rogier, M. Moeneclaey, and J. Verhaevert, "Wireless communication for firefighters using dual-polarized textile antennas integrated in their garment," *IEEE Transactions on Antennas and Propagation*, vol. 58, no. 4, pp. 1357–1368, 2010.

[65] Y. Bayram, Y. Zhou, B. S. Shim, S. Xu, J. Zhu, N. A. Kotov, and J. L. Volakis, "E-textile conductors and polymer composites for conformal lightweight antennas," *IEEE Transactions on Antennas and Propagation*, vol. 58, no. 8, pp. 2732–2736, 2010.

[66] N. Chahat, M. Zhadobov, L. Le Coq, and R. Sauleau, "Wearable endfire textile antenna for on-body communications at 60 GHz," *IEEE Antennas and Wireless Propagation Letters*, vol. 11, pp. 799–802, 2012.

[67] N. H. M. Rais, P. J. Soh, M. F. A. Malek, and G. A. Vandenbosch, "Dual-band suspended-plate wearable textile antenna," *IEEE Antennas and Wireless Propagation Letters*, vol. 12, pp. 583–586, 2013.

[68] J. Tak, S. Lee, and J. Choi, "All-textile higher order mode circular patch antenna for on-body to on-body communications," *IET Microwaves, Antennas & Propagation*, vol. 9, no. 6, pp. 576–584, 2015.

[69] J. Tak, Y. Hong, and J. Choi, "Textile antenna with ebg structure for body surface wave enhancement," *Electronics Letters*, vol. 51, no. 15, pp. 1131–1132, 2015.

[70] A. Yadav, V. K. Singh, P. Yadav, A. K. Beliya, A. K. Bhoi, and P. Barsocchi, "Design of circularly polarized triple-band wearable textile antenna with safe low sar for human health," *Electronics*, vol. 9, no. 9, p. 1366, 2020.

[71] E. Wissem, I. Sfar, L. Osman, and J.-M. Ribero, "A textile EBG-based antenna for future 5G-IoT millimeter-wave applications," *Electronics*, vol. 10, no. 2, p. 154, 2021.

[72] S. J. Chen, T. Kaufmann, R. Shepherd, B. Chivers, B. Weng, A. Vassallo, A. Minett, and C. Fumeaux, "A compact, highly efficient and flexible polymer ultra-wideband antenna," *IEEE Antennas and Wireless Propagation Letters*, vol. 14, pp. 1207–1210, 2015.

[73] L. Marnat and A. Shamim, "Liquid crystal polymer (LCP) based antenna for flexible system on package (SoP) applications," in *2012 15 International Symposium on Antenna Technology and Applied Electromagnetics*. IEEE, 2012, pp. 1–4.

[74] Q. H. Abbasi, M. U. Rehman, X. Yang, A. Alomainy, K. Qaraqe, and E. Serpedin, "Ultrawideband band-notched flexible antenna for wearable applications," *IEEE Antennas and Wireless Propagation Letters*, vol. 12, pp. 1606–1609, 2013.

[75] Z. Hamouda, J.-L. Wojkiewicz, A. Pud, L. Kone, B. Belaabed, S. Bergheul, and T. Lasri, "Dual-band elliptical planar conductive polymer antenna printed on a flexible substrate," *IEEE Transactions on Antennas and Propagation*, vol. 63, no. 12, pp. 5864–5867, 2015.

[76] S. J. Chen, C. Fumeaux, P. Talemi, B. Chivers, and R. Shepherd, "Progress in conductive polymer antennas based on free-standing polypyrrole and PEDOT: PSS," in *2016 17th International Symposium on Antenna Technology and Applied Electromagnetics (ANTEM)*. IEEE, 2016, pp. 1–4.

[77] J. Pourahmadazar and T. A. Denidni, "Millimeter-wave planar antenna on flexible polyethylene terephthalate substrate with water base silver nanoparticles conductive ink," *Microwave and Optical Technology Letters*, vol. 60, no. 4, pp. 887–891, 2018.

[78] R. H. Cichewicz and S. A. Kouzi, "Chemistry, biological activity, and chemotherapeutic potential of betulinic acid for the prevention and treatment of cancer and hiv infection," *Medicinal research reviews*, vol. 24, no. 1, pp. 90–114, 2004.

[79] I. Marasco, G. Niro, F. Rizzi, M. De Vittorio, A. D'Orazio, and M. Grande, "Design of a PEN-based flexible PIFA antenna operating in the sub-6GHz band for 5G applications," in *2020 22nd International Conference on Transparent Optical Networks (ICTON)*. IEEE, 2020, pp. 1–4.

[80] I. Marasco, G. Niro, L. Lamanna, L. Piro, F. Guido, L. Algieri, V. Mastronardi, A. Qualtieri, E. Scarpa, D. Desmaele *et al.*, "Compact and flexible meander antenna for surface acoustic wave sensors," *Microelectronic Engineering*, vol. 227, p. 111322, 2020.

[81] T. Inui, H. Koga, M. Nogi, N. Komoda, and K. Suganuma, "A miniaturized flexible antenna printed on a high dielectric constant nanopaper composite," *Advanced Materials*, vol. 27, no. 6, pp. 1112–1116, 2015.

[82] D. Unnikrishnan, D. Kaddour, S. Tedjini, E. Bihar, and M. Saadaoui, "CPW-fed inkjet printed uwb antenna on abs-pc for integration in molded interconnect devices technology," *IEEE Antennas and Wireless Propagation Letters*, vol. 14, pp. 1125–1128, 2015.

[83] M. R. Abdul-Aziz, S. A. Mohassieb, N. A. Eltresy, M. M. Yousef, B. Anis, S. O. Abdellatif, and A. S. Khalil, "Enhancing the performance of polygon monopole antenna using graphene/tmdcs heterostructures," *IEEE Transactions on Nanotechnology*, vol. 19, pp. 269–273, 2020.

[84] Z. Wang, L. Qin, Q. Chen, W. Yang, and H. Qu, "Flexible uwb antenna fabricated on polyimide substrate by surface modification and in situ self-metallization technique," *Microelectronic Engineering*, vol. 206, pp. 12–16, 2019.

[85] D. Cang, Z. Wang, and H. Qu, "A polyimide-based flexible monopole antenna fed by a coplanar waveguide," *Electronics*, vol. 10, no. 3, p. 334, 2021.

[86] Y. Zhang, B.-h. Wu, H.-l. Wang, H. Wu, Y.-c. An, X.-x. Zhi, and J.-g. Liu, "Preparation and characterization of transparent polyimide nanocomposite films with potential applications as spacecraft antenna substrates with low dielectric features and good sustainability in atomic-oxygen environments," *Nanomaterials*, vol. 11, no. 8, p. 1886, 2021.

[87] R. B. Simorangkir, Y. Yang, L. Matekovits, and K. P. Esselle, "Dual-band dual-mode textile antenna on pdms substrate for body-centric communications," *IEEE Antennas and Wireless Propagation Letters*, vol. 16, pp. 677–680, 2016.

[88] A. Bakar, F. Hasnan, A. Razali, A. Rahim, M. Osman, T. Ali, and R. Radzali, "Polydimethylsiloxane as a potential antenna substrate." *Acta Physica Polonica, A.*, vol. 135, no. 5, 2019.

[89] S. Abbas, S. Desai, K. Esselle, J. Volakis, and R. Hashmi, "Design and characterization of a flexible wideband antenna using polydimethylsiloxane composite substrate," *International Journal of Antennas and Propagation*, vol. 2018, 2018.

[90] A. Hassan, S. Ali, J. Bae, and C. H. Lee, "All printed antenna based on silver nanoparticles for 1.8 GHz applications," *Applied Physics A*, vol. 122, no. 8, pp. 1–7, 2016.

[91] S. Ahmed, F. A. Tahir, A. Shamim, and H. M. Cheema, "A compact kapton-based inkjet-printed multiband antenna for flexible wireless devices," *IEEE Antennas and Wireless Propagation Letters*, vol. 14, pp. 1802–1805, 2015.

[92] S. F. Jilani, M. O. Munoz, Q. H. Abbasi, and A. Alomainy, "Millimeter-wave liquid crystal polymer based conformal antenna array for 5G applications," *IEEE Antennas and Wireless Propagation Letters*, vol. 18, no. 1, pp. 84–88, 2018.

[93] G. J. Hayes, J.-H. So, A. Qusba, M. D. Dickey, and G. Lazzi, "Flexible liquid metal alloy (egain) microstrip patch antenna," *IEEE transactions on Antennas and Propagation*, vol. 60, no. 5, pp. 2151–2156, 2012.

[94] Z. Li, S. K. Sinha, G. M. Treich, Y. Wang, Q. Yang, A. A. Deshmukh, G. A. Sotzing, and Y. Cao, "All-organic flexible fabric antenna for wearable electronics," *Journal of Materials Chemistry C*, vol. 8, no. 17, pp. 5662–5667, 2020.

[95] M. A. Riheen, T. Nguyen, T. K. Saha, T. Karacolak, and P. K. Sekhar, "CPW fed wideband bowtie slot antenna on PET substrate," *Progress In Electromagnetics Research C*, vol. 101, pp. 147–158, 2020.

[96] M. A. Rahman, M. F. Hossain, M. A. Riheen, and P. K. Sekhar, "Early brain stroke detection using flexible monopole antenna," *Progress In Electromagnetics Research C*, vol. 99, pp. 99–110, 2020.

[97] F. Tariq, Q. Amjad, A. Kamran, A. Hassan, and R. Karim, "A flexible antenna on cost-effective pen substrate for sub-6 GHz 5G wireless transceivers," in *2019 International Conference on Frontiers of Information Technology (FIT)*. IEEE, 2019, pp. 89–895.

[98] C. M. Lee, Y. Kim, Y. Kim, I. K. Kim, and C. W. Jung, "A flexible and transparent antenna on a polyamide substrate for laptop computers," *Microwave and Optical Technology Letters*, vol. 57, no. 5, pp. 1038–1042, 2015.

[99] J. Kulkarni, A. G. Alharbi, A. Desai, C.-Y.-D. Sim, A. Poddar *et al.*, "Design and analysis of wideband flexible self-isolating MIMO antennas for sub-6 GHz 5G and wlan smartphone terminals," *Electronics*, vol. 10, no. 23, p. 3031, 2021.

[100] H. R. Khaleel, H. M. Al-Rizzo, D. G. Rucker, and Y. Al-Naiemy, "Flexible printed monopole antennas for WLAN applications," in *2011 IEEE International Symposium on Antennas and Propagation (APSURSI)*. IEEE, 2011, pp. 1334–1337.

[101] S. Mohandoss, S. K. Palaniswamy, R. R. Thipparaju, M. Kanagasabai, B. R. B. Naga, and S. Kumar, "On the bending and time domain analysis of compact wideband flexible monopole antennas," *AEU-International Journal of Electronics and Communications*, vol. 101, pp. 168–181, 2019.

[102] F. Faisal, Y. Amin, Y. Cho, and H. Yoo, "Compact and flexible novel wideband flower-shaped CPW-fed antennas for high data wireless applications," *IEEE Transactions on Antennas and Propagation*, vol. 67, no. 6, pp. 4184–4188, 2019.

[103] M. Venkateswara Rao, B. T. P. Madhav, T. Anilkumar, and B. Prudhvinadh, "Circularly polarized flexible antenna on liquid crystal polymer substrate material with metamaterial loading," *Microwave and Optical Technology Letters*, vol. 62, no. 2, pp. 866–874, 2020.

[104] S. F. Jilani, B. Greinke, Y. Hao, and A. Alomainy, "Flexible millimetre-wave frequency reconfigurable antenna for wearable applications in 5G networks," in *2016 URSI International Symposium on Electromagnetic Theory (EMTS)*. IEEE, 2016, pp. 846–848.

[105] A. Rida, L. Yang, R. Vyas, and M. M. Tentzeris, "Conductive inkjet-printed antennas on flexible low-cost paper-based substrates for RFID and WSN applications," *IEEE Antennas and Propagation Magazine*, vol. 51, no. 3, pp. 13–23, 2009.

[106] D. C. Thompson, O. Tantot, H. Jallageas, G. E. Ponchak, M. M. Tentzeris, and J. Papapolymerou, "Characterization of liquid crystal polymer (LCP) material and transmission lines on LCP substrates from 30 to 110 ghz," *IEEE Transactions on Microwave Theory and Techniques*, vol. 52, no. 4, pp. 1343–1352, 2004.

[107] R. J. Vyas, A. Rida, L. Yang, and M. M. Tentzeris, "Design and development of the first entirely paper-based wireless sensor module," in *2008 IEEE Antennas and Propagation Society International Symposium*. IEEE, 2008, pp. 1–4.

[108] D. E. Anagnostou, A. A. Gheethan, A. K. Amert, and K. W. Whites, "A direct-write printed antenna on paper-based organic substrate for flexible displays and WLAN applications," *Journal of Display Technology*, vol. 6, no. 11, pp. 558–564, 2010.

[109] A. Gheethan, D. Anagnostou, A. Amert, and K. Whites, "Printed paper-based low-cost pifa antenna for handheld devices," in *Proc. 8th Annu. Flexible Electron. Displays Conf.(FEDC'09)*, 2009, pp. 2–5.

[110] D. E. Anagnostou, A. A. Gheethan, T. Amert, and K. W. Whites, "A low-cost wlan "green" pifa antenna on eco-friendly paper substrate," in *2009 IEEE Antennas and Propagation Society International Symposium*. IEEE, 2009, pp. 1–4.

[111] A. A. Gheethan and D. E. Anagnostou, "Dual band-reject uwb antenna with sharp rejection of narrow and closely-spaced bands," *IEEE transactions on antennas and propagation*, vol. 60, no. 4, pp. 2071–2076, 2012.

[112] H. Lee, G. Shaker, K. Naishadham, X. Song, M. McKinley, B. Wagner, and M. Tentzeris, "Carbon-nanotube loaded antenna-based ammonia gas sensor," *IEEE Transactions on Microwave Theory and Techniques*, vol. 59, no. 10, pp. 2665–2673, 2011.

[113] A. Mansour, N. Shehata, B. Hamza, and M. Rizk, "Efficient design of flexible and low cost paper-based inkjet-printed antenna," *International Journal of Antennas and Propagation*, vol. 2015, 2015.

[114] A. Mansour, M. Azab, and N. Shehata, "Flexible paper-based wideband antenna for compact-size IoT devices," in *2017 8th IEEE Annual Information Technology, Electronics and Mobile Communication Conference (IEMCON)*. IEEE, 2017, pp. 426–429.

[115] B. S. Cook and A. Shamim, "Inkjet printing of novel wideband and high gain antennas on low-cost paper substrate," *IEEE Transactions on Antennas and Propagation*, vol. 60, no. 9, pp. 4148–4156, 2012.

[116] T. Leng, X. Huang, K. Chang, J. Chen, M. A. Abdalla, and Z. Hu, "Graphene nanoflakes printed flexible meandered-line dipole antenna on paper substrate for low-cost RFID and sensing applications," *IEEE Antennas and Wireless Propagation Letters*, vol. 15, pp. 1565–1568, 2016.

[117] H. Prakash, N. Chandra, R. Prakash *et al.*, "Effect of decoherence on fidelity in teleportation using entangled coherent states," *Journal of Physics B: Atomic, Molecular and Optical Physics*, vol. 40, no. 8, p. 1613, 2007.

[118] G. Xiao, P. Aflaki, S. Lang, Z. Zhang, Y. Tao, C. Py, P. Lu, C. Martin, and S. Change, "Printed UHF RFID reader antennas for potential retail applications," *IEEE Journal of Radio Frequency Identification*, vol. 2, no. 1, pp. 31–37, 2018.

[119] K. Zack, H. Khaleel, A. Isaac, and A. Bihnam, "Compact spiral antenna for space based applications," in *2014 IEEE Antennas and Propagation Society International Symposium (APSURSI)*. IEEE, 2014, pp. 1708–1709.

[120] W. G. Whittow, A. Chauraya, J. Vardaxoglou, Y. Li, R. Torah, K. Yang, S. Beeby, and J. Tudor, "Inkjet-printed microstrip patch antennas realized on textile for wearable applications," *IEEE Antennas and Wireless Propagation Letters*, vol. 13, pp. 71–74, 2014.

[121] K. N. Paracha, S. K. A. Rahim, H. T. Chattha, S. S. Aljaafreh, Y. C. Lo *et al.*, "Low-cost printed flexible antenna by using an office printer for conformal applications," *International Journal of Antennas and Propagation*, vol. 2018, 2018.

[122] Z. Wang, C. Pang, Y. Li, and X. Wang, "A method for radiation pattern reconstruction of phased-array antenna," *IEEE Antennas and Wireless Propagation Letters*, vol. 19, no. 1, pp. 168–172, 2019.

[123] H. R. Khaleel, "Design and fabrication of compact inkjet printed antennas for integration within flexible and wearable electronics," *IEEE transactions on components, packaging and manufacturing technology*, vol. 4, no. 10, pp. 1722–1728, 2014.

[124] Z. Stempien, E. Rybicki, A. Patykowska, T. Rybicki, and M. Szynkowska, "Shape-programmed inkjet-printed silver electro-conductive layers on textile surfaces," *Journal of Industrial Textiles*, vol. 47, no. 6, pp. 1321–1341, 2018.

[125] B. K. Tehrani, B. S. Cook, and M. M. Tentzeris, "Inkjet printing of multilayer millimeter-wave Yagi-Uda antennas on flexible substrates," *IEEE Antennas and Wireless Propagation Letters*, vol. 15, pp. 143–146, 2015.

[126] H. F. Abutarboush and A. Shamim, "A reconfigurable inkjet-printed antenna on paper substrate for wireless applications," *IEEE Antennas and Wireless Propagation Letters*, vol. 17, no. 9, pp. 1648–1651, 2018.

[127] M. Grouchko, A. Kamyshny, C. F. Mihailescu, D. F. Anghel, and S. Magdassi, "Conductive inks with a "built-in" mechanism that enables sintering at room temperature," *ACS nano*, vol. 5, no. 4, pp. 3354–3359, 2011.

[128] D. Xu, X. Tian, X. Guo, W. Jiang, W. Liu, and S. Xing, "Design and research of flexible wearable textile antenna based on GNPS/PANI/PDMS composites for 2.45 ghz," *Nanoscience and Nanotechnology Letters*, vol. 9, no. 4, pp. 476–480, 2017.

[129] A. Lamminen, K. Arapov, G. de With, S. Haque, H. G. Sandberg, H. Friedrich, and V. Ermolov, "Graphene-flakes printed wideband elliptical dipole antenna for low-cost wireless communications applications," *IEEE Antennas and Wireless Propagation Letters*, vol. 16, pp. 1883–1886, 2017.

[130] A. Meredov, K. Klionovski, and A. Shamim, "Screen-printed, flexible, parasitic beam-switching millimeter-wave antenna array for wearable applications," *IEEE open journal of antennas and propagation*, vol. 1, pp. 2–10, 2019.

[131] B. Li, D. Li, and J. Wang, "Copper deposition on textiles via an automated dispensing process for flexible microstrip antennas," *Textile Research Journal*, vol. 84, no. 19, pp. 2026–2035, 2014.

[132] J. Virkki, Z. Wei, A. Liu, L. Ukkonen, and T. Björninen, "Wearable passive e-textile UHF RFID tag based on a slotted patch antenna with sewn ground and microchip interconnections," *International Journal of Antennas and Propagation*, vol. 2017, 2017.

[133] T. N. Kapetanakis, M. Pavec, M. P. Ioannidou, C. D. Nikolopoulos, A. T. Baklezos, R. Soukup, and I. O. Vardiambasis, "Embroidered bow-tie wearable antenna for the 868 and 915 MHZ ISM bands," *Electronics*, vol. 10, no. 16, p. 1983, 2021.

[134] A. Chauraya, R. Seager, W. Whittow, S. Zhang, and Y. Vardaxoglou, "Embroidered frequency selective surfaces on textiles for wearable applications," in *2013 Loughborough Antennas & Propagation Conference (LAPC)*. IEEE, 2013, pp. 388–391.

[135] B. A. Babu, B. Madhav, Y. P. Reddy, and M. Rao, "Embroidered quad-band electro-textile wearable antenna for WBAN applications," in *AIP Conference Proceedings*, vol. 2352, no. 1. AIP Publishing LLC, 2021, p. 020050.

[136] M. El Gharbi, M. Martinez-Estrada, R. Fernández-García, S. Ahyoud, and I. Gil, "A novel ultra-wide band wearable antenna under different bending conditions for electronic-textile applications," *The Journal of The Textile Institute*, vol. 112, no. 3, pp. 437–443, 2021.

[137] P. Ramya *et al.*, "Design of embroidery antenna for wearable applications," *Turkish Journal of Computer and Mathematics Education (TURCOMAT)*, vol. 12, no. 10, pp. 1191–1196, 2021.

[138] J. DicCbshfsE, M. K. Abd Rahim, N. A. Samsuri, H. A. M. Salim, and M. F. Ali, "Embroidered fully textile wearable antenna for medical monitoring applications," *Progress In Electromagnetics Research*, vol. 117, pp. 321–337, 2011.

[139] L. Corchia, G. Monti, E. De Benedetto, and L. Tarricone, "Wearable antennas for remote health care monitoring systems," *International Journal of Antennas and Propagation*, vol. 2017, 2017.

[140] M. Sharma and H. Singh, "Substrate integrated waveguide based leaky wave antenna for high frequency applications and IoT," *International Journal of Sensors Wireless Communications and Control*, vol. 11, no. 1, pp. 5–13, 2021.

[141] A. Iqbal, M. A. Selmi, L. F. Abdulrazak, O. A. Saraereh, N. K. Mallat, and A. Smida, "A compact substrate integrated waveguide cavity-backed self-triplexing antenna," *IEEE Transactions on Circuits and Systems II: Express Briefs*, vol. 67, no. 11, pp. 2362–2366, 2020.

[142] M. Z. Ali and Q. U. Khan, "High gain backward scanning substrate integrated waveguide leaky wave antenna," *IEEE Transactions on Antennas and Propagation*, vol. 69, no. 1, pp. 562–565, 2020.

[143] N. Javanbakht, R. E. Amaya, J. Shaker, and B. Syrett, "Side-lobe level reduction of half-mode substrate integrated waveguide leaky-wave antenna," *IEEE Transactions on Antennas and Propagation*, vol. 69, no. 6, pp. 3572–3577, 2020.

[144] A. A. Althuwayb, "Enhanced radiation gain and efficiency of a metamaterial-inspired wideband microstrip antenna using substrate integrated waveguide technology for sub-6 GHz wireless communication systems," *Microwave and Optical Technology Letters*, vol. 63, no. 7, pp. 1892–1898, 2021.

[145] S. S. Kharintsev, A. I. Noskov, G. G. Hoffmann, and J. Loos, "Near-field optical taper antennas fabricated with a highly replicable ac electrochemical etching method," *Nanotechnology*, vol. 22, no. 2, p. 025202, 2010.

[146] M. Kubo, X. Li, C. Kim, M. Hashimoto, B. J. Wiley, D. Ham, and G. M. Whitesides, "Stretchable microfluidic radiofrequency antennas," *Advanced materials*, vol. 22, no. 25, pp. 2749–2752, 2010.

[147] S. D. Tie JC and R. Liu., *Metamaterials: Theory, Design and Application.* Springer, 2010.

[148] M. Lapine and S. Tretyakov, "Contemporary notes on metamaterials," *IET microwaves, antennas & propagation*, vol. 1, no. 1, pp. 3–11, 2007.

[149] A. Sihvola, "Metamaterials in electromagnetics," *Metamaterials*, vol. 1, no. 1, pp. 2–11, 2007.

[150] G. V. Eleftheriades and K. G. Balmain, *Negative-refraction metamaterials: fundamental principles and applications.* John Wiley & Sons, 2005.

[151] R. W. Ziolkowski and N. Engheta, "Metamaterials: two decades past and into their electromagnetics future and beyond," *IEEE Transactions on Antennas and Propagation*, vol. 68, no. 3, pp. 1232–1237, 2019.

[152] A. R. Alhawari, A. Almawgani, A. T. Hindi, H. Alghamdi, and T. Saeidi, "Metamaterial-based wearable flexible elliptical UWB antenna for WBAN and breast imaging applications," *AIP Advances*, vol. 11, no. 1, p. 015128, 2021.

[153] U. Ali, S. Ullah, M. Shafi, S. A. Shah, I. A. Shah, and J. A. Flint, "Design and comparative analysis of conventional and metamaterial-based textile antennas for wearable applications," *International Journal of Numerical Modelling: Electronic Networks, Devices and Fields*, vol. 32, no. 6, p. e2567, 2019.

[154] K. Hossain, T. Sabapathy, M. Jusoh, M. A. Abdelghany, P. J. Soh, M. N. Osman, M. N. M. Yasin, H. A. Rahim, and S. S. Al-Bawri, "A negative index nonagonal CSRR metamaterial-based compact flexible planar monopole antenna for ultrawideband applications using viscose-wool felt," *Polymers*, vol. 13, no. 16, p. 2819, 2021.

[155] S. Ibnyaich, L. Wakrim, and M. M. Hassani, "Nonuniform semi-patches for designing an ultra wideband pifa antenna by using genetic algorithm optimization," *Wireless Personal Communications*, vol. 117, no. 2, pp. 957–969, 2021.

[156] T. Saeidi, S. N. Mahmood, S. Alani, S. M. Ali, I. Ismail, and A. R. Alhawari, "Sub-6g metamaterial-based flexible wearable uwb antenna for iot and wban," in *2020 IEEE Intl Conf on Dependable, Autonomic and Secure Computing, Intl Conf on Pervasive Intelligence and Computing, Intl Conf on Cloud and Big Data Computing, Intl Conf on Cyber Science and Technology Congress (DASC/PiCom/CBDCom/CyberSciTech).* IEEE, 2020, pp. 7–13.

[157] A. Al-Adhami and E. Ercelebi, "A flexible metamaterial based printed antenna for wearable biomedical applications," *Sensors*, vol. 21, no. 23, p. 7960, 2021.

[158] S. Roy and U. Chakraborty, "Metamaterial based dual wideband wearable antenna for wireless applications," *Wireless Personal Communications*, vol. 106, no. 3, pp. 1117–1133, 2019.

[159] M. Wang, Z. Yang, J. Wu, J. Bao, J. Liu, L. Cai, T. Dang, H. Zheng, and E. Li, "Investigation of sar reduction using flexible antenna with metamaterial

structure in wireless body area network," *IEEE Transactions on Antennas and Propagation*, vol. 66, no. 6, pp. 3076–3086, 2018.

[160] D. Negi, R. Khanna, and J. Kaur, "Design and performance analysis of a conformal cpw fed wideband antenna with mu-negative metamaterial for wearable applications," *International Journal of Microwave and Wireless Technologies*, vol. 11, no. 8, pp. 806–820, 2019.

[161] T. A. Elwi, "A further realization of a flexible metamaterial-based antenna on nickel oxide polymerized palm fiber substrates for RF energy harvesting," *Wireless Personal Communications*, vol. 115, no. 2, pp. 1623–1634, 2020.

[162] Z. Wang, J. Volakis, and A. Kiourti, "Embroidered antennas for communication systems," in *Electronic Textiles*. Elsevier, 2015, pp. 201–237.

[163] G. N. Islam, A. Ali, and S. Collie, "Textile sensors for wearable applications: A comprehensive review," *Cellulose*, vol. 27, no. 11, pp. 6103–6131, 2020.

[164] K.-J. Baeg and J. Lee, "Flexible electronic systems on plastic substrates and textiles for smart wearable technologies," *Advanced Materials Technologies*, vol. 5, no. 7, p. 2000071, 2020.

[165] H. Peng, X. Sun, W. Weng, and X. Fang, "Flexible electronic devices based on polymers," *Polymer Materials for Energy and Electronic Applications*, vol. 325, pp. 325–354, 2017.

[166] K. N. Paracha, S. K. A. Rahim, P. J. Soh, and M. Khalily, "Wearable antennas: A review of materials, structures, and innovative features for autonomous communication and sensing," *IEEE Access*, vol. 7, pp. 56 694–56 712, 2019.

[167] C. Riedel, "Dielectric and mechanical properties of polymers at macro and nanoscale," Ph.D. dissertation, Université Montpellier II-Sciences et Techniques du Languedoc, 2010.

[168] Y. Ouyang and W. J. Chappell, "High frequency properties of electro-textiles for wearable antenna applications," *IEEE Transactions on Antennas and Propagation*, vol. 56, no. 2, pp. 381–389, 2008.

[169] J. C. McDonald and G. M. Whitesides, "Poly (dimethylsiloxane) as a material for fabricating microfluidic devices," *Accounts of chemical research*, vol. 35, no. 7, pp. 491–499, 2002.

[170] J. Trajkovikj, J.-F. Zürcher, and A. K. Skrivervik, "Soft and flexible antennas on permittivity adjustable pdms substrates," in *2012 Loughborough Antennas & Propagation Conference (LAPC)*. IEEE, 2012, pp. 1–4.

[171] N. Tiercelin, P. Coquet, R. Sauleau, V. Senez, and H. Fujita, "Polydimethylsiloxane membranes for millimeter-wave planar ultra flexible antennas," *Journal of Micromechanics and Microengineering*, vol. 16, no. 11, p. 2389, 2006.

[172] H. Jeong and S. Lim, "A stretchable radio-frequency strain sensor using screen printing technology," *Sensors*, vol. 16, no. 11, p. 1839, 2016.

[173] M. Seki, R. Aoyama, J. W. Hong, T. Fujii, and I. Endo, "Multiple diagnostic analyses by enzymatic and chemical reaction on a pdms microchip," in *1st Annual International IEEE-EMBS Special Topic Conference on Microtechnologies in Medicine and Biology. Proceedings (Cat. No. 00EX451)*. IEEE, 2000, pp. 21–24.

[174] N. Y. Li, Z. Zakaria, N. A. Shairi, H. Alsariera, and R. Alahnomi, "Design and investigation on wideband antenna based on polydimethylsiloxane (PDMS) for medical imaging application," *no*, vol. 3, pp. 89–92, 2020.

[175] P. Du, X. Lin, and X. Zhang, "Dielectric constants of pdms nanocomposites using conducting polymer nanowires," in *2011 16th International Solid-State Sensors, Actuators and Microsystems Conference*. IEEE, 2011, pp. 645–648.

[176] H. Mirza, T. M. Hossain, P. J. Soh, M. F. Jamlos, M. N. Ramli, A. A. Al-Hadi, E. S. Hassan, and S. Yan, "Deployable linear-to-circular polarizer using pdms based on unloaded and loaded circular FSS arrays for pico-satellites," *Ieee Access*, vol. 7, pp. 2034–2041, 2018.

[177] A. Nag, R. B. Simorangkir, E. Valentin, T. Björninen, L. Ukkonen, R. M. Hashmi, and S. C. Mukhopadhyay, "A transparent strain sensor based on pdms-embedded conductive fabric for wearable sensing applications," *IEEE Access*, vol. 6, pp. 71 020–71 027, 2018.

[178] K. Raj M and S. Chakraborty, "PDMS microfluidics: A mini review," *Journal of Applied Polymer Science*, vol. 137, no. 27, p. 48958, 2020.

[179] Z. Si, S. Hu, D. Cai, P. Qin, and Q. Xu, "Performance enhancement of a polydimethylsiloxane membrane for effective n-butanol pervaporation by bonding multi-silyl-functional mcm-41," *RSC advances*, vol. 8, no. 10, pp. 5127–5135, 2018.

[180] B. Zheng, W. Li, L. Liu, X. Wang, C. Chen, Z. Yu, and H. Li, "Determination of phenols isomers in water by novel nanosilica/polydimethylsiloxane-coated stirring bar combined with high performance liquid chromatography-fourier transform infrared spectroscopy," *Scientific reports*, vol. 7, no. 1, pp. 1–10, 2017.

[181] P.-Y. Cresson, Y. Orlic, J.-F. Legier, E. Paleczny, L. Dubois, N. Tiercelin, P. Coquet, P. Pernod, and T. Lasri, "1 to 220 GHz complex permittivity behavior of flexible polydimethylsiloxane substrate," *IEEE Microwave and Wireless Components Letters*, vol. 24, no. 4, pp. 278–280, 2014.

[182] C. Tomassoni, L. Silvestri, A. Ghiotto, M. Bozzi, and L. Perregrini, "Substrate-integrated waveguide filters based on dual-mode air-filled resonant cavities," *IEEE Transactions on Microwave Theory and Techniques*, vol. 66, no. 2, pp. 726–736, 2018.

[183] Online, *IPC TM-650 2.5.5.5 Test Methods Manual (1998).* Online IPC, 1998.

[184] P. I. Dankov, M. I. Tsatsova, and V. P. Levcheva, "Investigation of uniaxial dielectric anisotropy of textile fabrics and its influence over the wearable antennas' behaviour," in *2017 Progress in Electromagnetics Research Symposium-Fall (PIERS-FALL).* IEEE, 2017, pp. 1101–1108.

[185] L.-F. Chen, C. Ong, C. Neo, V. Varadan, and V. K. Varadan, *Microwave electronics: measurement and materials characterization.* John Wiley & Sons, 2004.

[186] J. W. Schultz, *Focused beam methods: measuring microwave materials in free space.* John Schultz, 2012.

[187] W. E. Courtney, "Analysis and evaluation of a method of measuring the complex permittivity and permeability microwave insulators," *IEEE Transactions on Microwave Theory and Techniques*, vol. 18, no. 8, pp. 476–485, 1970.

[188] G. Kent, "An evanescent-mode tester for ceramic dielectric substrates," *IEEE transactions on microwave theory and techniques*, vol. 36, no. 10, pp. 1451–1454, 1988.

[189] E. J. Vanzura, R. G. Geyer, M. D. Janezic *et al.*, "The nist 60-millimeter diameter cylindrical cavity resonator: Performance evaluation for permittivity measurements," 1993.

[190] A. Note *et al.*, "Basics of measuring the dielectric properties of materials," *Agilent Technologies*, p. 1e31, 2006.

[191] D. V. Blackham and R. D. Pollard, "An improved technique for permittivity measurements using a coaxial probe," *IEEE Transactions on Instrumentation and Measurement*, vol. 46, no. 5, pp. 1093–1099, 1997.

[192] X. Zhao, C. Liu, and L. C. Shen, "Numerical analysis of a tm/sub 010/cavity for dielectric measurement," *IEEE transactions on microwave theory and techniques*, vol. 40, no. 10, pp. 1951–1959, 1992.

[193] B. Hadjistamov, V. P. Levcheva, and P. I. Dankov, "Dielectric substrate characterization with re-entrant resonators," in *Proc. Vth Mediterranean Microwave Symposium (MMS'2007)*, 2007, pp. 183–186.

[194] Y. Kato and M. Horibe, "Broadband permittivity measurements up to 170-GHz using balanced-type circular-disk resonator excited by 0.8-mm coaxial line," *IEEE Transactions on Instrumentation and Measurement*, vol. 68, no. 6, pp. 1796–1805, 2019.

[195] P. I. Dankov, "Concept for equivalent dielectric constant of planar transmission lines on anisotropic substrates," in *2016 46th European Microwave Conference (EuMC).* IEEE, 2016, pp. 158–161.

[196] A. Gaebler, F. Goelden, S. Mueller, and R. Jakoby, "Triple-mode cavity perturbation method for the characterization of anisotropic media," in *2008 38th European Microwave Conference*. IEEE, 2008, pp. 909–912.

[197] J. Krupka, D. Cros, M. Aubourg, and P. Guillon, "Study of whispering gallery modes in anisotropic single-crystal dielectric resonators," *IEEE transactions on microwave theory and techniques*, vol. 42, no. 1, pp. 56–61, 1994.

[198] G. Mumcu, K. Sertel, and J. L. Volakis, "A measurement process to characterize natural and engineered low-loss uniaxial dielectric materials at microwave frequencies," *IEEE transactions on microwave theory and techniques*, vol. 56, no. 1, pp. 217–223, 2008.

[199] J. C. Rautio, R. L. Carlson, B. J. Rautio, and S. Arvas, "Shielded dual-mode microstrip resonator measurement of uniaxial anisotropy," *IEEE Transactions on Microwave Theory and Techniques*, vol. 59, no. 3, pp. 748–754, 2011.

[200] P. I. Dankov, "Material characterization in the microwave range, when the materials become composite, reinforced, 3d-printed, artificially mixed, nanomaterials and metamaterials," in *Forum for Electromagnetic Research Methods and Application Technologies (FERMAT Journal). Available online: https://www. e-fermat. org/articles. php (accessed on 20 December 2020)*, 2020.

[201] P. I. Dankov and B. N. Hadjistamov, "Characterization of microwave substrates with split-cylinder and split-coaxial-cylinder resonators," in *2007 European Microwave Conference*. IEEE, 2007, pp. 933–936.

[202] V. Levcheva, B. Hadjistamov, and P. Dankov, "Two-resonator method for characterization of dielectric substrate anisotropy," *Bulg. J. Phys*, vol. 35, no. 1, pp. 33–52, 2008.

[203] P. I. Dankov, *Dielectric anisotropy of modern microwave substrates*. IntechOpen, 2010.

[204] P. Dankov, "A method for determination of equivalent dielectric constant of planar transmission lines on anisotropic substrates with dielectric overlay," in *2017 International Workshop on Antenna Technology: Small Antennas, Innovative Structures, and Applications (iWAT)*. IEEE, 2017, pp. 56–59.

[205] R. Garg, I. Bahl, and M. Bozzi, *Microstrip lines and slotlines*. Artech house, 2013.

[206] M. Barbuto, A. Alu, F. Bilotti, A. Toscano, and L. Vegni, "Characteristic impedance of a microstrip line with a dielectric overlay," *COMPEL: The International Journal for Computation and Mathematics in Electrical and Electronic Engineering*, 2013.

[207] N. Bowden, W. T. Huck, K. E. Paul, and G. M. Whitesides, "The controlled formation of ordered, sinusoidal structures by plasma oxidation of an elastomeric polymer," *Applied Physics Letters*, vol. 75, no. 17, pp. 2557–2559, 1999.

[208] Online, *SYLGARD^{TM} 184 Silicone Elastomer, Technical Data Sheet, The Dow Chemical Company Form No. 11-3184- 01 C; www.sylgard.com.* SYLGARD.

[209] A. Müller, M. C. Wapler, and U. Wallrabe, "A quick and accurate method to determine the poisson's ratio and the coefficient of thermal expansion of pdms," *Soft Matter*, vol. 15, no. 4, pp. 779–784, 2019.

[210] Online, *Isola Astra® MT data sheet; online available.* Isola Astra® MT data sheet; online available.

[211] K.-L. Wong, *Design of nonplanar microstrip antennas and transmission lines*. John wiley & sons, 2004, vol. 163.

[212] R. Sanchez-Montero, P.-L. Lopez-Espi, C. Alen-Cordero, and J.-A. Martinez-Rojas, "Bend and moisture effects on the performance of a U-shaped slotted wearable antenna for off-body communications in an industrial scientific medical (ism) 2.4 GHz band," *Sensors*, vol. 19, no. 8, p. 1804, 2019.

[213] P. Escobedo, J. de Pablos-Florido, M. A. Carvajal, A. Martínez-Olmos, L. F. Capitán-Vallvey, and A. J. Palma, "The effect of bending on laser-cut electrotextile inductors and capacitors attached on denim as wearable structures," *Textile Research Journal*, vol. 90, no. 21-22, pp. 2355–2366, 2020.

[214] N. P. Gupta, M. Kumar, and R. Maheshwari, "Development and performance analysis of conformal uwb wearable antenna under various bending radii," in *IOP Conference Series: Materials Science and Engineering*, vol. 594, no. 1. IOP Publishing, 2019, p. 012025.

[215] M. El Gharbi, R. Fernández-García, S. Ahyoud, and I. Gil, "A review of flexible wearable antenna sensors: design, fabrication methods, and applications," *Materials*, vol. 13, no. 17, p. 3781, 2020.

[216] M. E. B. Jalil, M. K. Abd Rahim, N. A. Samsuri, N. A. Murad, H. A. Majid, K. Kamardin, and M. A. Abdullah, "Fractal koch multiband textile antenna performance with bending, wet conditions and on the human body," *Progress In Electromagnetics Research*, vol. 140, pp. 633–652, 2013.

[217] D. Ferreira, P. Pires, R. Rodrigues, and R. F. Caldeirinha, "Wearable textile antennas: Examining the effect of bending on their performance." *IEEE Antennas and Propagation Magazine*, vol. 59, no. 3, pp. 54–59, 2017.

[218] Y. Ye, J. Yuan, and K. Su, "A volume-surface integral equation solver for radiation from microstrip antenna on anisotropic substrate," *International Journal of Antennas and Propagation*, vol. 2012, 2012.

[219] H. Odabasi and F. L. Teixeira, "Analysis of cylindrically conformal patch antennas on isoimpedance anisotropic substrates," in *2011 XXXth URSI General Assembly and Scientific Symposium.* Citeseer, 2011, pp. 1–4.

[220] S. Baloda, Z. A. Ansari, S. Singh, and N. Gupta, "Development and analysis of graphene nanoplatelets (gnps)-based flexible strain sensor for health monitoring applications," *IEEE Sensors Journal*, vol. 20, no. 22, pp. 13 302–13 309, 2020.

[221] M. I. Ahmed, M. F. Ahmed, and A. H. A. Shaalan, "Novel electro-textile patch antenna on jeans substrate for wearable applications," *Progress In Electromagnetics Research C*, vol. 83, pp. 255–265, 2018.

[222] A. Yadav, V. Kumar Singh, A. Kumar Bhoi, G. Marques, B. Garcia-Zapirain, and I. de la Torre Díez, "Wireless body area networks: UWB wearable textile antenna for telemedicine and mobile health systems," *Micromachines*, vol. 11, no. 6, p. 558, 2020.

[223] P. S. Hall and Y. Hao, *Antennas and propagation for body-centric wireless communications*. Artech house, 2012.

[224] S. Gabriel, R. Lau, and C. Gabriel, "The dielectric properties of biological tissues: Iii. parametric models for the dielectric spectrum of tissues," *Physics in medicine & biology*, vol. 41, no. 11, p. 2271, 1996.

[225] R. Alkhamis, J. Wigle, and H. Song, "Global positioning system and distress signal frequency wrist wearable dual-band antenna," *Microwave and Optical Technology Letters*, vol. 59, no. 8, pp. 2057–2064, 2017.

[226] M. Karlsson and S. Gong, "Circular dipole antenna for mode 1 UWB radio with integrated balun utilizing a flex-rigid structure," *IEEE transactions on antennas and propagation*, vol. 57, no. 10, pp. 2967–2971, 2009.

[227] Y. Sun, S. W. Cheung, and T. I. Yuk, "Design of a textile ultra-wideband antenna with stable performance for body-centric wireless communications," *IET Microwaves, Antennas & Propagation*, vol. 8, no. 15, pp. 1363–1375, 2014.

[228] S. R. Zahran, M. A. Abdalla, and A. Gaafar, "Time domain analysis for foldable thin UWB monopole antenna," *AEU-International Journal of Electronics and Communications*, vol. 83, pp. 253–262, 2018.

[229] F. Alsharif and Ç. Kurnaz, "Wearable microstrip patch ultra wide band antenna for breast cancer detection," in *2018 41st International Conference on Telecommunications and Signal Processing (TSP)*. IEEE, 2018, pp. 1–5.

[230] H. A. Elmobarak, S. K. A. Rahim, X. Castel, and M. Himdi, "Flexible conductive fabric/e-glass fibre composite ultra-wideband antenna for future wireless networks," *IET Microwaves, Antennas & Propagation*, vol. 13, no. 4, pp. 455–459, 2019.

[231] B. Prudhvi Nadh, B. Madhav, M. Siva Kumar, M. Venkateswara Rao, and T. Anilkumar, "Circular ring structured ultra-wideband antenna for wearable applications," *International Journal of RF and Microwave Computer-Aided Engineering*, vol. 29, no. 4, p. e21580, 2019.

[232] B. B. Qas Elias, P. J. Soh, A. Abdullah Al-Hadi, and G. A. Vandenbosch, "Design of a compact, wideband, and flexible rhombic antenna using cma for WBAN/WLAN and 5G applications," *International Journal of Numerical Modelling: Electronic Networks, Devices and Fields*, vol. 34, no. 5, p. e2841, 2021.

[233] R. K. Singh and A. Gupta, "Design and development of u-shaped slot wearable antenna for WLAN/Wi-Fi and wban applications," in *2018 International Conference on Advances in Computing, Communication Control and Networking (ICACCCN)*. IEEE, 2018, pp. 1063–1067.

[234] H. Yalduz, B. Koç, L. Kuzu, and M. Turkmen, "An ultra-wide band low-SAR flexible metasurface-enabled antenna for WBAN applications," *Applied Physics A*, vol. 125, no. 9, pp. 1–11, 2019.

[235] M. Kanagasabai, P. Sambandam, G. N. A. Mohammed, N. Dinesh, M. S. Morais, A. Viswanathan, S. K. Palaniswamy, and A. Shrivastav, "On the design of frequency reconfigurable tri-band miniaturized antenna for wban applications," *AEU-International Journal of Electronics and Communications*, vol. 127, p. 153450, 2020.

[236] D. Chaturvedi and S. Raghavan, "A dual-band half-mode substrate integrated waveguide-based antenna for WLAN/WBAN applications," *International Journal of RF and Microwave Computer-Aided Engineering*, vol. 28, no. 5, p. e21239, 2018.

[237] P. Vasina and J. Lacik, "Circularly polarized rectangular ring-slot antenna with chamfered corners for off-body communication at 5.8 GHz ISM band," *Radioengineering*, vol. 26, no. 1, pp. 85–90, 2017.

[238] S. Agneessens and H. Rogier, "Compact half diamond dual-band textile hmsiw on-body antenna," *IEEE Transactions on Antennas and Propagation*, vol. 62, no. 5, pp. 2374–2381, 2014.

[239] P. K. Sharma and N. Gupta, "Design and analysis polydimethylsiloxane (PDMS) and jean substrate based flexible antenna for ultra-wideband applications." IEEE IMaRC 2021, 2021.

[240] K. Kandasamy, B. Majumder, J. Mukherjee, and K. P. Ray, "Dual-band circularly polarized split ring resonators loaded square slot antenna," *IEEE Transactions on antennas and Propagation*, vol. 64, no. 8, pp. 3640–3645, 2016.

[241] H. Rahman and S. A. Rahim, "Dual band pdms based flexible antenna for wearable application," in *2015 IEEE MTT-S 2015 International Microwave Workshop Series on RF and Wireless Technologies for Biomedical and Healthcare Applications (IMWS-BIO)*. IEEE, 2015, pp. 193–194.

List of Publications

Peer Reviewed Journals:

[1] **Praveen Kumar Sharma** and Navneet Gupta, "A CPW Fed SRR Inspired Flexible Antenna using Polydimethylsiloxane (PDMS) Substrate for WLAN and WBAN Applications." *IEEE Journal on Flexible Electronics*, vol. 1 (1), pp. 39-46, 2022.

[2] **Praveen Kumar Sharma**, Navneet Gupta and Plamen I. Dankov, "Analysis of Dielectric Properties of Polydimethylsiloxane (PDMS) as a Flexible Substrate for Sensors and Antenna Applications." *IEEE-Sensors Journal*, vol. 21 (17), pp. 19492-19504, Sep. 2021. **(SCIE and SCOPUS indexed, Q1)**.

[3] Plamen I. Dankov, **Praveen Kumar Sharma**, and Navneet Gupta, "Numerical and Experimental Investigation of the Opposite Influence of Dielectric Anisotropy and Substrate Bending on Planar Radiators and Sensors." *MDPI-Sensors Journal*, vol. 21 (16), pp. 1-23, 2021. **(SCIE and SCOPUS indexed, Q1)**.*[1]

[4] **Praveen Kumar Sharma**, Navneet Gupta and Plamen I. Dankov, "Characterization of Polydimethylsiloxane (PDMS) as a Wearable Antenna Substrate using Resonance and Planar Structure Methods." *AEU- International Journal of Electronics and Communications-Elsevier*, vol. 127, 153455 (11 pages), 2020.**(SCIE and SCOPUS indexed, Q1)**.

[1]Work contributed by Praveen Kumar Sharma only is included in this thesis*

Peer Reviewed Conferences:

[1] **Praveen Kumar Sharma** and Navneet Gupta, "Design and Analysis of Polydimethylsiloxane and Jean Substrate Flexible Antenna for Ultra-wideband Applications." In *2021 IEEE MTT-S International Microwave and RF Conference (IMARC)*, pp. 1-4. **IEEE**, 2021.

[2] **Praveen Kumar Sharma** and Navneet Gupta, "Design and Analysis of a Compact CSRR Loaded Defected Ground Plane Antenna for Ultra-wideband Applications." In *2021 2nd International Conference on Communication, Computing and Industry 4.0 (C2I4)*,pp. 1-4. **IEEE**, 2021.

[3] **Praveen Kumar Sharma**, Navneet Gupta and Plamen I. Dankov, "Wideband Transmission Line Characterization of Polydimethylsiloxane (PDMS) as a Wearable Antenna Substrate." In *2020 IEEE International Conference on Electronics, Computing and Communication Technologies (CONECCT)*, pp. 1-4. **IEEE**, 2020.

[4] **Praveen Kumar Sharma** and Navneet Gupta, "Design of Metamaterial Based Patch Antenna for Ultra-Wide Band Applications." In *8th Int. Conf. on Computing, Communication and Sensor Networks (CCSN-2019)*, pp. 22-25, 2019, ISBN: 81-85824-46-5.

Biography of the Supervisor

Prof. Navneet Gupta is Professor in the Electrical and Electronics Engineering Department at Birla Institute of Technology and Science, Pilani, Rajasthan, India. Currently, he is the Associate Dean of Sponsored Research and Consultancy Division at the same Institute. He was also formerly the Head, Electrical and Electronics Engineering Department (September 2016 to August 2018). Prof. Gupta has research interests in the area of Modeling of Micro/Nano Electronic Devices, Flexible and Wearable Electronics, Computational Material Science and Electromagnetics. He has published 70+ research papers in international journals of high repute. He has also presented 65+ papers in various conferences in India and abroad. 7 Ph.D. students have graduated working under his supervision. Prof. Gupta has received research funding from various Government agencies which include UGC, DST, SERB, DRDO and MHRD. Currently he is also involved in two international projects; one with University of Sofia, Bulgaria and another with Tel-Aviv University, Israel. He received Outstanding Engineering Services to Society Award by Institution of Engineers (India), Rajasthan State Centre, DST Young Scientist Award in Physical Sciences, Gold Medal in Master's degree. He is a Fellow of Institution of Engineers (India), Senior member of IEEE and life members of renowned professional bodies such as Semiconductor Society of India, Material Research Society of India (MRSI) and Optical Society of India (OSI). He is an expert reviewer of many reputed International Journals including IEEE, Springer, Elsevier and IE (I).

Biography of the Student

Praveen Kumar Sharma received his Bachelor of Engineering (BE-Honors) degree in Electronics and Communication Engineering from the University of Rajasthan, India, in 2008. He received his Master of Engineering (ME) degree in Electronics and Communication Engineering from the National Institute of Technical Teachers Training and Research (NITTTR), Chandigarh, India, in 2015. He is currently working towards the Ph.D. degree in the Department of Electrical and Electronics Engineering, Birla Institute of Technology and Science, Pilani, (BITS-Pilani) Rajasthan, India. His research Interest includes Antennas, Material Science, Microwaves, and Electromagnetics. He is a member of professional, scientific and industrial research organizations such as Institution of Engineering and Technology (IET) and The Institute of Electrical and Electronics Engineers (IEEE). He is also working as an Assistant Professor in the Department of Electronics and Communication Engineering in BK Birla Institute of Engineering and Technology, Pilani, Rajasthan, India since 2008. He visited IUT Angouleme, France in Jan-Feb 2016 under faculty exchange program and Sofia University "St. Kliment Ohridski", Sofia University Sofia, Bulgaria to work as a Co-PI on DST joint research project in between BITS, Pilani, India and Sofia University, Bulgaria.